

UCSF

UC San Francisco Electronic Theses and Dissertations

Title

Quantitative proteomics of the thyroid hormone receptor coregulator interactions

Permalink

<https://escholarship.org/uc/item/1bj12385>

Author

Moore, Jamie M. R

Publication Date

2004

Peer reviewed|Thesis/dissertation

Quantitative Proteomics of the Thyroid Hormone Receptor Coregulator Interactions

by

Jamie M. R. Moore

DISSERTATION

Submitted in partial satisfaction of the requirements for the degree of

DOCTOR OF PHILOSOPHY

in

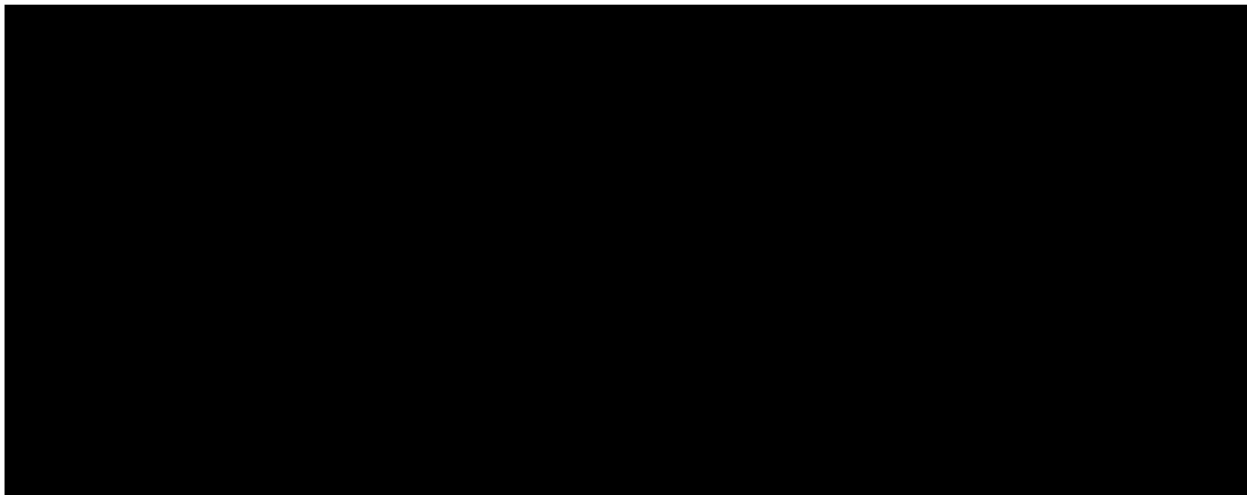
Chemistry and Chemical Biology

in the

GRADUATE DIVISION

of the

UNIVERSITY OF CALIFORNIA, SAN FRANCISCO



Date

University Librarian

Degree Conferred:.....

**Copyright 2004
By
Jamie M. R. Moore**

DEDICATION

The completion of my doctoral thesis would not have been possible without the unwavering support of my husband, and therefore this dissertation is dedicated to Michael James Moore. His faith, guidance, and continual support allowed me to overcome all of the obstacles I hit along the way. He endured many all night study sessions during the first year of course work and tolerated my extreme stress during oral examinations with sympathy and providing delicious brain-fortifying meals. He was at my side during abdominal surgery and the birth of our first son. During those stressful, restless times, his continual belief in me kept me going. Now with the completion of my dissertation and the start of a new career, I hope to return the favor and allow Michael to find his chosen career path.

There are several other critical people that I would like to mention, Dr. R. Kiplin Guy who was a great mentor and provided much needed guidance, Sarah Galicia for all of her help and for being a good friend, Dr. Timothy Geistlinger for good advice and friendship, Dr. Robert Fletterick, Dr. Holly Ingraham and Dr. Kevan Shokat for support, Dr. Tom Patapoff and Mary Cromwell for encouraging me to return to school, my parents Joe and Gloria Rasmussen for always believing in me, my brother Craig Rasmussen for sharing the graduate experience with me, my in-laws Brian and Sue Moore, and Drs. Olof and McKay Sohlberg for love and support, my crafty-lady friends Michelle, JP, Tracey, Sara,

Lani, Stephanie, Renais, Sally, Rebecca, Julia, and Kathleen for good times and much needed breaks, and my son Jackson Boyd Moore who always makes me smile.

Quantitative Proteomics of the Thyroid Hormone Receptor Coregulator Interactions

By

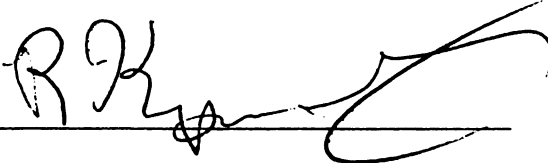
Jamie M. R. Moore

ABSTRACT

Department of Chemistry and Chemical Biology, University of California at San Francisco, Genentech Hall, Mission Bay, 600 16th Street, San Francisco, CA 94143-2280

The thyroid hormone receptor regulates a diverse set of genes involved in processes including growth, differentiation, and metabolism. Most of the effects of thyroid hormone are mediated through the thyroid hormone receptor (TR). TR belongs to the nuclear hormone receptor superfamily of ligand activated transcription factors. Upon binding of thyroid hormone, TR releases corepressor proteins and undergoes a conformational change that allows for the interaction of coactivating proteins necessary for gene transcription. This interaction is mediated by a conserved motif, termed the NR box, found in many coregulators. Recent work has demonstrated that differentially assembled coregulator complexes can elicit specific biological responses. However, the mechanism for the selective assembly of these coregulator complexes has yet to be elucidated.

Here we present the synthesis of a library of coregulator protein mimetics and design of a high-throughput *in vitro* binding assay to measure the equilibrium affinity of thyroid receptor to a library of potential coregulators. To further understand the principles underlying TR-coregulator selectivity, the binding studies were carried out in the presence of different ligands including the endogenous thyroid hormone T3, synthetic thyroid receptor β -selective agonist GC-1, and antagonist NH-3. Using this homogenous method several coregulator NR boxes capable of associating with thyroid receptor at physiologically relevant concentrations were identified including ones found in traditional coactivating proteins such as SRC1, SRC2, TRAP220, TRBP, p300 and ARA70; and those in coregulators known to repress gene activation including RIP140 and DAX-1. In addition, it was discovered that the thyroid receptor-coregulator binding patterns vary with ligand and that this differential binding can be used to predict biological responses. Finally, it is demonstrated that this is a general method that can be applied to other nuclear receptors including the androgen receptor, estrogen receptor and orphan receptors such as steroidogenic factor 1 and liver receptor homolog.

A handwritten signature in black ink, appearing to read 'R. Kiplin Guy', written over a horizontal line.

R. Kiplin Guy, Ph.D.

Graduate Committee Chairperson

TABLE OF CONTENTS

Copyright	ii
Dedication	iii
Abstract	v
Table of Contents	vii
List of Tables	x
List of Figures	xi
Chapter 1: Thyroid Hormone Receptor and Coregulators	1
Chapter 2: Synthesis of a Nuclear Receptor Coregulator Fluorescent Peptide Library	16
Introduction.....	17
Results and Discussion.....	20
Conclusions.....	32
Materials and Methods.....	36
Acknowledgments.....	38
Chapter 3: Development of a High-Throughput Fluorescence Polarization Method for Quantitative Determination of Nuclear Receptor-Coregulator Interactions	40
Introduction.....	41
Results and Discussion.....	43

Conclusions.....	54
Materials and Methods.....	55
Acknowledgments.....	57
Chapter 4: Elucidating Thyroid Hormone Receptor β-Coregulator	
Interactions.....	58
Summary.....	59
Introduction.....	60
Results.....	60
Conclusion.....	61
Materials and Methods.....	73
Acknowledgments.....	76
Chapter 5: The Mechanism of Ligand Dependent Transactivation by the	
Androgen Receptor.....	77
Summary.....	78
Introduction.....	79
Results and Discussion.....	82
Conclusion.....	96
Materials and Methods.....	96
Acknowledgements.....	103
Chapter 6: Ligand Affects on the Recruitment of Coregulators to Estrogen	
Receptor α.....	104
Summary.....	105

Introduction.....	107
Results and Discussion.....	111
Conclusion.....	120
Materials and Methods.....	122
Acknowledgements.....	125
Chapter 7: Biophysical Characterization of AF-2 Activation of LRH-1 and SF-1.....	126
Summary.....	127
Introduction.....	128
Results and Discussion.....	129
Conclusion.....	136
Materials and Methods.....	137
Acknowledgements.....	139
Appendix.....	140
A. Protocol for Peptide Library Synthesis.....	140
B. Protocol for Measuring Binding Affinities of the Thyroid Receptor β to NCOA Peptide using Fluorescence Polarization.....	158
References.....	165

LIST OF TABLES

1-1. *List of Coregulators*.....14

2-1. *Nuclear Receptor Coregulator (NCOA) Fluorescent Peptide Library*...20

2-2. *Summary of NCOA Peptide Libraries Synthesized*.....22

2-3. *Mass Accuracy, Purity, and Yields for Fluorescently Labeled NCOA Peptides*.....33

4-1. *Dissociation Constants for NR box peptides for TR β*72

7-1. *Comparison of Mouse and Human "LXXLL" Sequences for DAX1 and SHP*.....134

LIST OF FIGURES

1-1. *Physiological Affects of Thyroid Hormone*.....2

1-2. *Primary Structure of TR Isoforms*.....4

1-3. *Nuclear Receptor Superfamily*.....6

1-4. *A Simple Model of TR Activation*.....7

1-5. *Models for Negative Regulation of Thyroid Hormone Gene Expression*...9

1-6. *SRC Family Primary Structure*.....10

1-7. *Structural Features of the Thyroid Hormone -SRC2-2 Interaction*.....13

2-1. *Mapping Nuclear Receptor-Coregulator Interactions Utilizing Fluorescence Polarization*.....17

2-2. *General Peptide Synthesis Scheme*.....24

2-3. *Proposed Mechanism for Methionine Reduction During Cleavage Using TFA, Ammonium Iodide, and Dimethylsulphide*.....26

2-4. *Purification of Crude Unlabeled Peptides*.....29

2-5. *Labeling Strategies*.....31

2-6. *Purification of Labeled Peptides in the Presence and Absence of TCEP*.....34

2-7. *LCMS Traces for SRC2-2 and SRC2-3*.....35

3-1. *Fluorescence Polarization*.....42

3-2. *Klotz Plot of TR β -LBD and SRC2-2*.....44

3-3. *The Effect of pH on TR β -LBD–Coregulator Interactions*.....45

3-4. *The Effect of Detergents on TR β -LBD–Coregulator Interactions*.....47

3-5. *Scatchard and Hill Plot Analysis*.....48

3-6. *Four Binding Modes for TR β -LBD*.....50

<i>3-7. Dissociation Constants for TRβ-LBD-Coregulators.....</i>	<i>53</i>
<i>4-1. Coregulator Binding Patterns and Specificity Determinants.....</i>	<i>62</i>
<i>5-1. AR Model of Activation.....</i>	<i>80</i>
<i>5-2. AR-LBD Coregulator Interactions.....</i>	<i>84</i>
<i>5-3. Comparison of AR and TR NCOA Recruitment.....</i>	<i>87</i>
<i>5-4. AR Interacts with LXXLL and FXXLF Coregulator NR Boxes.....</i>	<i>89</i>
<i>5-5. AR-LBD Confers AF-2 Activity.....</i>	<i>90</i>
<i>5-6. AR-LBD Structures with ARA70-2 and SRC2-3.....</i>	<i>92</i>
<i>5-7. Affects of AR-LBD Mutations.....</i>	<i>94</i>
<i>6-1. Pathways Regulated by Activated ER.....</i>	<i>108</i>
<i>6-2. Structures of ERα-DES and ERα-OHT with SRC2-2.....</i>	<i>110</i>
<i>6-3. ERα-LBD Binding Curves.....</i>	<i>112</i>
<i>6-4. Coregulator Binding Patterns for Nuclear Receptor.....</i>	<i>114</i>
<i>6-5. Specificity Determinants.....</i>	<i>118</i>
<i>6-6. Ligand Affects on ERα-LBD Coregulator Recruitment.....</i>	<i>119</i>
<i>6-7. Affects of Indene Ligands on p160 Coregulator Binding to ER.....</i>	<i>121</i>
<i>7-1. LRH-1 and SF-1 Coregulator Binding Patterns.....</i>	<i>130</i>
<i>7-2. Comparison of Mouse and Human Coregulator Recruitment to LRH-1 and SF-1.....</i>	<i>134</i>
<i>7-3. Crystals obtained with mouse SF-1 ligand binding domain and box 1 of mouse SHP.....</i>	<i>135</i>
<i>7-4. SF-1 with SHP box 1 in Coregulator Binding Pocket.....</i>	<i>136</i>

Chapter 1: Thyroid Hormone Receptor and Coregulators

Jamie M. R. Moore and R. Kip Guy, Thyroid Hormone Receptor Interactions with Coregulators, *Molecular and Cellular Proteomics*, December 2004, In Preparation

Jamie M. R. Moore, Sarah J. Galicia, Andrea C. McReynolds, Ngoc-Ha Nguyen, Thomas S. Scanlan, and R. Kiplin Guy, Quantitative proteomics of the thyroid hormone receptor coregulator interactions, *Journal of Biological Chemistry* 2004 Jun 25; 279(26): 27584-90

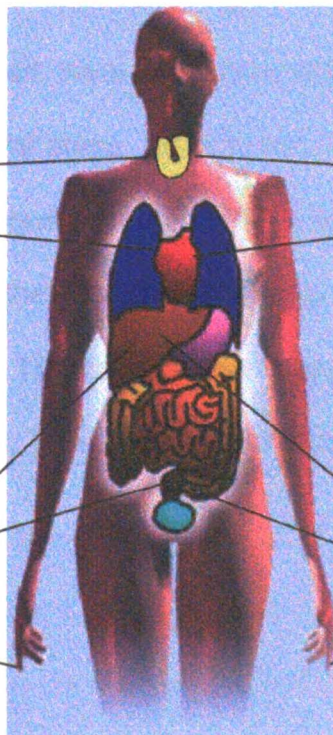
Copyright © 2004 by the American Society for Biochemistry and Molecular Biology

INTRODUCTION

Thyroid hormone controls essential functions in growth, development, and metabolism and is important for normal function of almost all tissues. Studying diseased states of hypo and hyperthyroidism has elucidated some of the important physiological affects of thyroid hormone (Figure 1-1). Specifically, thyroid hormone has critical roles in the regulation of the cardiovascular system including heart rate, cardiac contractility, and output [1]. In addition, it has been linked to several metabolic processes such as basal metabolism, and lipid and carbohydrate homeostasis [2]. Other regulatory roles of thyroid hormone are associated with the reproductive and central nervous system.

Hypothyroidism

- Dry, Coarse Hair
- Puffy Face
- Enlarged Thyroid (Goiter)
- Slow Heartbeat**
- Arthritis
- Cold Intolerance**
- Depression
- Fatigue
- Heavy Menstrual Periods
- Infertility
- Weight Gain**
- High Cholesterol**
- Constipation
- Brittle Nails



Hyperthyroidism

- Hair loss
- Bulging Eyes
- Enlarged Thyroid (Goiter)
- Rapid Heartbeat**
- Difficulty Sleeping
- Heat Intolerance**
- Irritability
- Fatigue
- Scant Menstrual Periods
- Infertility
- Weight Loss**
- Low Cholesterol**
- Frequent Bowel Movements
- Soft Nails

FIGURE 1-1. Physiological Affects of Thyroid Hormone

In hypothyroidism patients experience low energy, cold intolerance, hair loss and reproductive failure. In addition, weight gain, increased cholesterol levels and

slower heartbeats have been associated with hypothyroidism. Common symptoms of hyperthyroidism include insomnia, nervousness and anxiety, increased heart rate, weight loss, lowering of cholesterol levels and heat intolerance. These effects highlight some of the tissues that thyroid hormone regulates including the heart, liver, thyroid gland, reproductive organs and colon.

Most of the effects of thyroid hormone are mediated by a family of high-affinity receptor proteins known as the thyroid hormone receptors (TR). However, recent work by Thomas Scanlan demonstrated that metabolites of thyroid hormone can also exert biological effects through the G-protein coupled receptors [3]. There are two different genes that express different TR subtypes, TR α and TR β . Each transcript can be alternatively spliced generating different isoforms (TR α_1 , TR α_2 , TR β_1 , TR β_2 ,) [4, 5] (Figure 1-2). While most of these isoforms are widely expressed, there are distinct patterns of expression that vary with tissue and developmental stage. In particular, TR β_2 is found almost exclusively in the hypothalamus, anterior pituitary, and developing ear. In addition, mice deficient in either TR α or TR β display unique phenotypes suggesting that the different TR isoforms have unique regulatory roles [6-11]. Unlike the other TR proteins, TR α_2 , does not bind thyroid hormone and it may function to inhibit other TR

[6].

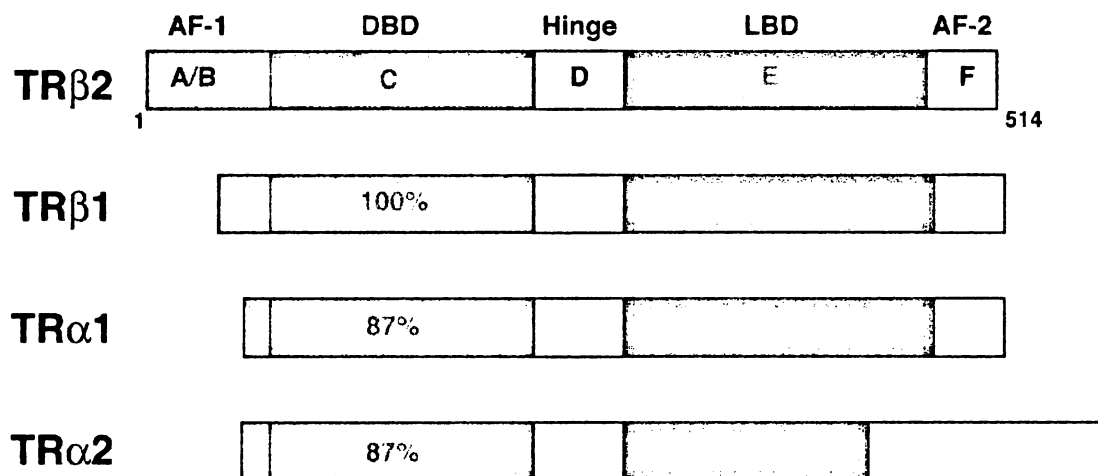


FIGURE 1-2. Primary Structure of TR Isoforms

There are two genes that encode 4 different TR proteins, TRβ2, TRβ1, TRα1, TRα2. TRα2 does not bind thyroid hormone and may function to inhibit the other TRs. Like other nuclear receptors, they are highly homologous proteins with approximately 500 amino acids comprised of a five domains labeled A through F. There are two activation function domains, AF-1 and AF-2, a DNA-binding domain (DBD), hinge domain, and ligand binding domain (LBD). The percent homology for the TRs is indicated.

The TRs belong to the large superfamily of nuclear hormone receptors that regulate gene transcription (Figure 1-3). These proteins control a diverse set of target genes in response to specific physiological signals. Members include the endocrine receptors, e.g. estrogen (ER), androgen (AR) and thyroid receptors (TR), the adopted orphan receptors, e.g. retinoid X receptor (RXR) and peroxisome proliferator activated receptor (PPAR), and the orphan receptors, e.g. steroidogenic factor 1 (SF-1) and liver receptor homolog 1 (LRH-1).

It postulated that this superfamily of proteins arose from a common ancestry as indicated by their highly conserved DNA-binding domains (DBD) and structurally conserved ligand binding domains (LBD) ([12]) (Figure 1-2, Figure 1-7).

Activation of Gene Expression by Thyroid Hormone

Like nearly all NRs, TRs contain a DNA binding domain that recognizes and interacts with short, repeated sequences of DNA found in thyroid hormone-responsive genes, termed the thyroid hormone response elements (TREs). TR can bind to this half-site, AGGTCA, as a monomer, homodimer, or heterodimer with the retinoid X receptor (RXR) [13]. However, receptor activation from the heterodimer complex is generally believed to be favored as RXR enhances the DNA-binding affinity of TR. Structurally it has been shown that the TR/RXR heterodimer binds to a classical DR4 TRE, in which two half-sites are directly repeated with a spacing of 4 base pairs [14].

In the absence of thyroid hormone, TR/RXR heterodimer associates with corepressor proteins at the TRE, such as nuclear receptor corepressor (N-CoR) and silencing mediator of retinoid and thyroid receptors (SMRT) [15]. These corepressor proteins interact with the C-terminal domain of TR and RXR and recruit large multiprotein complexes containing histone deacetylase activity (HDAC) that maintain the chromatin in a compact state repressing gene

activation. Upon binding of thyroid hormone, TR undergoes a conformational change, releasing corepressor

Ligands:	<u>Endocrine Receptors</u> High-affinity, hormonal lipids	<u>Adopted Orphan Receptors</u> Low-affinity, dietary lipids	<u>Orphan Receptors</u> Unknown
	<div style="background-color: #4a86e8; color: white; padding: 5px;"> ER α, β PR AR GR MR </div> <div style="background-color: #e91e63; color: white; padding: 5px;"> RAR α, β, γ TR α, β VDR EcR </div>	<div style="background-color: #ffff00; padding: 5px;"> RXR α, β, γ PPAR α, β, γ LXR α, β FXR PXR/SXR CAR </div>	<div style="background-color: #ff4500; color: white; padding: 5px;"> SF-1 LRH-1 DAX-1 SHP TLX PNR NGFI-B α, β, γ ROR α, β, γ ERR α, β, γ RVR α, β, γ GCNF TR 2,4 HNF-4 COUP-TF α, β, γ </div>

FIGURE 1-3. Nuclear Receptor Superfamily

Nuclear receptors (NR) are a family of transcription factors. They include the endocrine receptors such as the estrogen (ER), androgen (AR) and thyroid receptors (TR). This class of NR activates transcription upon binding high affinity hormonal lipids. The NR boxed in blue, typically form homodimers upon binding to specific DNA response elements, whereas the NR boxed in pink usually form heterodimers with the retinoid X receptor (RXR). The next class of NRs, boxed in yellow, is termed adopted orphan receptors as it has been shown that these receptors are capable of binding an array of low affinity dietary lipids. The final class of NRs, boxed in orange, is termed orphan receptors, e.g. steroidogenic factor 1 (SF-1) and liver receptor homolog 1 (LRH-1). These are receptors for which no physiological ligand has been identified as of yet and it is unclear rather these NR require a ligand for transactivation [16].

UCSF LIBRARY

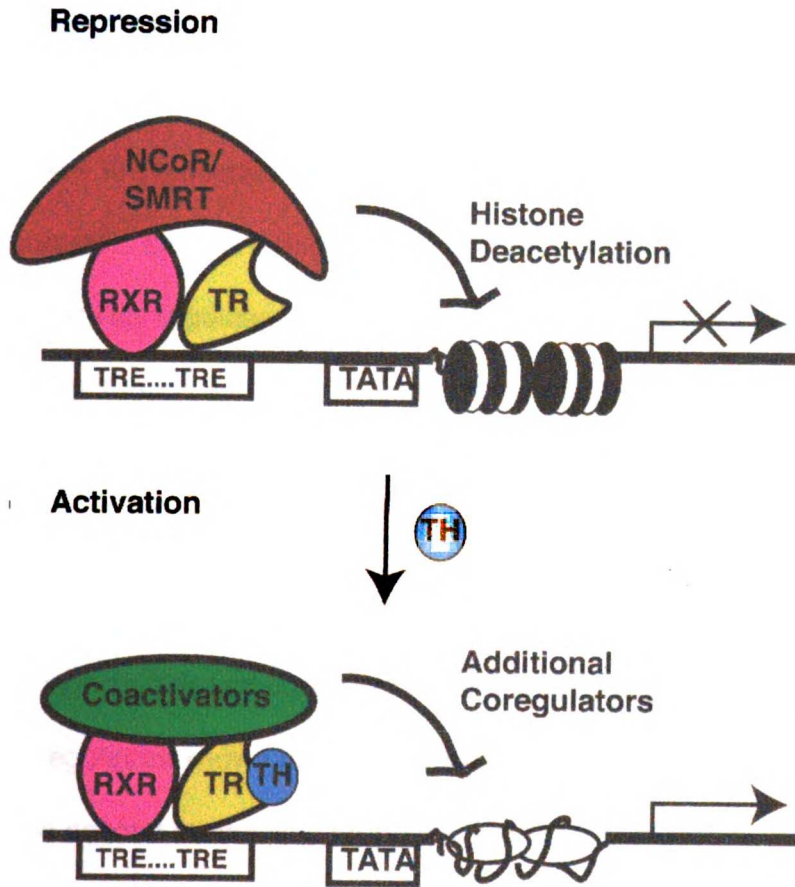


FIGURE 1-4. A Simple Model of TR Activation

Thyroid hormone acts as a switch between activation and repression of thyroid hormone (TH) responsive genes. In the absence of TH, TR/RXR heterodimer is associated with corepressor proteins, which maintain the chromatin in a repressed state. Upon binding of TH, the heterodimer undergoes a conformational change releasing corepressors and allowing for the interaction of coactivator proteins

required for gene transcription.

proteins and allowing for the interaction with coactivator proteins that enhance TRE driven gene transcription (Figure 1-4).

Down Regulation of Gene Expression by Thyroid Hormone

Studies utilizing cDNA microarrays have revealed that thyroid hormone can both positively and negatively regulate genes [17]. The mechanism for thyroid hormone-dependent negative regulation of genes has yet to be fully elucidated. There are several models that have been proposed (Figure 1-5). The first model suggests that TR can directly interact with a "negative" TRE (nTRE) in a negatively regulated gene (Figure 1-5A). Recent work has identified a nTRE in TSH β subunit and thyroid hormone dependent HDAC activity was observed at this nTRE [18]. The precise mechanism for the down-regulation of genes by nTRE remains unclear though. One possible mechanism is that the nTRE confers structural determinants altering the coregulator binding pocket to recognize different coregulators such as corepressors, NCoR/SMRT, or coregulators known to repress transcription such as RIP140, SHP, and DAX1. The second model also proposes that TR is recruited to a negatively regulated gene, but in this case the TR does not directly interact with the DNA but instead recognizes DNA binding proteins such as jun and fos at AP-1 sites. Structural determinants arising from protein-protein interactions might then alter the coregulator binding pocket [19] (Figure 1-5B). The final model has been termed the "squelching model" [20] [21], This model suggests that the TR/RXR complex selectively recruits corepressors or coactivators away from NRs or transcriptional factors that regulate the expression of thyroid responsive genes (Figure 1-5C).

NOV 1 2004

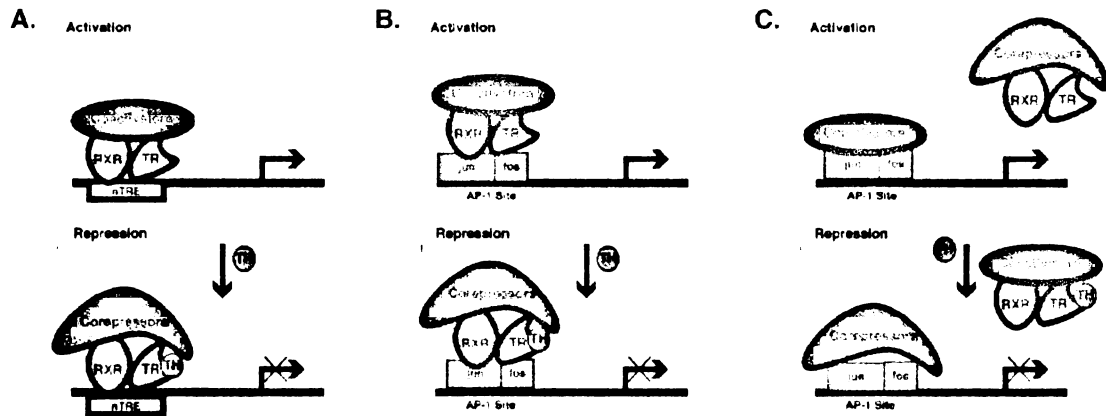


FIGURE 1-5. Models for Negative Regulation of Thyroid Hormone Gene Expression

A. TR/RXR complex binds to a nTRE resulting in a conformational change such that thyroid hormone bound state now recognizes corepressor. B. TR/RXR complex interacts with other transcriptional factors. The resulting protein-protein interactions convey differential structural determinants allowing the thyroid hormone bound state to interact with corepressor. C. Thyroid hormone complexed to TR/RXR recruits coactivators away from other transcriptional factors such as jun and fos at AP-1 sites [21].

Coregulators

The regulation of gene expression by NR involves interaction with a complex network of coregulator proteins. Structural, biochemical, and genetic studies have provided a considerable amount of information about NR-coregulator interactions. The best-studied coregulators belong to the p160 protein family of steroid receptor coactivators (SRC) [22]. Members of this family include SRC1, SRC2 (GRIP1/TIF2), and SRC3 (AIB1/TRAM1/RAC3/ACTR). These proteins contain several functional domains including the nuclear receptor interaction domain (NID) and activation domains that interact with other coregulatory proteins such as pCAF, CBP/p300 and CARM-1 (Figure 1-6). In addition, it has

been shown that SRCs contain a histone acetyltransferase activity (HAT) domain. Other domains such as the basic helix loop helix (bHLH), PasA/B, and glutamine rich domains are believed to serve as DNA-binding or protein-protein interaction surfaces. Within the NID, there are three repeated motifs with the consensus sequence LXXLL, often termed the NR box. In addition there is a unique fourth LXXLL motif found in the extreme carboxy-terminus of an alternatively spliced variant of SRC1, SRC1-a.

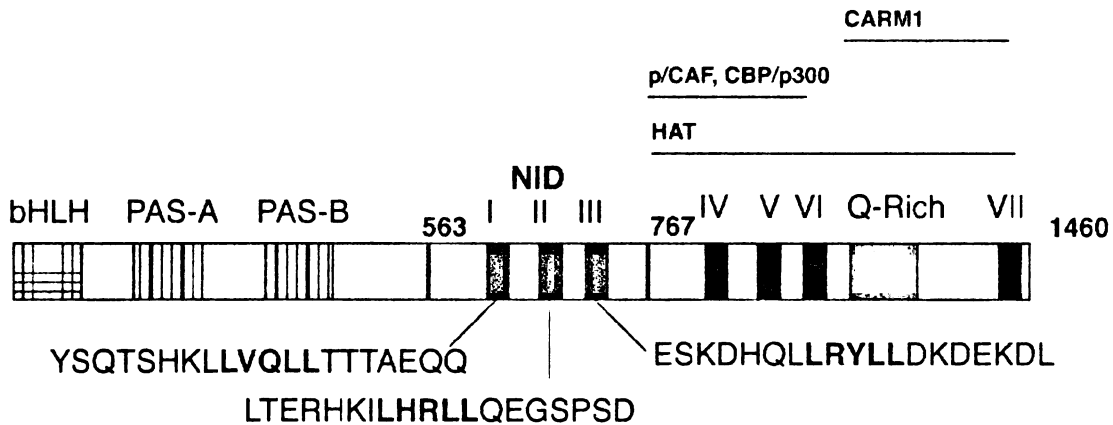


FIGURE 1-6. SRC Family Primary Structure

A block diagram of SRC identifying some of the functional domains is displayed. The amino terminus contains highly conserved basic helix loop helix (bHLH) and Pas A/B domains. These domains are believed to function as DNA-binding domains or protein-protein interaction surfaces for other transcription factors. The central nuclear interaction domain (NID) contains three nuclear receptor interaction motifs, LXXLL (NR boxes), that are known to interact with NR (SRC1-1, SRC1-2, SRC1-3). In addition, SRC1 has two isoforms, SRC1a and SRC1e. SRC1-a has an additional NR box at the carboxy terminus designated SRC1-7 that has been shown to interact with some NR. There is a glutamine rich domain located in the carboxy terminus that is also believed to serve as a protein-protein interaction surface. Interaction surfaces for other coregulators such as p/CAF, CBP/p300 and CARM1 are indicated as well as the histone acetyltransferase activity domain (HAT) [22].

Several investigations have shown that the LXXLL motif is necessary and sufficient for interaction with NR [23, 24]. Work in the Yamamoto lab has demonstrated that peptides from the SRC2 family which contain an LXXLL motif bind to TR with comparable affinities to full-length SRC2 protein [24]. Structural characterization of this interaction revealed that the LXXLL motif of SRC2-2 binds to a hydrophobic groove in the ligand binding domain of TR β (TR β -LBD) as an α -helix (Figure 1-7) [25]. Like most NR, TR β -LBD is comprised of 12 α -helical bundles and 4 β -strands arranged in three layers. Ligand binding to NR allosterically modulates the conformation of the NR-LBD to form protein-protein interaction surfaces for coregulators, either coactivators or corepressor, depending on the nature of the ligand. In the case of an agonist ligand, thyroid hormone, helix 12 rearranges to form a hydrophobic cleft consisting of helices 3,4,5, and 12 allowing for interactions with coactivators such as SRC2. The leucine side chains of the LXXLL motif interact with the hydrophobic pocket of TR β -LBD. In addition a charge clamp is formed between the SRC2-2 backbone with a glutamic acid and lysine of TR β -LBD, holding the coregulator peptide in place. Conversely an antagonist ligand causes helix 12 to rearrange concealing the hydrophobic pocket or altering it such that corepressor motifs, IXXLXXII, are instead recognized. It has been postulated that in the absence of ligand, helix 12 fluctuates between the two states and it appears that different ligands can shift this equilibrium [26].

In addition to the p160 family, there are many other coregulators available for interaction with NR including CREB binding protein (CBP)/p300 [27], [28], thyroid receptor activating protein (TRAP)/ vitamin D receptor interacting protein (DRIPs)/peroxisome proliferating activated receptor binding protein (PBP) [29], [30] androgen receptor activator 70/55 (ARA70/55) [31], [32] receptor interacting protein 140 (RIP140) [33], PPAR γ coactivator 1 (PGC-1) [34], thyroid receptor binding protein (TRBP)/PPAR interacting protein (PRIP) [35], [36], DAX-1 [37], and small heterodimer partner (SHP) [38] (Table 1-1). The interaction of these coregulators with nuclear receptors is also mediated by LXXLL motifs. An extended helical motif, IXXLXXII, has been identified in corepressors such as nuclear receptor corepressor (NCoR) and silencing mediator of retinoic acid (SMRT).

NR-Coregulator Specificity

There is a large pool of coregulators available for interaction with TR. Although there appears to be some functional redundancy within the SRCs, there is also evidence that SRCs have distinct biological regulatory roles. While mice deficient in SRC1 exhibit resistance to thyroid hormone (RTH), the phenotypes for mice deficient in SRC2 and SRC3 are distinct with no evidence of RTH [39], [40], [41]. These studies, along with recent work with the progesterone and glucocorticoid receptors, have demonstrated that interaction with specific coregulators can elicit specific biological responses [42]. However, it remains

unclear how NRs discriminate between different coregulators. In this study we sought to define rules that govern TR-coregulator selectivity.

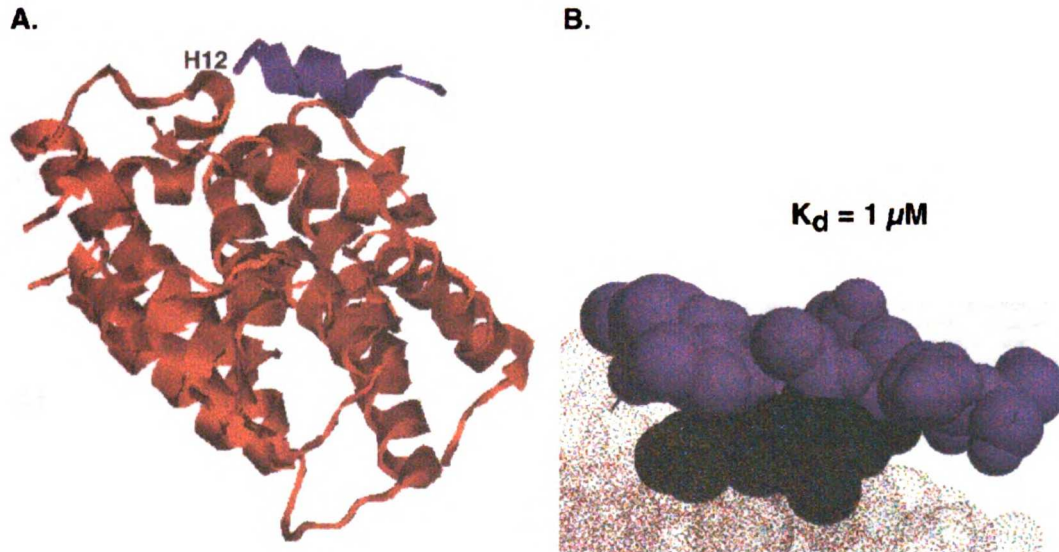


FIGURE 1-7. Structural Features of the Thyroid Hormone -SRC2-2 Interaction

A. Ribbon diagram of the ligand binding domain of TR (TR-LBD) complexed with the SRC2-2 coregulator peptide. TR-LBD is comprised of 12 alpha helical bundles. Upon binding of thyroid hormone, helix 12 (labeled) rearranges to form the coregulator binding pocket. TR-LBD is shown in orange, SRC2-2 peptide is shown in purple. B. A close view of the coregulator binding pocket. The LXXLL backbone is shown in purple with the leucine side-chains in green fitting tightly into the TR-LBD coregulator binding pocket (orange). Binding to TR-LBD induces α -helical formation of the coregulator peptide with a K_d close to $1 \mu\text{M}$ [24].

Combinatorial peptide libraries have been used to define NR-coregulator specificity, and have revealed that the sequences immediately flanking the NR box are critical for specificity [43], [44]. However the peptides in these studies were generated from random libraries that do not represent the true NR box sequences. Other investigations focused on defining SRC NR box selectivity using a subset of coregulator NR boxes from the SRCs. This work has shown

TABLE 1-1. List of Coregulators

Coregulator	Other Common Names	NCBI Protein Accession Number	Number of LXXLL Motifs	Other Information
SRC1	NCoA-1	AAC50305	4	Intrinsic HAT activity Targeted gene disruption resulted in decreased growth and development, resistance to thyroid hormone, increased expression of SRC2
SRC2	NCoA-2/GRIP1/TIF2	Q15596	3	Intrinsic HAT activity 40% sequence homology to SRC1
SRC3	NCoA-3 /AIB1/TRAM1/RAC3/A CTR	Q9Y6Q9	3	Intrinsic HAT activity 33% identity with SRC1, 45% identity with SRC2 Targeted gene disruption resulted in dwarfism, delayed puberty, reduced female reproductive function, and blunted mammary gland development
PGC-1		AAF19083	1	Tissue-specific expression and is inducible by various stimuli such as exposure to cold temperatures and exercise
TRAP220	PBP/DRIP205	Q15648	2	Involved in the regulation of adaptive thermogenesis and hepatic gluconeogenesis General Coactivator Targeted gene disruption is embryonic lethal
TRBP	PRIP	Q14686	2	No intrinsic HAT activity Targeted gene disruption resulted in similar results to PBP
TRAP100		Q75448	7	Component of TRAP Complex Targeted gene disruption resulted in cell viability
ARA70		Q13772	1	No intrinsic HAT activity Interacts with p/CAF
ARA55		NP_057011	1	
p300		Q92831	1	Intrinsic HAT activity Helps recruit RNA Pol II holoenzyme to the promoter
RIP140		P48552	9	Generally down-regulates receptor activity
NCoR		AA032941	3	Suppresses gene expression
SMRT		Q9Y618	2	Suppresses gene expression
DAX1		P51843	3	Orphan NR lacking DBD Generally down-regulates receptor
SHP		Q15466	1	Orphan NR lacking DBD Generally down-regulates receptor activity

that ligands can allosterically modulate the coregulator binding pocket and therefore differentially alter specific SRC recruitment and NR box usage [45], [46], [47]. However, to date there has been no comprehensive study of the interactions of TR and natural coregulator NR boxes. To address this issue, we

designed an in vitro binding assay to measure the equilibrium binding of TR β to a library of potential coregulators in a high-throughput manner using fluorescence polarization. With this method, binding constants for TR β to coregulator NR boxes were determined in a consistent format, including NR boxes from SRCs and 9 other known coregulators. In addition the TR β -coregulator binding patterns for three different ligands including the thyroid hormone T3, the synthetic TR β -selective agonist GC-1, and the T3 antagonist NH-3 were defined. This quantitative information can be used to establish rules for TR β coregulator selectivity and these rules can be used for predicting biological responses. We also demonstrate that this is a general method that can be used with other NR to answer mechanistic questions about NR transcriptional regulation.

CHAPTER 2

Synthesis of a Fluorescent NCOA Peptide Library

Jamie M. R. Moore, Sarah J. Galicia, Andrea C. McReynolds, Ngoc-Ha Nguyen, Thomas S. Scanlan, and R. Kiplin Guy, Quantitative proteomics of the thyroid hormone receptor coregulator interactions, *Journal of Biological Chemistry* 2004 Jun 25; 279(26): 27584-90.

Copyright © 2004 by the American Society for Biochemistry and Molecular Biology

INTRODUCTION

The interaction of nuclear receptors (NR) with coregulators is an important signaling step that potentiates biological responses. However, it remains unclear how NRs discriminate between different coregulators. In this study we sought to define rules that govern NR-coregulator selectivity. To that end, we designed an in vitro binding assay to measure the equilibrium binding of NR to a library of potential coregulators in a high-throughput manner using fluorescence polarization (Figure 2-1).

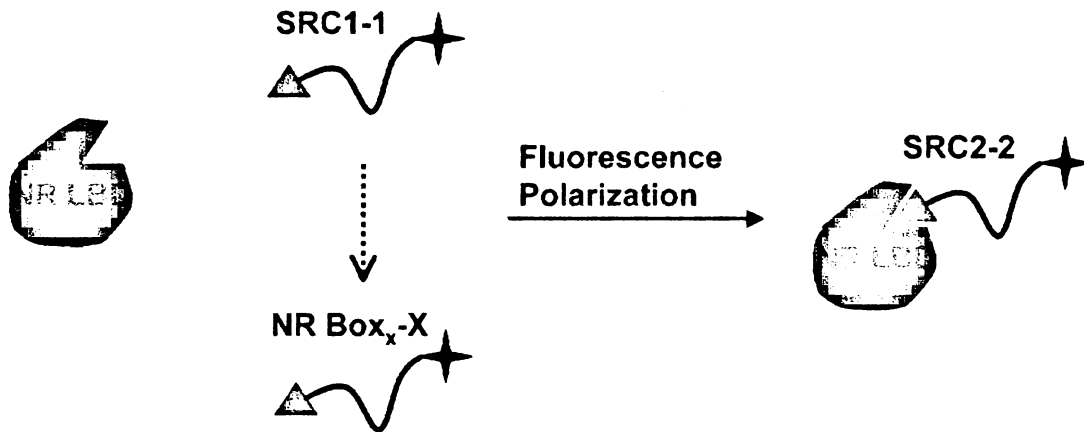


FIGURE 2-1. Mapping Nuclear Receptor-Coregulator Interactions Utilizing Fluorescence Polarization

Fluorescence polarization can be used to quantitatively determine the binding affinity of nuclear receptors to a library of known coregulator peptides that contain a fluorescent tag.

The first step in designing our high-throughput assay was the assembly of a library of known coregulator peptides. We identified several crucial requirements for this library. First of all we wanted to include sequences from known coregulator proteins. We abstracted NR box sequences from the following

coregulator proteins: SRC family (SRC1, SRC2, SRC3), CREB binding protein (CBP)/p300 [27], [28], thyroid receptor activating protein (TRAP)/ vitamin D receptor interacting protein (DRIPs)/peroxisome proliferating activated receptor binding protein (PBP) [29], [30] androgen receptor activator 70/55 (ARA70/55) [31], [32] receptor interacting protein 140 (RIP140) [33], PPAR γ coactivator 1 (PGC-1) [34], thyroid receptor binding protein (TRBP)/PPAR interacting protein (PRIP) [35], [36], DAX-1[37], and small heterodimer partner (SHP) [38]. In addition, to capture specificity determinants, peptides of 20 amino acid length were chosen and therefore consisted of the LXXLL motif plus 7-8 flanking residues (Figure 2-2). Previous screens with coactivator peptides established amino acid residues at +6 to +12 as critical for binding [47], [48]. Negative controls were also constructed by replacing L+4 and L+5 with alanine (LXXAA), as this substitution has been shown to abolish interactions with NR [47]. The coregulator peptides also required a fluorescence tag. Finally, to accurately and consistently measure binding constants these coregulator peptides needed to be individually synthesized at moderate yields (1-10mg) and high quality (>80% pure).

The use of solid-phase chemistry fluorenylmethyloxycarbonyl (Fmoc) was chosen to synthesize our library of coregulator peptides. The first free dipeptide was synthesized in 1901 by Emil Fisher [49], however it was not until the 1950s that bioactive peptides were synthesized [50]. These methods were labor

intensive, racemization occurred frequently, and overall yields were low. To overcome these problems, Merrifield introduced solid-phase peptide synthesis [51], [52] [53], [54]. Polymer chemistry has continued to grow and improve and still remains the method of choice for peptide synthesis today. The application of Fmoc protection to solid-phase synthesis was introduced in the 1970s [55], [56]. This approach is operationally simple and the chemistry is less complex in comparison to other methods. Standard Fmoc protocols are now available and are widely used for the synthesis of parallel peptide libraries [57].

There is now a wide range of high-throughput equipment available for Fmoc synthesis of solid-phase peptides from the nanogram to gram scale including systems that are completely automated. Despite the fact that peptide chemistry has been around for decades and there is now accessible high-throughput equipment, there is very little literature available on the generation of parallel peptide libraries. Most industrial laboratories use sophisticated automated systems that are cost prohibitive for an academic setting. The libraries generated in academia tend to be combinatorial libraries, libraries comprised of 3-4mers, or small scale libraries [58]. Therefore, there were several challenges we had to overcome to assemble our library of 94 coregulator peptides including obtaining milligram quantities of pure peptides and synthesizing hydrophobic peptides consisting of 20 amino acids. Described here are some of the

challenges we faced in generating the coregulator peptide library and the steps we took to overcome them.

RESULTS AND DISCUSSION

TABLE 2-1. Nuclear Receptor Coregulator (NCOA) Fluorescent Peptide Library

Sequence alignment of the coregulator fluorescent peptides synthesized, including the gene accession number to signify where these sequences were obtained. The coregulator peptides are listed in the far left column, where SRC1-1, SRC1-2, SRC1-3 represents the first, second and third NR boxes in SRC1, respectively. This nomenclature, first proposed by O'Malley, is applied to all of the coregulator peptides studied in this research project[39]. The conserved NR box, LXXLL, is enclosed in a box. Negative control peptides were also synthesized with leucine +4 and +5 replaced with alanines (LXXAA).

NCBI Protein Accession Number	PEPTIDE	-8	-7	-6	-5	-4	-3	-2	-1	L	X	X	L/A	L/A	6	7	8	9	10	11	12
										1	2	3	4	5							
AAC80305	SRC1-1	C	Y	S	Q	T	S	H	K	I	L	V	Q	L	L	T	T	A	E	Q	Q
	SRC1-2	C	L	T	A	R	H	K	Q	L	L	H	R	Y	L	L	E	G	S	P	D
	SRC1-3	C	E	S	K	D	H	Q	S	L	L	R	Y	A	A	D	D	E	K	D	L
Q15596	SRC1-7	C	Q	A	Q	Q	K	Q	L	L	L	Q	Q	A	A	T	T	E			
	SRC2-1	C	D	S	K	G	Q	T	K	I	L	L	Q	A	A	T	T	K	S	D	Q
	SRC2-2	C	L	K	E	K	H	K	L	L	L	H	R	Y	A	A	D	D	S	S	P
Q9Y909	SRC2-3	C	K	K	K	E	N	A	K	L	L	R	Y	A	A	D	D	S	S	T	K
	SRC3-1	C	E	S	K	G	H	K	K	I	L	L	Q	A	A	T	T	C	S	D	D
	SRC3-2	C	L	Q	E	K	H	R	A	L	L	H	Y	A	A	D	D	N	G	D	P
AAF19083	SRC3-3	C	K	K	E	N	N	A	L	L	L	R	Y	A	A	D	D	N	D	P	S
	mPGC-1	C	E	A	E	E	P	S	L	L	L	K	K	A	A	D	D	A	P	A	N
	PBP-1	C	K	V	S	Q	N	P	P	L	L	T	S	A	A	D	D	I	T	G	N
Q15448	PBP-2	C	N	T	K	N	H	P	M	L	L	M	N	A	A	D	D	N	P	A	Q
	PRIP-1	C	V	T	L	T	S	P	L	L	L	V	S	A	A	D	D	I	S	A	A
	PRIP-2	C	M	R	E	A	P	T	S	A	L	L	S	Q	A	A	D	D	N	S	G
Q75448	TRAP100-1	C	R	A	L	L	S	A	L	L	L	H	W	A	A	D	D	C	T	A	A
	TRAP100-2	C	A	F	E	F	L	K	S	L	L	T	P	L	L	D	D	K	A	A	D
	TRAP100-3	C	H	M	L	S	G	K	S	L	L	D	L	A	A	A	A	A	A	A	A
	TRAP100-4	C	D	S	T	K	V	E	S	L	L	V	A	A	A	A	N	N	S	S	E
	TRAP100-5	C	L	V	L	L	G	H	I	L	L	P	G	A	A	A	D	D	S	S	K
	TRAP100-6	C	D	D	V	Q	P	S	K	Q	L	L	M	R	A	A	S	S	N	E	N
Q13772	ARA70	C	L	Q	Q	Q	A	Q	Q	L	L	Y	S	A	A	G	Q	E	F	L	N
	NP_057011	C	L	G	T	G	L	C	Q	E	L	D	R	L	L	Q	R	E	S	L	N
	Q82831	C	A	A	S	K	H	L	K	Y	L	S	E	A	A	M	S	G	S	A	P
P48552	RIP140-1	C	D	S	I	V	L	T	Y	L	L	E	G	A	A	R	H	Q	A	S	G
	RIP140-2	C	G	K	Q	D	S	T	L	L	L	A	S	A	A	A	Q	S	F	S	V
	RIP140-3	C	Y	G	V	A	S	S	L	H	L	K	T	A	A	A	K	K	S	K	V
AA032941	RIP140-4	C	P	S	V	A	C	S	Q	L	L	A	L	A	A	S	S	S	E	A	H
	RIP140-5	C	Q	A	A	N	N	S	L	L	L	L	H	A	A	A	K	S	Q	T	I
	RIP140-6	C	S	H	Q	K	V	T	L	L	L	Q	L	A	A	G	H	K	N	E	N
	RIP140-7	C	L	L	E	R	R	T	V	L	L	Q	L	A	A	G	N	P	N	K	G
	RIP140-8	C	S	F	S	K	N	G	V	L	L	S	R	A	A	R	Q	N	Q	C	S
	RIP140-9	C	E	S	K	S	F	N	V	V	L	L	K	Q	A	A	L	S	E	N	D
	NCOR-1	C	D	P	A	S	N	L	G	H	L	E	D	A	A	A	R	Q	A	L	M
	NCOR-2	C	L	I	T	L	A	D	F	I	L	C	Q	A	A	A	T	K	D	F	A
	NCOR-3	C	T	I	T	A	A	N	F	I	L	I	D	V	A	A	R	Q	Q	I	L
Q8Y618	SMRT-1	C	H	A	S	T	A	N	M	F	L	L	E	A	A	A	T	R	K	A	A
	SMRT-2	C	V	V	T	L	A	Q	H	I	L	I	S	E	A	A	A	Q	Q	A	D
	DAX1-1	C	H	Q	W	Q	G	S	I	L	L	Y	N	A	A	A	M	T	A	K	Y
P51843	DAX1-2	C	H	P	R	Q	G	S	I	L	L	Y	S	A	A	T	S	S	A	K	Q
	DAX1-3	C	H	P	R	Q	G	S	I	L	L	Y	S	A	A	T	S	S	A	K	Q
	SHP	C	A	A	S	R	P	A	I	L	L	Y	A	A	A	S	S	S	L	K	A
AAC80305	SRC1-1	C	Y	S	Q	T	S	H	K	I	L	V	Q	A	A	T	T	A	E	Q	Q
	SRC1-2	C	L	T	A	R	H	K	Q	L	L	H	R	Y	A	A	E	G	S	P	D
	SRC1-3	C	E	S	K	D	H	Q	S	L	L	R	Y	A	A	D	D	E	K	D	L
Q15596	SRC1-7	C	Q	A	Q	Q	K	Q	L	L	L	Q	Q	A	A	T	T	E			
	SRC2-1	C	D	S	K	G	Q	T	K	I	L	L	Q	A	A	T	T	K	S	D	Q
	SRC2-2	C	L	K	E	K	H	K	L	L	L	H	R	Y	A	A	D	D	S	S	P
Q9Y909	SRC2-3	C	K	K	K	E	N	A	K	L	L	R	Y	A	A	D	D	C	D	S	T
	SRC3-1	C	E	S	K	G	H	K	K	I	L	L	Q	A	A	T	T	C	S	S	D
	SRC3-2	C	L	Q	E	K	H	R	A	L	L	H	Y	A	A	D	D	N	G	D	P
AAF19083	SRC3-3	C	K	K	E	N	N	A	L	L	L	R	Y	A	A	D	D	N	D	P	S
	mPGC-1	C	E	A	E	E	P	S	L	L	L	K	K	A	A	D	D	A	P	A	N
	PBP-1	C	K	V	S	Q	N	P	P	L	L	T	S	A	A	D	D	I	T	G	N
Q15448	PBP-2	C	N	T	K	N	H	P	M	L	L	M	N	A	A	D	D	N	P	A	Q
	PRIP-1	C	V	T	L	T	S	P	L	L	L	V	S	A	A	D	D	I	S	A	A
	PRIP-2	C	M	R	E	A	P	T	S	A	L	L	S	Q	A	A	D	D	N	S	G
Q75448	TRAP100-1	C	R	A	L	L	S	A	L	L	L	H	W	A	A	D	D	C	T	A	A
	TRAP100-2	C	A	F	E	F	L	K	S	L	L	T	P	L	L	D	D	K	A	A	D
	TRAP100-3	C	H	M	L	S	G	K	S	L	L	D	L	A	A	A	A	A	A	A	A
	TRAP100-4	C	D	S	T	K	V	E	S	L	L	V	A	A	A	A	N	N	S	S	E
	TRAP100-5	C	L	V	L	L	G	H	I	L	L	P	G	A	A	A	D	D	S	S	K
	TRAP100-6	C	D	D	V	Q	P	S	K	Q	L	L	M	R	A	A	S	S	N	E	N
Q13772	ARA70	C	L	Q	Q	Q	A	Q	Q	L	L	Y	S	A	A	G	Q	E	F	L	N
	NP_057011	C	L	G	T	G	L	C	Q	E	L	D	R	L	L	Q	R	E	S	L	N
	Q82831	C	A	A	S	K	H	L	K	Y	L	S	E	A	A	M	S	G	S	A	P
P48552	RIP140-1	C	D	S	I	V	L	T	Y	L	L	E	G	A	A	R	H	Q	A	S	G
	RIP140-2	C	G	K	Q	D	S	T	L	L	L	A	S	A	A	A	Q	S	F	S	V
	RIP140-3	C	Y	G	V	A	S	S	L	H	L	K	T	A	A	A	K	K	S	K	V
AA032941	RIP140-4	C	P	S	V	A	C	S	Q	L	L	A	L	A	A	S	S	S	E	A	H
	RIP140-5	C	Q	A	A	N	N	S	L	L	L	L	H	A	A	A	K	S	Q	T	I
	RIP140-6	C	S	H	Q	K	V	T	L	L	L	Q	L	A	A	G	H	K	N	E	N
	RIP140-7	C	L	L	E	R	R	T	V	L	L	Q	L	A	A	G	N	P	N	K	G
	RIP140-8	C	S	F	S	K	N	G	V	L	L	S	R	A	A	R	Q	N	Q	C	S
	RIP140-9	C	E	S	K	S	F	N	V	V	L	L	K	Q	A	A	L	S	E	N	D
	NCOR-1	C	D	P	A	S	N	L	G	H	L	E	D	A	A	A	R	Q	A	L	M
	NCOR-2	C	L	I	T	L	A	D	F	I	L	C	Q	A	A	A	T	K	D	F	A
	NCOR-3	C	T	I	T	A	A	N	F	I	L	I	D	V	A	A	R	Q	Q	I	L
Q8Y618	SMRT-1	C	H	A	S	T	A	N	M	F	L	L	E	A	A	A	T	R	K	A	A
	SMRT-2	C	V	V	T	L	A	Q	H	I	L	I	S	E	A	A	A	Q	Q	A	D
	DAX1-1	C	H	Q	W	Q	G	S	I	L	L	Y	N	A	A	A	M	T	A	K	Y
P51843	DAX1-2	C	H	P	R	Q	G	S	I	L	L	Y	S	A	A	T	S	S	A	K	Q
	DAX1-3	C	H	P	R	Q	G	S	I	L	L	Y	S	A	A	T	S	S	A	K	Q
	SHP	C	A	A	S	R	P	A	I	L	L	Y	A	A	A	S	S	S	L	K	A

A 94-member fluorescent coactivator peptide library was synthesized utilizing standard Fmoc chemistry (Table 2-1). Of the 94 compounds synthesized, 69 were successfully recovered, purified, and labeled. However, it took 7 library synthesis attempts (JR1-JR7) to obtain these 69 fluorescent peptides. Some of these libraries were unsuccessful due to analyst error (JR 3), others due to instrument error (JR6), but with the majority of the libraries (JR1, JR2, JR4, JR6, and JR7) we lacked the instrumentation and expertise. Each library was a learning process that allowed us to develop in the end a successful synthesis protocol (Appendix A). A summary of each library is listed in Table 2-2. In general the synthesis proceeded smoothly for the addition of the first 8 amino

TABLE 2-2. Summary of NCOA Peptide Libraries Synthesized

The seven libraries that were synthesized (JR1-JR7) are listed including the composition of the library and the final results. In addition, problems associated with each library are described.

LIBRARY	PEPTIDES	RESULTS	PROBLEMS/OBSERVATIONS
JR1	SRC2 Specificity Library	Unsuccessful	Labeled on-bead, mostly unlabeled recovered, single peptide purification
JR2	SRC Family Peptides	Unsuccessful	Labeled on-bead, mostly unlabeled recovered, single peptide purification
JR3	SRC Family Peptides	Unsuccessful	Technical Error
JR4	NCOA Peptide Library	Partial Recovery	Optimization of labeling conditions
JR5	NCOA Peptide Library	Partial Recovery	Optimization of cleaving time and conditions, delay due to back-ordered columns, excess TFA exposure
JR6	NCOA Peptide Library	Unsuccessful	Genvac Failure
JR7	NCOA Peptide Library	Successful	Successfully applied new protocol

acids. However, after introduction of leucines in the NR box, the coupling became sluggish and complete coupling was difficult to achieve. The steps following synthesis which include cleavage and side-chain deprotection, post-cleavage work-up, purification, and fluorescent labeling all required significant optimization. For most of these steps, it was found that reduction in TFA exposure resulted in higher yields of intact peptides.

The parallel synthesis of 94 peptides was conducted in a two 48 well Robbins Reaction block. Preloaded Wang resin (Novabiochem) was dispersed into individual wells and synthesis proceeded through a series of deprotection and coupling steps (Figure 2-2). All coupling reactions were run for 2-2 1/2 hours and were monitored by the Kaiser test. Based on Kaiser test results, the first eight amino acids were added successfully with one coupling reaction. However, as the peptide grew in length, it became increasingly difficult to couple additional amino acid residues. Several reports have shown that peptide coupling becomes increasingly difficult with peptide length [59], [60]. In addition, these groups have shown that amino acids such as leucine and isoleucine are difficult to couple and acylate. To overcome these obstacles we initially performed additional coupling reactions until a negative Kaiser test was observed. This strategy proved to be unsuccessful as it was time consuming, cost prohibitive, and in many cases more than one amino acid residue was attached to the growing peptide. It was determined that by performing only two

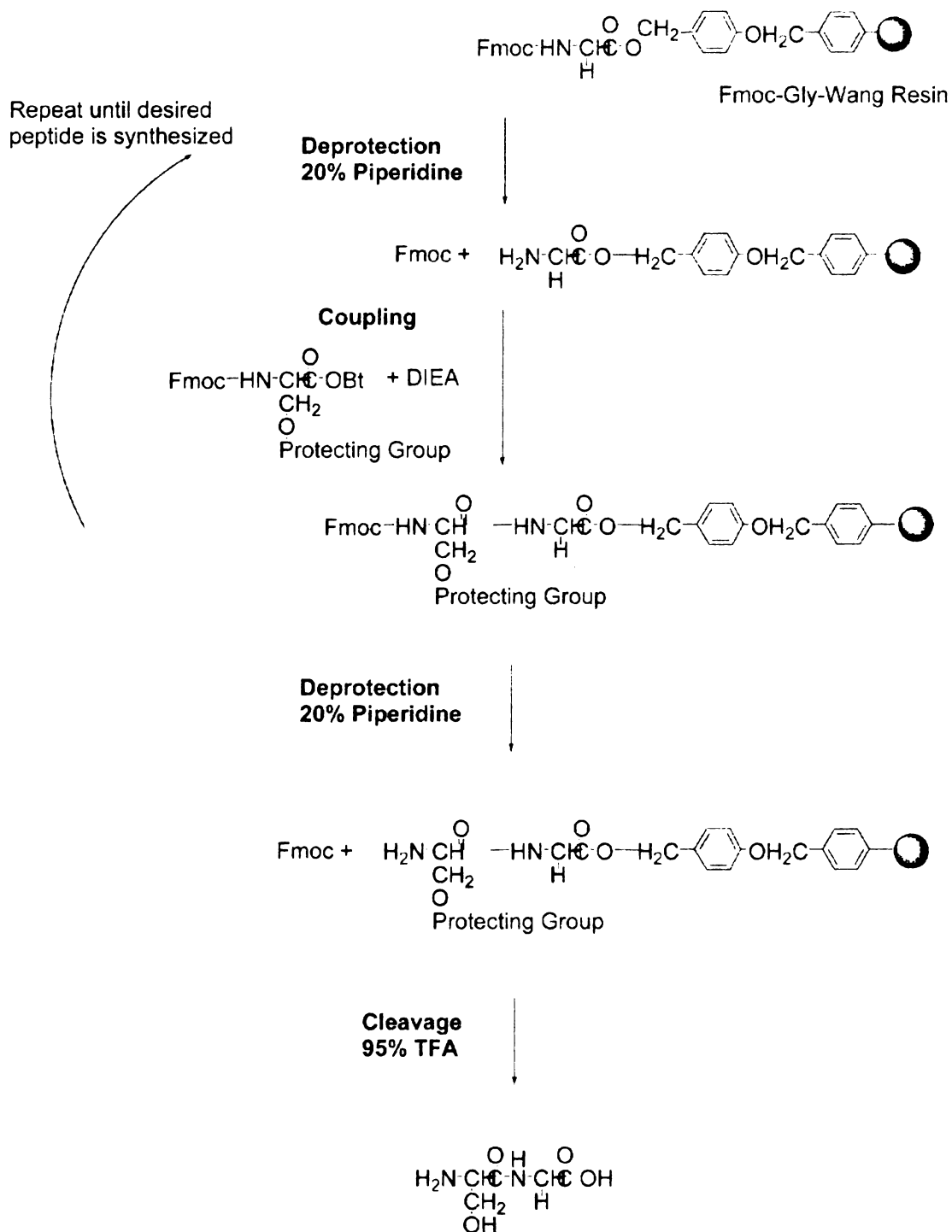


FIGURE 2-2. General Peptide Synthesis Scheme

Solid phase peptide synthesis consists of assembling amino acids from the C-terminal to the N-terminal. The α -carboxyl group is attached via an acid-labile linker to a solid support. Resins commonly used are composed of polystyrene

(P). The amino terminal end of the amino acid is protected by a base-labile Fmoc (9-fluorenylmethoxycarbonyl) protecting group while the side chains are protected by acid-labile groups such as tertiary-butyl (tBu). After the first amino acid is loaded onto the resin, the Fmoc group is removed using piperidine (Deprotection). A Kaiser test is then performed to confirm that all of the Fmoc protecting groups are removed. The next Fmoc-amino acid is then attached to the growing peptide by activation of its carboxyl group (Coupling). A Kaiser test is then performed to confirm that complete coupling has occurred on all the free amines on the resin. Synthesis then proceeds through a cycle of 1) deprotection of Fmoc amino terminus groups and 2) coupling of the next amino acid until the peptide is completely synthesized. The completely synthesized peptide is then cleaved from the resin and side chain protection groups are removed using trifluoroacetic acid and scavengers.

rounds of coupling with 3 equivalents of protected amino acid, sufficient coupling was achieved with minimum double couplings observed. The second round of coupling was only allowed to proceed for 1-1 1/2 hours. It was also determined that the addition of methylene chloride (DCM) to the coupling cocktail ameliorated the coupling process [61]. In dimethylformamide (DMF) alone it has been shown that growing peptides have a propensity to form β -sheets than can complicate the coupling step. By adding more polar solvents, the β -sheet formation is disrupted. The optimal ratio of DMF:DCM is 3:1. Once synthesis was complete, the peptides were thoroughly washed and resin was prepared for cleavage reaction by shrinking with methanol.

Optimal cleavage conditions are dependent not only on the individual amino acid residues present, but on their number, sequence, and side-chain protecting groups. Therefore, finding universal cleavage conditions for 94 peptides was

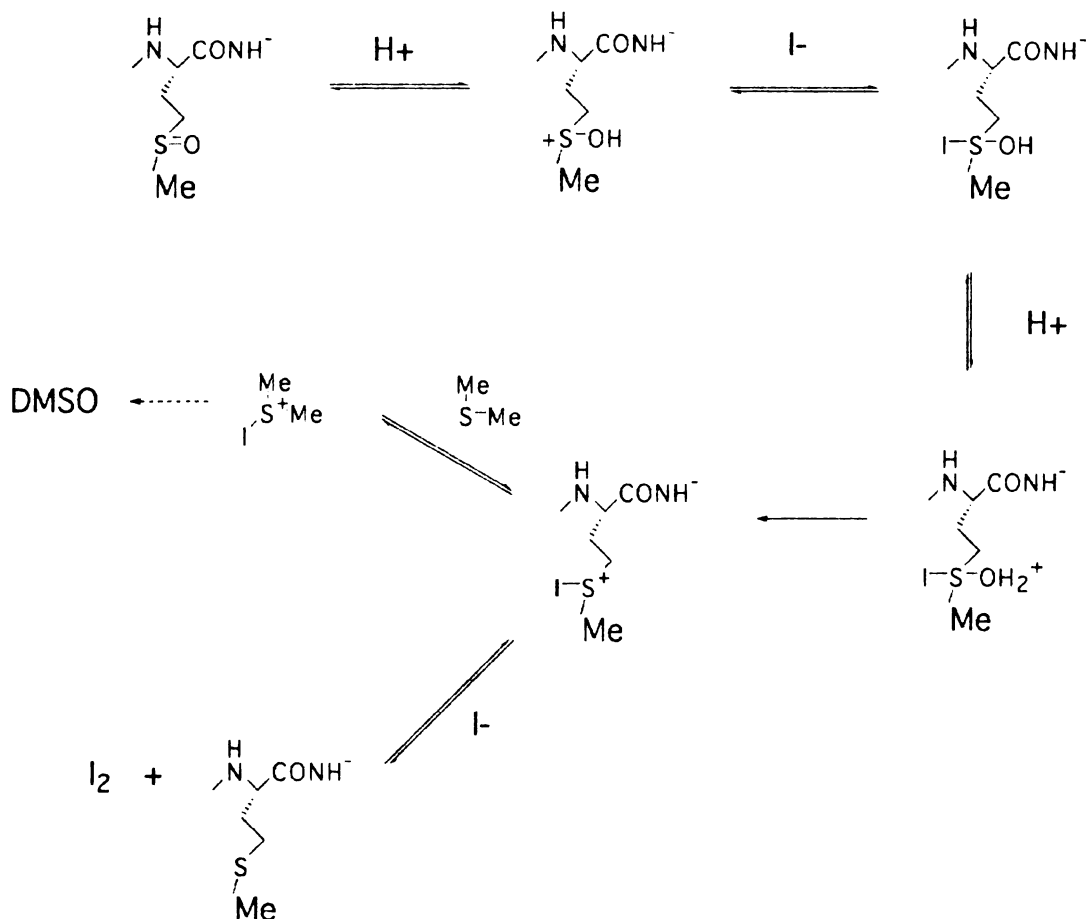


FIGURE 2-3. Proposed Mechanism for Methionine Reduction During Cleavage Using TFA, Ammonium Iodide, and Dimethylsulphide [62]

difficult. Two factors, the cleavage cocktail and time of the cleavage reaction, required adjustment. A cocktail recently reported in the literature, Reagent H, ((trifluoroacetic acid 81%, phenol 5%, thioanisole 5%, 1,2-ethanedithiol 2.5%, water 3%, dimethylsulphide 2%, ammonium iodide 1.5% w/w) was found to be effective in simultaneously cleaving and deprotecting the peptides [62]. The scavengers in this cocktail have been shown to remove difficult protecting groups, such as the trityl group found on cysteines as well as minimize acid-

catalyzed methionine oxidation (Figure 2-3). It was also determined that the cleavage reaction time was critical for the recovery of intact peptides. Initial cleavage reactions proceeded for 12-24 hours to insure complete removal of less acid-labile protecting groups. However, this long exposure to TFA was determined to be detrimental to the peptides (JR5) and efficient cleavage and deprotection could be completed in 4 hours.

Once the peptides were fully deprotected and cleaved, they were collected into 48 well titer plates and dried down immediately using a speedvac (Genevac) to remove as much TFA as possible. The dried peptides were then reconstituted using 50:50 acetonitrile:water, filtered, and HPLC purified (Biotage). Again, it was determined purification needed to occur immediately, as residual TFA in the dried samples could also cause degradation. This was discovered during the synthesis of JR5 where after we cleaved and dried the peptides we were delayed as we waited for back-ordered purification columns to arrive. The yields from JR5 were very low and in some cases intact peptides were not recovered due to degradation.

Crude peptides were purified using reversed-phase HPLC (See Appendix A for details). Early libraries such as JR1 and JR2 were purified using Waters Semi-Prep HPLC (Waters Delta 600) and pure samples were lyophilized. One peptide could be purified at a time, and therefore only 8 peptides could be purified and

identified in a single day. This was not only cumbersome and time-consuming (40 samples/week), it also proved to be detrimental to the peptide as the crude peptides were exposed to TFA for up to 3 weeks in some cases. The Biotage HPLC sped up the purification process tremendously, reducing purification of 40 samples down to one day (JR4-JR7). Using the Biotage, HPLC fractions were collected based upon peak absorption at 214 and 280 (Figure 2-4), then were dried down using a speedvac (Genevac HT-4 or Mega). Peptides were identified using either MADLI-TOF or electrospray ionization (ESI) mass spectrometry by reconstituting dried fractions in 50:50 acetonitrile:water. It was found that by limiting the exposure time to TFA, the recovery of the peptides was greatly enhanced, including any residual TFA that was not evaporated by the speedvac and the small amount of TFA (0.01%) present in the HPLC fractions. This was achieved by immediately proceeding to the purification step after cleavage and storing samples in the dried state at -80°C .

B

Plate 102301 MW 0.00 Name JR4a-A6
 Well A6 Method 219_10-100 in 12 Reg. Code JR4a_A6
 Owner Start 10/23/01 11:34:32 A End 10/23/01 11:51:47 AM

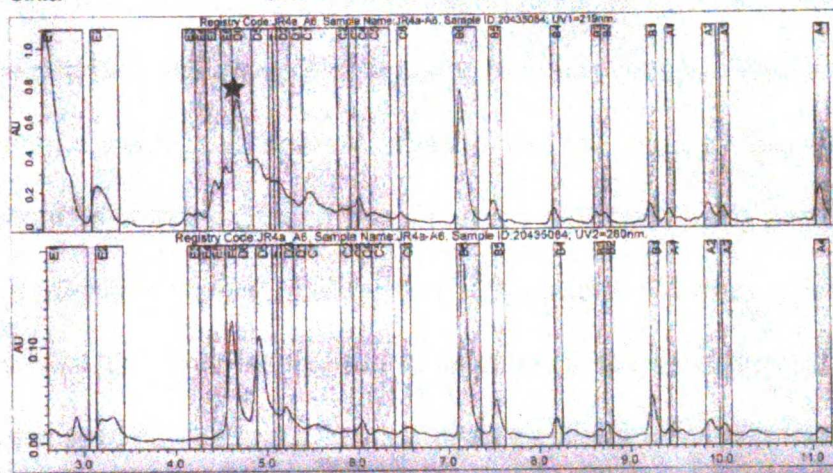


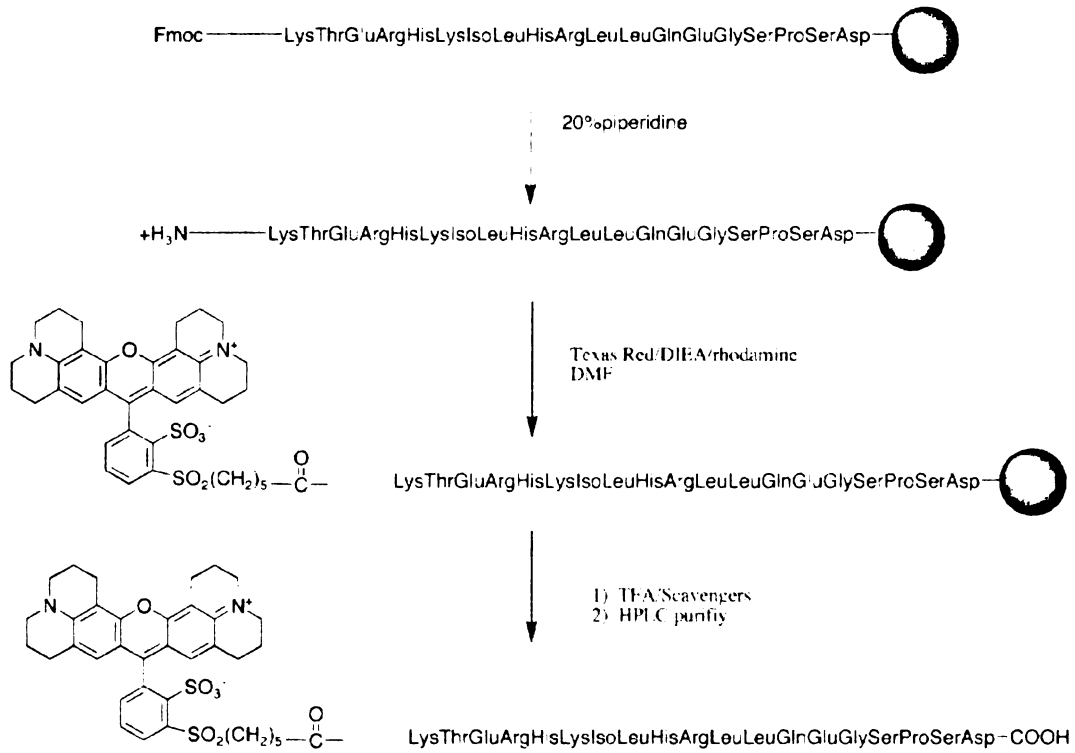
FIGURE 2-4. Purification of Crude Unlabeled Peptides

The HPLC trace of crude unlabeled SRC2-2 purified on the Biotage is shown. The star indicates the location of pure SRC2-2. The chromatogram on top was detected at 214 nm, and the bottom trace was detected at 280 nm. The other peaks represent side products, larger peptides, smaller peptides, and protecting groups.

The final step of this synthesis was to attach a fluorescent probe to all of the peptides. Three different strategies were considered (Figure 2-5). The first approach consisted of coupling a hexanoic amino acid fluorophore to the terminal amine while the peptide remained on resin. This would allow for specific labeling of the terminal amine and only one purification step would be required. Low labeling efficiency was observed with this strategy as a result of the resin absorbing significant amounts of activated fluorophore. In an attempt to overcome this problem, inactivated rhodamine was added as a blocking agent

(ref). In the presence of rhodamine, it was still found that 10-20 equivalents of activated fluorophore were required for complete labeling. Due to the cost of the hexanoic amino acid fluorophores, this strategy was abandoned (JR1-JR2). The second tactic involved labeling cleaved, deprotected, and purified peptides with inexpensive fluorophores capable of coupling to amino groups. The drawback to this approach is the loss of specific labeling and the need for two purification steps. A variation of this approach was ultimately employed using a thiol reactive fluorophore, 5-iodoacetamido fluorescein (Molecular Probes) (JR4). This fluorophore is inexpensive relative to the hexanoic amino acid fluorophores, but still allows for specific labeling. Purified dried peptides were reconstituted in a phosphate buffer (pH 7) and reduced using 10-fold excess of TCEP. Then 10 eq. of 5-iodoacetamido fluorescein dissolved in DMF was added. The coupling reaction was conducted in 48 well Robbins reaction blocks and was allowed to proceed for 2 hours at room temperature. The reaction was then quenched with β -mercaptoethanol and HPLC purified. Initial analysis indicated that labeling efficiency was close to 100%. However, upon further investigation it was determined that there was a peak co-eluting with labeled peptides. This peak turned out to be a TCEP-fluorescein complex (Figure 2-5). To avoid this problem, we attempted to reduce the peptides using a TCEP immobilized resin(Pierce). This proved to be unsuccessful and the reduction step was deleted from the labeling procedure. Removal of the reduction step did result in lower labeling efficiency, however enough labeled peptide was obtained

A. Fluorescent Labeling on Bead



B. Fluorescent Labeling off Bead with Thiol Reactive Fluorophore

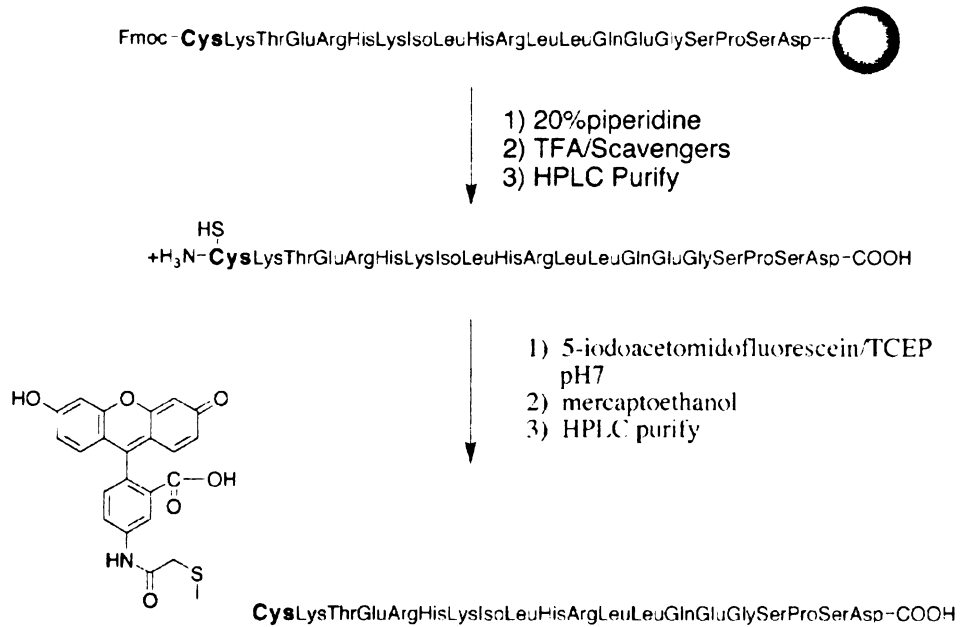


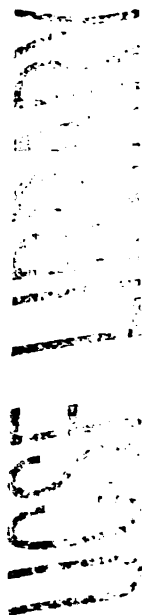
FIGURE 2-5. Labeling Strategies

The two labeling strategies that were attempted are shown. A) The first method employed labeling on bead. The completed peptide on the resin was Fmoc deprotected then allowed to react with Texas Red in the presence of base and a non-reactive rhodamine blocker. The peptides were then simultaneously cleaved and side-chain deprotected using TFA. The crude peptides were purified using HPLC. B) The second method was performed off bead. The completed peptides were first cleaved and sidechain protecting groups were removed. This was followed by HPLC purification. The purified peptides were then allowed to react with a 5-iodoacetomido fluorescein. An additional HPLC purification step was performed to recover pure labeled peptides.

to justify removal of TCEP. The purified labeled peptides were identified by MALDI-TOF or ESI. Yields were determined by UV absorption of the fluorophore and LCMS was used to assess purity (Table 2-3, see protocol Appendix A for LCMS conditions). Some peptides were not successfully ionized by electrospray. In those cases, the pure peptides were collected by HPLC and MALDI-TOF was used to confirm mass. Representative LCMS traces are shown in Figure 2-6.

CONCLUSIONS

The synthesis of 20-mer fluorescently labeled peptides proved to be much more difficult and time-consuming than originally thought. Although, peptide synthesis has been around for several decades, most groups do not synthesize multiple peptides of this length, quantity, and purity in a parallel fashion. As a consequence, there were many hurdles to overcome. Firstly, the synthesis was optimized to accommodate the length and hydrophobicity of these peptides by increasing equivalents of coupled amino acids and adding polar solvents to the coupling reaction. Additionally, it was found that TFA exposure needed to be limited to reduce peptide degradation, including optimizing and reducing cleaving



conditions. Purification and labeling also required optimization. It was found that the best labeling conditions were achieved using a thiol-reactive fluorophore (5-iodoacetomido fluorescein) which was attached to an amino-terminus cysteine. Finally, the acquisition of high-throughput purification technology greatly streamlined and enhanced yields of peptides including the Biotage HPLC, Genevac HT-4/Mega, and LCMS (Water Alliance 2948, Micromass ZQ).

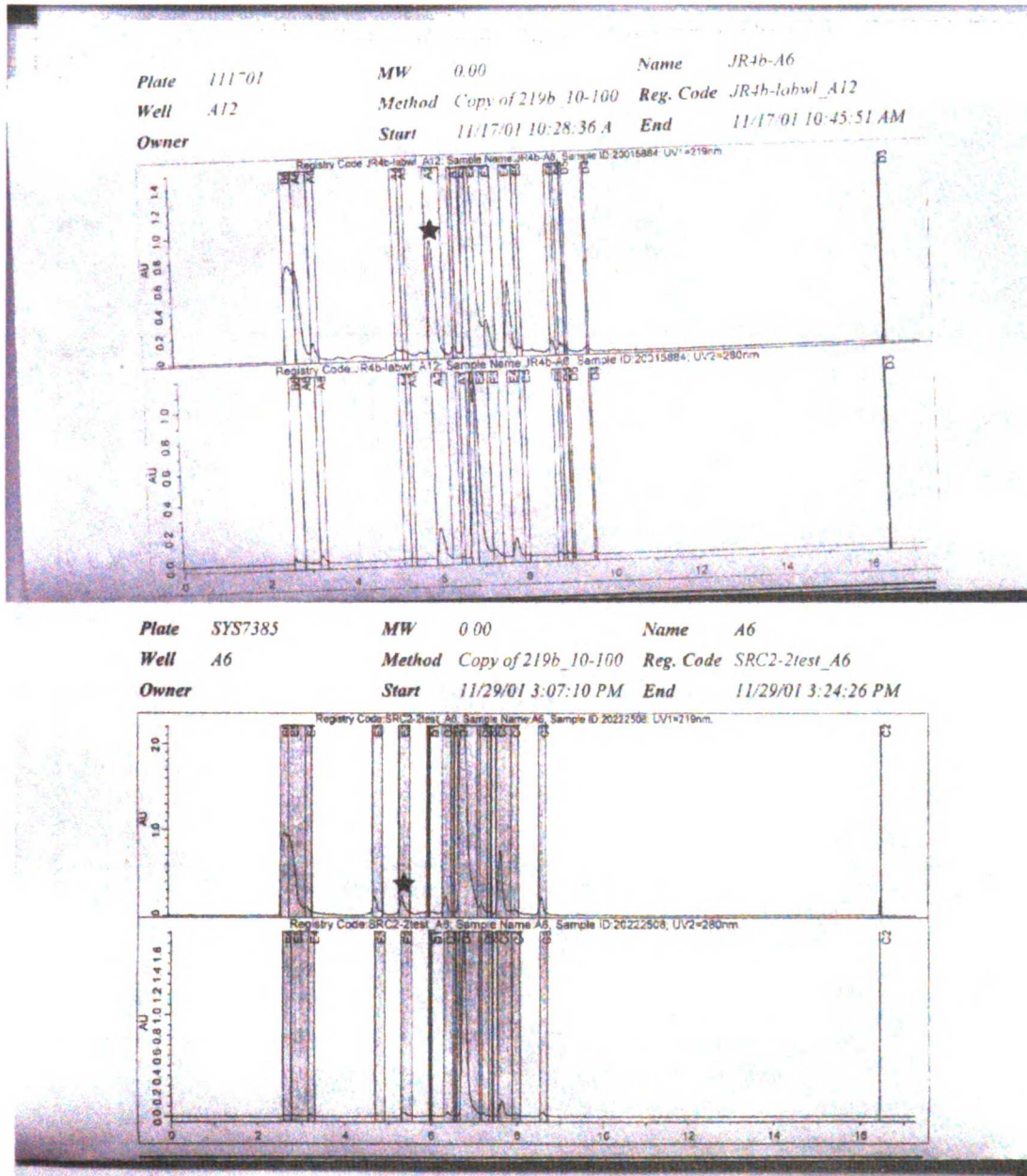
TABLE 2-3. Mass Accuracy, Purity, and Yields for Fluorescently Labeled NCOA Peptides

Purity and mass accuracy were determined for most peptides using LCMS. In some cases, as noted, peptides were collected using HPLC and mass was determined using MALDI-TOF. Yields were determined by measuring the UV absorption of the fluorescein.

Coregulator-Peptides	Positive NR Box Peptides (LXXLL)				Negative NR Box Peptides (LXXAA)			
	Expected Mass (z=+3)	Observed Mass*	% Purity*	% Yield*	Expected Mass (z=+3)	Observed Mass*	% Purity*	% Yield*
SRC1-1	889.80	890.17	100	0.10	861.79	862.02	89	0.04
SRC1-2	888.19	888.20	100	0.01	860.17	860.34	67	0.16
SRC1-3	950.52	950.93	78	0.04	922.57	922.59	87	0.05
SRC2-1	876.17	876.23	82	0.27	848.17	848.23	96	0.07
SRC2-2	907.21	907.46	100	0.42	879.21	879.25	98	0.07
SRC2-3	**2797.61	2798.97	98	0.24	905.25	905.34	83	0.01
SRC3-1	883.83	883.97	100	0.52	855.83	853.76	95	0.05
SRC3-2	896.54	896.77	98	0.18	868.50	868.72	75	0.01
SRC3-3	922.84	922.65	100	0.07	894.89	894.91	80	0.08
TRAP220-1	**2431.52	2431.81	83	0.05	783.11	X	X	X
TRAP220-2	**2685.42	2686.09	87	1.42	867.82	867.90	100	0.05
TRBP-1	*1276.73	1216.73	99	0.45	783.47	X	X	X
TRBP-2	831.45	831.45	99	0.29	*1204.64	1203.27	99	0.26
TRAP100-2	870.51	870.63	93	1.44	842.52	842.56	89	2.06
TRAP100-3	*1166.20	1160.02	94	2.84	749.77	749.65	98	1.63
TRAP100-4	852.80	89.90	75	3.18	824.79	824.44	99	0.91
TRAP100-6	864.20	864.11	100	1.87	836.17	X	X	X
TRAP100-7	875.45	875.26	100	0.25	847.50	847.46	90	1.81
ARA70	896.50	896.12	91	0.16	*1302.19	1301.88	91	0.25
ARA55	860.16	860.83	99	1.49	*1247.70	1247.71	91	2.13
p300	834.48	834.48	100	0.00	806.44	806.12	90	0.00
RIP140-1	827.15	827.44	95	0.32	799.11	798.87	79	3.23
RIP140-3	865.20	865.45	100	0.08	837.18	836.89	90	0.03
RIP140-5	860.85	861.32	100	0.13	832.82	832.90	98	0.01
RIP140-6	898.19	898.68	75	0.64	870.15	870.14	98	2.67
RIP140-7	885.24	885.65	96	0.90	857.19	857.22	89	1.10
RIP140-8	906.51	907.12	100	0.09	878.49	878.48	92	2.40
RIP140-9	900.17	900.67	93	1.22	872.15	872.33	99	2.91
DAX1-1	**2767.52	2767.11	89	0.54	889.15	889.15	98	0.13
DAX1-2	**2656.49	2657.02	88	0.85	852.14	852.43	99	0.00
DAX1-3	**2628.53	2628.86	83	0.45	848.80	848.79	91	1.30
SHP	808.16	808.32	100	0.16	780.13	780.25	98	0.15

* Determined by LCMS (m/z). † Determined by UV absorption.
 X Peptides which were unable to be synthesized or purified
 †(m/z) z=+2 was the predominant mass spectra peak observed
 ** Peptide did not ionize using electrospray, purity and mass were obtained by HPLC and MALDI-TOF (z=+1) on Voyager-EE STR (Applied Biosystems)

UCSF LIBRARY



UCSF LIBRARY

FIGURE 2-6. Purification of Labeled Peptides in the Presence and Absence of TCEP

The top two chromatograms are SRC2-2 labeled in the presence of TCEP at 214 and 280 nm, respectively. The star indicates where labeled SRC2-2 co-elutes with TCEP-fluorescein. The peaks after 6 minutes are free fluorescein. The bottom two chromatograms are SRC2-2 labeled in the absence of TCEP. The star indicates pure labeled SRC2-2. The peak at 5 minutes just before labeled SRC2-2 is unlabeled SRC2-2. In the absence of TCEP labeling efficiency drops.

Figure 2-7 A. SRC2-2

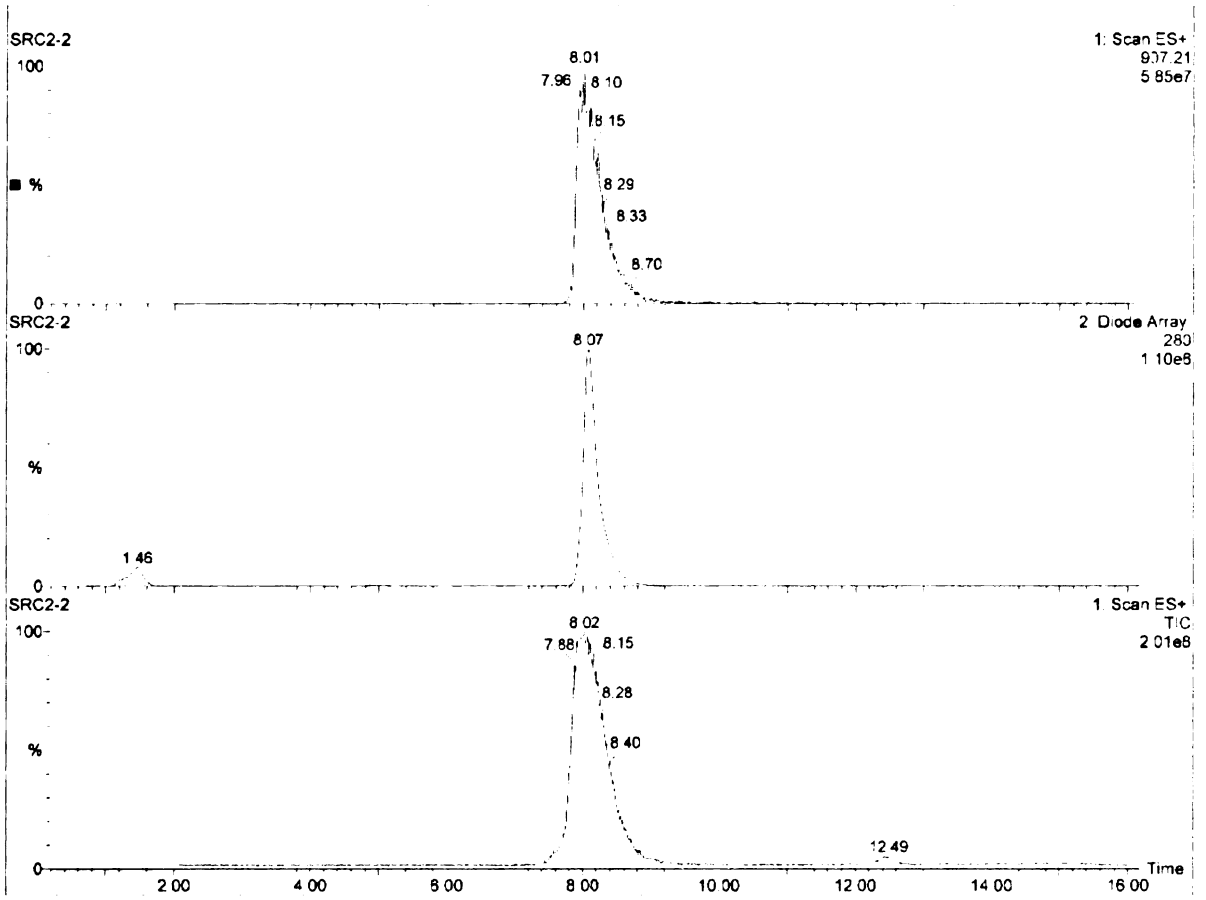


Figure 2-7B. SRC2-3

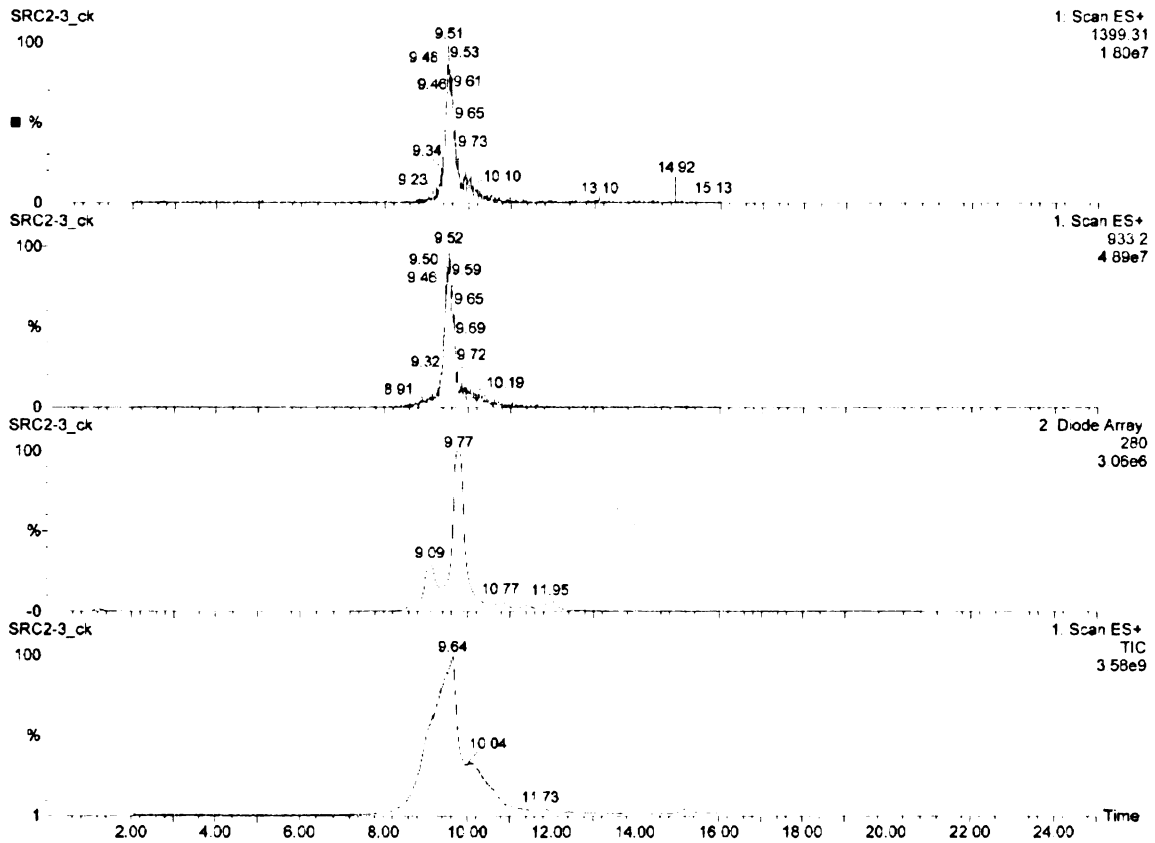


FIGURE 2-7. LCMS Traces for SRC2-2 and SRC2-3

A) The LCMS trace for SRC2-2 is shown. The purity was assigned as 100%. The bottom trace is the total ion count (TIC). The middle trace is the diode array detection at 280 nm. The top trace represents the total ion count for the triple charged species (907.21). All of the peaks line up and there is only one peak detected. B) The LCMS trace for SRC2-3 is shown. The purity was assigned as 85%. The bottom trace is TIC. The next trace up is the diode array detection at 280 nm. The top two traces represent the total ion count for the double (1399.31) and triple charged species (933.2), respectively. The peaks all line up, however, in this case there are additional peaks detected by UV.

METHODS

Protein Expression and Purification- Human TR β LBD (His6; residues E202-D461) was expressed from a pET28a construct (Novagen) in BL21(DE3) (20°C, 0.5 mM IPTG added at OD600 = 0.6) as previously described [24]. Cells were harvested, resuspended in sonication buffer (20 mM Tris, 300 mM NaCl, 0.025% tween, protease inhibitors, 10 mg lysozyme, pH 7.5, 30 minutes on ice), and sonicated for 3x3 minutes on ice. The lysed cells were centrifuged at 100,000 x g for 1 hr and the supernatant was loaded onto Talon resin (Clonetech). Liganded-protein was eluted with 500 mM imidazole plus ligand (3,3',5-triiodo-L-thyronine, Sigma). Protein purity was assessed by SDS-PAGE and HPSEC and protein concentration measured by coomassie protein assay.

Peptide Library Synthesis –(For more details see Appendix A) Coregulator peptides consisting of 20 amino acids with the general motif of **CXXXXXXXXLXXL/AL/AXXXXXXXXX** were constructed, where C is cysteine, L is leucine, A is alanine, and X is any amino acid. The sequences of all the coregulator peptides were obtained from human isoform candidate genes (SRC1/AAC50305, SRC2/Q15596, SRC3/Q9Y6Q9, PGC-1/AAF19083, TRAP220/Q15648, TRBP/Q14686, TRAP100/Q75448, ARA70/Q13772, ARA55/NP_057011, p300/Q92831, RIP140/P48552, DAX-1/P51843, SHP/Q15466). The peptides were synthesized in parallel using standard fluorenylmethoxycarbonyl (Fmoc) chemistry in 48 well synthesis blocks (FlexChem System, Robbins) [57]. Preloaded Wang (Novagen) resin was

deprotected with 20% piperidine in dimethylformamide. The next amino acid was then coupled using 2-(1H-Benzotriazole-1-yl)-1,1,3,3-tetramethyluronium hexafluorophosphate (2.38 equiv. wt.), Fmoc-protected amino acid (2.5 equiv. wt.), and diisopropylethylamine (5 equiv.wt.) in anhydrous dimethylformamide. Coupling efficiency was monitored by the Kaiser Test. Synthesis then proceeded through a cycle of deprotection and coupling steps until the peptides were completely synthesized. The completed peptides were cleaved from the resin with concomitant side chain deprotection (81% TFA, 5% phenol, 5% thioanisole, 2.5% ethanedithiol, 3% water, 2% dimethylsulphide, 1.5% ammonium iodide) and crude product was dried down using a speedvac (GeneVac). Reversed-phase chromatography followed by mass spectrometry (MALDI-TOF/ESI) was used to purify the peptides. The purified peptides were lyophilized. A thiol reactive fluorophore, 5-iodoacetamidofluorescein (Molecular Probes), was then coupled to the amino terminal cysteine following the manufacturer's protocol. Labeled peptide was isolated using reversed-phase chromatography and mass spectrometry. Peptides were quantified using UV spectroscopy. Purity was assessed using LCMS.

ACKNOWLEDGEMENTS

We would like to thank Dr. Timothy Geistlinger for technical advice. JMRR was funded by Department of Defense Breast Cancer Research Fund #DAMD17-01-1-0188. Additional financial support came from the Sandler Research

Foundation, and the NIH (DK-52798 and DK-58390). This portion of the research project could not have been completed without the tremendous technical assistance of Sarah J. Galicia and therefore we dedicate this chapter to her.

CHAPTER 3

Development of a High-Throughput Fluorescence Polarization Method for Quantitative Determination of Nuclear Receptor-Coregulator Interactions

United States Patent Application: 20040005636, Kind Code A1

January 8, 2004

Method for Obtaining the Binding Affinities of a Peptide Library to a Protein

Inventors: *Guy, Rodney Kiplin; (Concord, CA) ; Moore, Jamie Marie Rasmussen; (San Francisco, CA) ; Geistlinger, Timothy Ross; (San Francisco, CA*

Jamie M. R. Moore, Sarah J. Galicia, Andrea C. McReynolds, Ngoc-Ha Nguyen, Thomas S. Scanlan, and R. Kiplin Guy, Quantitative proteomics of the thyroid hormone receptor coregulator interactions, *Journal of Biological Chemistry* 2004 Jun 25; 279(26): 27584-90.

Copyright © 2004 by the American Society for Biochemistry and Molecular Biology

INTRODUCTION

The goals of our research project were to understand how nuclear receptors select from a pool of potential coregulators, determine how this selectivity changes under different conditions, and determine if this selectivity can be used to predict biological responses. We therefore needed to develop an *in vitro* binding assay that could quantitatively measure equilibrium binding constants of nuclear receptors to a library of physiologically relevant coregulators. This assay also needed to be performed using homogenous solutions and provide consistent results. There are many methods available for the determination of equilibrium binding constants including affinity chromatography and pull-downs, the Hummel-Dreyer method, surface plasmon resonance, analytical ultracentrifugation, and fluorescence methods. Many of these methods have been reported in the literature for investigating nuclear receptor-coregulator interactions (ref). Most of these methods, however, are not amendable to screening a large number of coregulators simultaneously and are more frequently used for elucidating individual protein-protein interactions. Library based methods, such as phage display, time-resolved fluorescence, and mammalian two-hybrids, have also been used to look at nuclear receptor-coregulator interactions [45], [44], [47]. Each of these techniques has drawbacks as well. Although phage display has been used effectively to define nuclear receptor-coregulator specificity, the peptides in these studies were generated from random libraries that do not represent true NR box sequences

[43], [44]. Both time-resolved fluorescence and mammalian two-hybrids have been used successfully to study physiologically relevant coregulators, but these methods are not homogenous techniques and as a consequence they are not capable of measuring accurate equilibrium binding affinities [45]. To capture all of our assay requirements we chose fluorescence polarization.

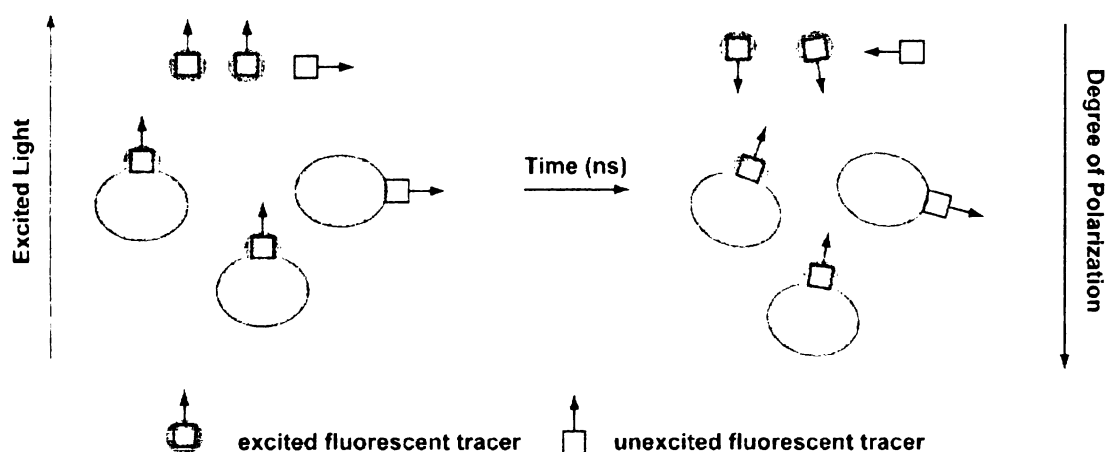


FIGURE 3-1. Fluorescence Polarization

The general theory of fluorescence polarization is presented. Fluorescence molecules are excited with linearly polarized light. The fluorescence molecules whose transition absorption vectors (arrows) are oriented in the same direction as the electric vector of the linearly polarized light will be selectively excited, as represented by the green squares. The white squares are fluorescent molecules that are not excited. Polarization is directly proportional to the rotational correlation times of the fluorescent molecules. Therefore, small fluorescent molecules (free dye, squares) rotate rapidly in solution and have low polarization whereas larger fluorescent molecules or dyes that are binding to larger molecules (orange ovals) rotate slower and have a higher polarization. To measure polarization, the fluorescence emission is monitored in both the parallel and perpendicular plane.

Fluorescence polarization is a technique that is sensitive to molecular motions and processes that can modify molecular motions (Figure 3-1). The long

lifetimes of common excited fluorescent molecules, such as 2-4 nanoseconds for fluorescein, can be used to monitor rotational motion of peptides that occur on that timescale. By exciting with plane-polarized light, polarization is determined by monitoring emission in the perpendicular and parallel planes. Since rotational correlation times are dependent on size, fluorescence polarization can be used to monitor the formation of complexes and for determining binding affinities.

Fluorescence polarization measurements can be performed on homogenous solutions using plate readers with no restrictions on the sequence of the fluorescent peptides. Using this technique we were able to design a high-throughput in vitro binding assay that allowed us to accurately and consistently determine thyroid receptor coregulator binding patterns.

RESULTS AND DISCUSSION

Optimization of Fluorescence Polarization Assay

A high throughput assay was designed to quantitatively measure the binding affinities of TR β -LBD to a library of coregulator peptides using fluorescence polarization. Before determining the binding affinities of TR β -LBD to all coregulator peptides, optimization studies were conducted by first studying only the interaction of TR β -LBD to SRC2-2 (the second NR box of SRC2). This interaction has been extensively studied in the literature and a measured binding dissociation constant has been reported (0.8 μ M) [24]. In an attempt to reproduce this binding constant, several parameters were investigated including

incubation time, buffer components, the presence of non-specific binding, the number of binding sites, and cooperativity.

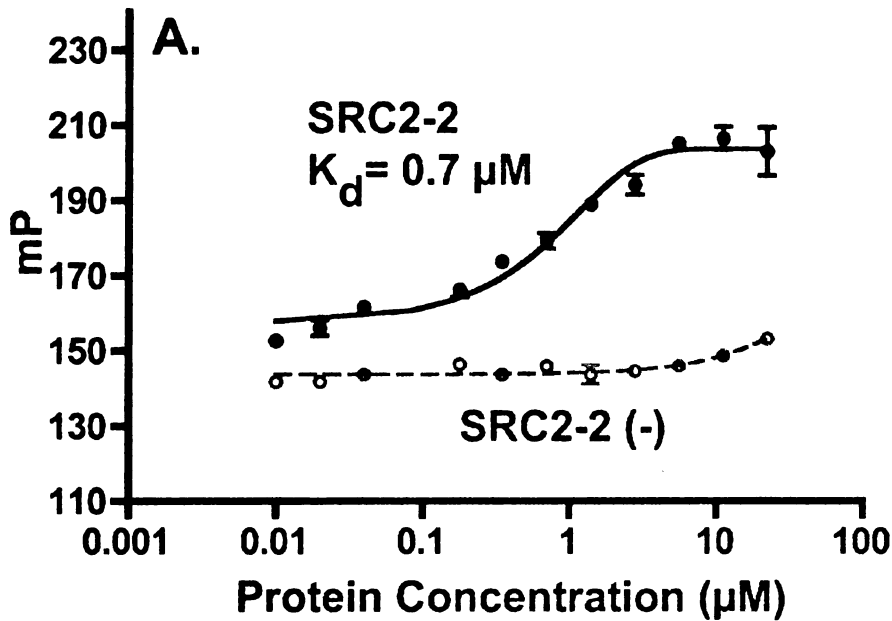


FIGURE 3-2. Klotz Plot of TR β -LBD and SRC2-2

A Klotz plot was constructed by titrating a fixed concentration of fluorescent SRC2-2 with increasing amounts of TR β -LBD. At low peptide concentration, there is mostly free peptide and therefore the polarization value is low. As protein concentration increases, there is more peptide complexed to TR β -LBD and polarization values increase until a maximal value is reached when all of the peptide is bound. Under these conditions, the time required to reach equilibrium was 30 minutes. The solid circles in green denote the native NR box peptide SRC2-2, solid green line represent fitted curves for native NR box SRC2-2, open red circles represent negative NR box SRC2-2(-) (LXXAA), and dashed red line is fitted curve for negative NR box SRC2-2(-).

The first parameter we investigated was the time required for the reaction of TR β -LBD and SRC2-2 to reach equilibrium. To determine this, we constructed a binding isotherm by holding fluorescent SRC2-2 constant at 10 nM, approximately 100-fold below expected K_d , and titrating in TR β -LBD. The

concentration of TR β -LBD was varied from 0.001- 30 μ M, at least 40 fold below and above the expected K_d . Fluorescence polarization was then measured to construct binding isotherms over several different timepoints: 5 minutes, 30 minutes, 1 hour, 2 hours, 6 hours, and 12 hours (data not shown). Shown in Figure 3-2, is the Klotz plot for the 30 minute timepoint. It was determined that 30 minutes was the optimal incubation time for SRC2-2 and TR β -LBD to reach equilibrium with a measured K_d of 0.7 μ M. At 5 minutes, the data was quite noisy with significant differences in polarization observed at each concentration of TR β -LBD. After 30 minutes, the binding isotherm did not change and therefore 30 minutes was the chosen incubation time.

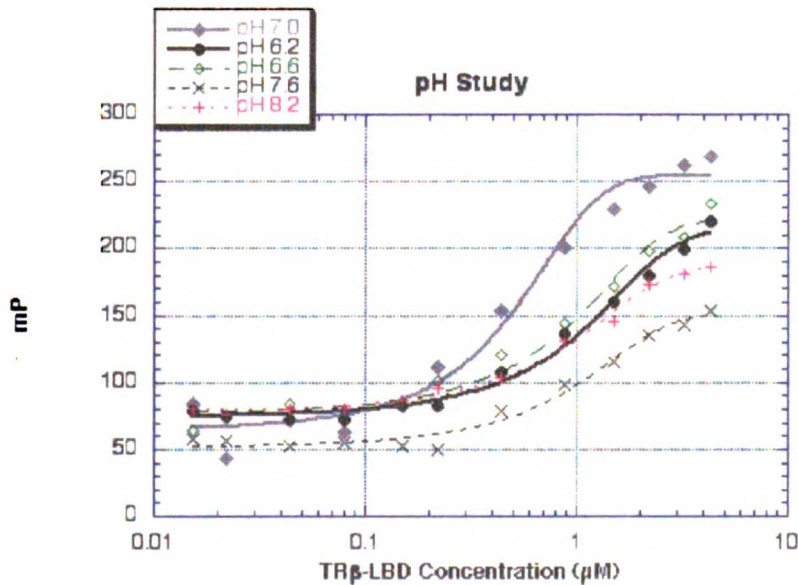


FIGURE 3-3. The Effect of pH on TR β -LBD–Coregulator Interactions
 To determine optimal buffer conditions for studying TR β -LBD-coregulator interactions, the pH of the buffer was varied from pH 6.2- pH 8.2 while holding all other buffer components constant. The best pH was determined to be at pH 7.0, with a measured K_d around 1 μ M, similar to literature reports [24]. The highest K_d value was observed at pH 7.6.

MSU LIBRARY
 10/22/04

The next step in designing the high-throughput fluorescence polarization assay was optimization of buffer conditions and components. There were two factors to consider. First off, it has been shown that protein stability can vary with pH and ionic strength (Moore, others). In addition, pH and ionic strength can affect protein-protein interactions by masking charges that may be critical in the interaction surface. Therefore, it was important to use a buffer that would provide the greatest stability for TR β -LBD as well as optimal conditions for interacting with coregulator peptides. To identify the best pH and ionic strength conditions, binding isotherms were constructed at different pH (Figure 3-3) and ionic strengths (data not shown). As seen in Figure 3-3, it was determined that pH 7.0 was optimal for binding to SRC2-2 ($K_d = 0.7 \mu\text{M}$). Interestingly, at pH 7.6 the highest K_d was observed while the K_d at pH 6.2 and pH 8.2 were similar. When the concentration of NaCl was varied from 100-500 mM there were no significant differences observed in the binding isotherms. Therefore, a concentration of 150 mM NaCl was chosen in order to mimic physiological conditions as close as possible. The next factor to consider was non-specific interactions of buffer components with the fluorescence tag, fluorescein. Detergents typically consist of large hydrophobic component and are capable of forming micelles. These hydrophobic groups could potentially interact with fluorescein. To investigate this possibility, we constructed binding isotherms with different detergents present in the binding buffer, including NP-40, Tween 20, TritonX100, TritonX114, and CHAPSO (Figure 3-4). Based on these studies NP-

40 appeared to be the best detergent ($K_d=1\mu\text{M}$). When CHAPSO was present in the binding buffer, a loss of binding was observed. This suggests that CHAPSO is interacting with the fluorescent peptide, disrupting interactions with TR β -LBD.

The results from all of the buffer studies with TR β -LBD led to the following

binding buffer: 50 mM Sodium Phosphate, 150 mM NaCl, 1 mM DTT, 1 mM

EDTA, 0.01% (w/v) NP-40, 10% glycerol, pH 7.2.

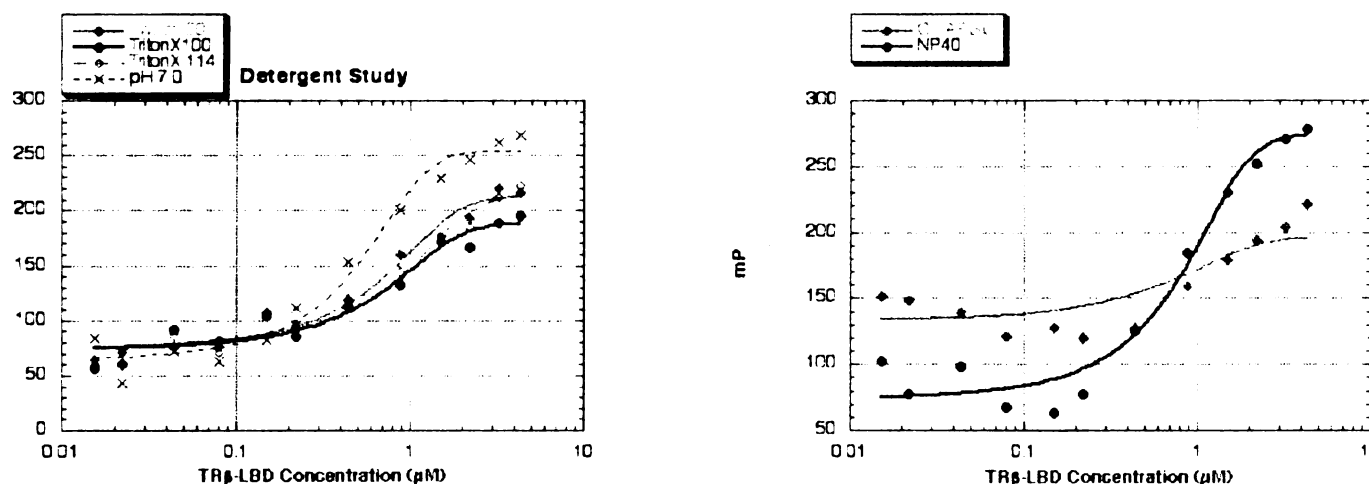


FIGURE 3-4. The Effect of Detergents on TR β -LBD–Coregulator Interactions

To determine optimal buffer conditions for studying TR β -LBD-coregulator interactions, the detergent in the buffer was varied while holding all other buffer components constant. The plot on the left is a comparison with Tween 20, TritonX100, TritonX114, and NP40 (designated pH 7.0 on plot). NP-40 appears to be the best detergent as the K_d under these buffer conditions is 1 μM . The plot on the right is a comparison of NP-40 and CHAPSO. It appears that the fluorescent peptide may non-specifically interact with CHAPSO, therefore this detergent will not be used in binding buffers.

Once a working binding buffer was established, the interaction between TR β -LBD and SRC2-2 was further analyzed for the presence of non-specific binding, multiple binding sites, and cooperativity by constructing Scatchard and Hill plots (Figure 3-5). Scatchard analysis is a plot of [bound TR β -LBD]/[free TR β -LBD] vs.

[bound TR β -LBD]. This type of analysis can provide information on the number of binding sites and the degree of cooperativity. The data fit best to a linear function as seen in Figure 3-5 left panel, suggesting that there was only a single class of binding sites. This result was expected and is consistent for a coregulator peptide binding to a single ligand binding domain of a nuclear receptor. The K_d determined from this plot was $0.55 \mu\text{M}$ (slope= $-1/K_d$), close to the value obtained from the klotz plot, $0.7 \mu\text{M}$ (Figure 3-2). Additionally, Hill plot analysis was also performed where the $\log [(bound/free)]$ vs. $\log [free]$ was plotted (Figure 3-5, right panel). The slope of the Hill plot is approximately 1 supporting the notion that there is a single identical interaction site. The K_d (x intercept = $\log K_d$) determined from this plot, $0.5 \mu\text{M}$, is consistent with both the Scatchard and Klotz plots.

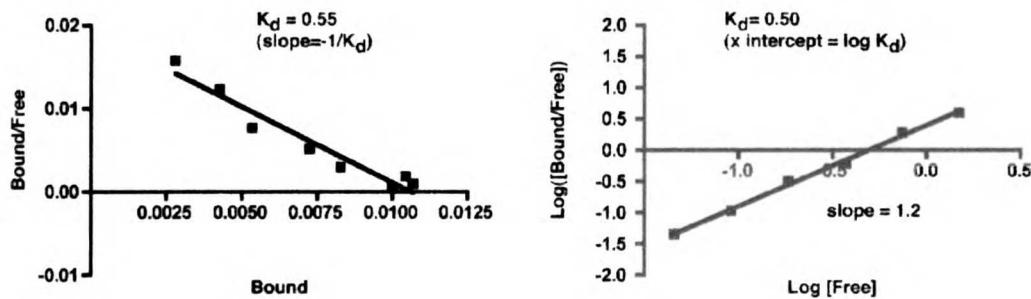


FIGURE 3-5. Scatchard and Hill Plot Analysis

Scatchard and Hill plot analysis were performed to identify non-specific binding, positive or negative cooperativity, and the presence of multiple binding sites. The plot on the left is a Scatchard plot. The data is best fit to a linear function, indicating that there is a single class of binding sites whose concentration is equal to the x intercept (10 nM). The K_d calculated from this plot (slope= $-1/K_d$), is $0.55 \mu\text{M}$, which agrees with the Klotz plot determination ($0.7 \mu\text{M}$). The plot on the right is a Hill plot. The slope of the Hill plot is approximately 1, supporting the notion that there is a single class of binding sites. The K_d determined from this plot is $0.5 \mu\text{M}$ (x intercept = $\log K_d$).

To further confirm that SRC2-2 specifically interacts with TR β -LBD, we conducted binding studies using a mutant SRC2-2, denoted SRC2-2(-). In this peptide, the LXXLL motif was changed to LXXAA. Previous work demonstrated that mutating the +4 and +5 leucines to alanine abolished the interaction with nuclear receptor ligand binding domains (38). As seen by the flat line in Figure 3-2, SRC2-2 (-) does not bind to TR β -LBD.

Using fluorescence polarization we were able to optimize conditions to demonstrate that TR β -LBD recruited SRC2-2 with a binding affinity similar to literature reports and that this interaction was specific with only one class of binding sites.

Interpreting Binding Isotherms and Data Presentation

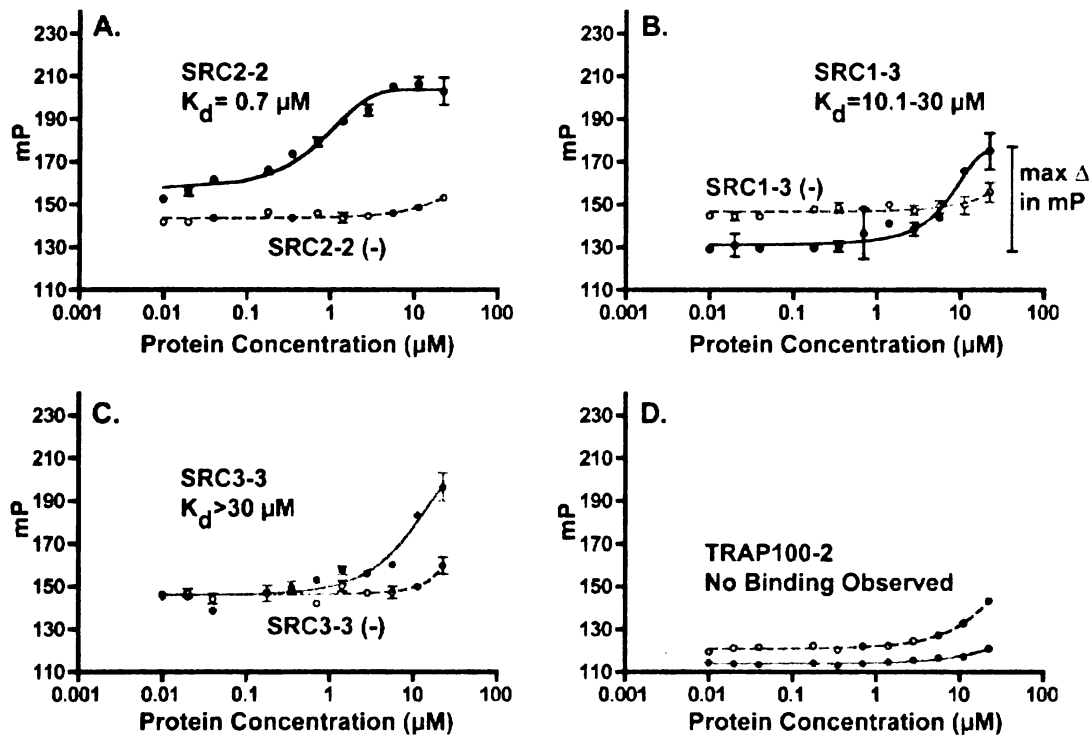


FIGURE 3-6. Four Binding Modes for TRβ-LBD

Panel A. The binding of TRβ SRC2-2 is plotted in dark green to signify that this is a saturable binding curve where a measurable $K_d = 0.7 \mu\text{M}$ is extracted by fitting to the equation $(y = \text{min} + (\text{max} - \text{min}) / (1 + (x/K_d)^{\text{Hillslope}}))$. The binding of TRβ to the negative control SRC2-2 peptide is also shown in red. Panel B. The binding curve for SRC1-3 is shown in light green. This binding curve appears to be reaching saturation, but no visible plateau is observed. The K_d is reported as $10.1-30 \mu\text{M}$. Panel C. The binding curve for SRC3-3 is shown in gray. Polarization is increasing with TRβ concentration but does not appear to be reaching saturation. The K_d is reported as $>30 \mu\text{M}$. Panel D. The binding curve for TRAP220-2 is plotted in red indicating that no binding is observed. The solid circles denote the native NR box peptides, solid lines represent fitted curves for native NR box peptides, open red circles represent negative NR box peptides (LXXAA), and dashed red line is fitted curve for negative NR box peptide.

Once we had a working direct binding assay for the interaction of TRβ-LBD with SRC2-2, we scaled up conditions to determine binding affinities for a library of known coregulator peptides (See Chapter 2, Synthesis of Fluorescent NCOA Peptide Library). Access to a fluorescence polarization plate reader (Analyst AD,

Molecular Probes) and liquid handlers (Biomek FX, Beckman Instruments) streamlined the scale-up process (See Appendix for Protocol). However, difficulty stemmed from data handling, interpretation, and presentation. When testing TR β -LBD against the whole library of 68 coregulators, the assay is performed two independent times in quadruplicate and therefore in the end there are 544 binding isotherms. Considerable amount of time and effort was required to handle all of this data.

The first step to tackle was data handling and manipulation of all of the binding data. To deal with the large amount of polarization data, we currently cut and paste into excel and use macros to manipulate the data. The data can then be exported into either Sigma plot (SPSS, Chicago, IL) or Prism (Graphpad, San Diego, CA) for analysis. Although this process is acceptable, it is fairly labor intensive and future work with Anang Shelat hopes to automate this process.

The next step in the data handling process was interpretation of binding isotherms. This proved to be quite challenging, as unfortunately the binding isotherms did not fall into the two categories of saturable binding or no binding. A wide range of binding isotherms was observed and after much debate and analysis we sorted the binding data into 4 modes. Example equilibrium affinity curves are summarized in Figure 3-6 (A-D) and K_d value ranges are reported in Figure 3-7.

The first binding mode consisted of peptides that bound in a dose dependent and saturable manner (Figure 3-6A) where a clear plateau was reached within the protein concentration range studied. Eight coregulator peptides exhibited this mode: SRC2-1, SRC2-2, SRC2-3, TRAP220-1, TRBP-1, p300, RIP140-5, and DAX1-3. The K_d values for this class ranged from 0.7 to 10 μM and are represented by a dark green color in Figure 3-7.

The next binding mode included peptides where binding appeared to be reaching saturation but did not have a clear plateau, as defined by at least two points with indistinguishable y-ordinates (Figure 3-6B). This assumption is based on previous binding studies conducted with these coregulator peptides where similar changes in polarization values were observed for saturating binding isotherms (data not shown). These peptides bound to TR β with a K_d range of 10-30 μM and included SRC1-2, SRC1-3, SRC3-2, TRAP220-2, TRBP-2, and ARA70. To accurately obtain K_d values, however, the binding studies would need to be carried out at protein concentrations varying from 1-300 μM as this would give the widest range of polarization values. Working with TR β protein concentrations higher than 100 μM is problematic due to protein aggregation and decreased protein stability. In order to reflect the inability to obtain an unambiguous K_d value, we report a K_d range, 10-30 μM , for coregulator peptides that exhibit this binding mode and represent the K_d as a light green colors in Figure 3-7.

Coregulator Peptides	TR β
SRC1-1	0.5-1.0
SRC1-2	1.1-5.0
SRC1-3	1.1-5.0
SRC1-4	5.1-10.0
SRC2-1	10.1-30.0
SRC2-2	0.5-1.0
SRC2-3	1.1-5.0
SRC3-1	0.5-1.0
SRC3-2	1.1-5.0
SRC3-3	0.5-1.0
PGC-1	5.1-10.0
TRAP220-1	10.1-30.0
TRAP220-2	1.1-5.0
TRBP-1	10.1-30.0
TRBP-2	1.1-5.0
TRAP100-2	No binding Obs.
TRAP100-3	No binding Obs.
TRAP100-4	No binding Obs.
TRAP100-6	No binding Obs.
TRAP100-7	No binding Obs.
ARA70	1.1-5.0
ARA55	5.1-10.0
p300	10.1-30.0
RIP140-1	5.1-10.0
RIP140-3	0.5-1.0
RIP140-5	10.1-30.0
RIP140-6	5.1-10.0
RIP140-7	5.1-10.0
RIP140-8	0.5-1.0
RIP140-9	5.1-10.0
DAX1-1	No binding Obs.
DAX1-2	No binding Obs.
DAX1-3	10.1-30.0
SHP	0.5-1.0

KD (μ M)	
0.5-1.0	0.5-1.0
1.1-5.0	1.1-5.0
5.1-10.0	5.1-10.0
10.1-30.0	10.1-30.0
>30.0	>30.0
No binding Obs.	No binding Obs.

FIGURE 3-7. Dissociation Constants for TR β -LBD-Coregulators

The equilibrium binding constants for TR β -coregulator NR boxes are reported. The coregulator peptides are listed in the left column where SRC1-1, SRC1-2, SRC1-3, SRC1-4 represent the first, second, third, and fourth NR box in SRC1, respectively. Each color represents a unique K_d range as defined by the legend on the left

MARY BERT SM

The third binding mode is one in which polarization increases with protein concentration but does not appear to be reaching saturation. This mode is exemplified by SRC3-3 (Figure 3-6C) where the polarization of SRC3-3 slowly increases with TR β concentration. Other coregulators included in this category are SRC1-1, SRC3-1, SRC3-3, RIP140-3, RIP140-8, and SHP. The binding isotherms for this group suggest that the coregulator peptides are binding non-specifically or that they bind with a K_d value significantly above the working assay range, (e.g. $> 30 \mu\text{M}$). In Figure 3-7, this binding mode is represented by a gray color. This class of coregulator peptides is distinguished from the final group of peptides where no binding is observed (Figure 6D) and is signified by red in Figure 3-7.

The final aspect of data handling was data presentation. We chose to use a colorimetric table to represent the measured K_d values (Figure 3-7). This type of table allows one to quickly see the differences in binding compared to a table of numbers. In addition, we maintained a color theme such that the four different binding modes could be distinguished (dark green, light green, gray, and red) as described above.

CONCLUSION

To quantitatively map thyroid receptor interactions with coregulators we chose the homogenous assay, fluorescence polarization. This assay allowed us to

simultaneously determine binding affinities of the thyroid receptor to a library of known coregulators peptides in solution in a consistent format. There were several parameters of the assay that required optimization including incubation time, buffer components, and data handling. Specific assay conditions and components were identified which allowed us to reproduce the binding of the TR β -LBD to SRC2-2 and demonstrate that this interaction is non-cooperative with only one class of binding sites. In addition, we were able to then screen an entire library of coregulator peptides for interactions with TR β -LBD and present the data in a clear format.

METHODS

Direct Binding Assay- (For more details see Appendix B)

In 96 well plates, hTR β -LBD was serially diluted from 70 μ M to 0.002 μ M in binding buffer (50 mM Sodium Phosphate, 150 mM NaCl, pH 7.2, 1 mM DTT, 1 mM EDTA, 0.01% NP40, 10% glycerol) containing 140 μ M ligand (T3). Then 10 μ L of diluted protein was added to 10 μ L of fluorescent coregulator peptide (20 nM) in 384 well plates yielding final protein concentrations of 35-0.001 μ M and 10 nM fluorescent peptide concentration. The samples were allowed to equilibrate for 30 minutes. Binding was then measured using fluorescence polarization (excitation λ 485 nm, emission λ 530 nm) on an Analyst AD (Molecular Devices). Two independent experiments were assayed for each state in quadruplicate. Data were analyzed using SigmaPlot 8.0 (SPSS, Chicago, IL) and the K_d values

were obtained by fitting data to the following equation ($y = \text{min} + (\text{max} - \text{min}) / (1 + (x/K_d)^{\text{Hillslope}})$)

Protein Expression and Purification- Human TR β LBD (His6; residues E202-D461) was expressed from a pET28a construct (Novagen) in BL21(DE3) (20°C, 0.5 mM IPTG added at OD600 = 0.6) as previously described [24] Cells were harvested, resuspended in sonication buffer (20 mM Tris, 300 mM NaCl, 0.025% tween, protease inhibitors, 10 mg lysozyme, pH 7.5, 30 minutes on ice), and sonicated for 3x3 minutes on ice. The lysed cells were centrifuged at 100,000 x g for 1 hr and the supernatant was loaded onto Talon resin (Clonetechn). Liganded-protein was eluted with 500 mM imidazole plus ligand (3,3',5-triiodo-L-thyronine, Sigma; GC-1; or NH-3;). Protein purity was assessed by SDS-PAGE and HPSEC and protein concentration measured by coomassie protein assay.

pH , Ionic Strength, and Detergent Studies

The direct binding assay was performed with hTR β -LBD and SRC2-2 while varying pH or detergent conditions. The buffer for all studies consisted of 50 mM Sodium Phosphate, pH 7.2, 300 mM NaCl, 1 mM DTT, 0.01% (w/v) NP-40. For the pH study all components were held constant while varying the pH from 6.2-8.2 using either concentrated HCl or NaOH. For the ionic strength study, all components of the buffer were held constant while varying the amount of NaCl:

100 mM, 200 mM, 300 mM, 400 mM, and 500 mM. For the detergent study, all buffer components were held constant including pH 7.2, and 300mM NaCl except the detergent. The following detergents were used: 0.01% NP-40, 0.01% Tween 20, 0.01% TritonX 100, 0.01% Triton X114 (percentages are w/v), and 20 mM CHAPSO.

ACKNOWLEDGEMENTS

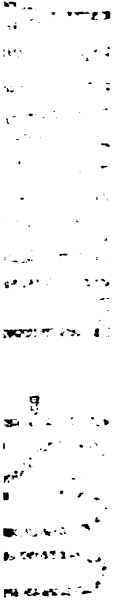
The authors thank Dr. Timothy Geistlinger and Dr. Kathleen Pendola-Novak for useful discussions and Dr. Adam Carroll and the Center for Advanced Technology for assistance and use of the Biomek FX and for School of Medicine REAC grant for financial support.

CHAPTER 4

Elucidating TR β -Coregulator Interactions

Jamie M. R. Moore, Sarah J. Galicia, Andrea C. McReynolds, Ngoc-Ha Nguyen, Thomas S. Scanlan, and R. Kiplin Guy, Quantitative proteomics of the thyroid hormone receptor coregulator interactions, *Journal of Biological Chemistry* 2004 Jun 25; 279(26): 27584-90.

Copyright © 2004 by the American Society for Biochemistry and Molecular Biology



SUMMARY

The thyroid hormone receptor regulates a diverse set of genes that regulate processes from embryonic development to adult homeostasis. Upon binding of thyroid hormone, thyroid receptor releases corepressor proteins and undergoes a conformational change that allows for the interaction of coactivating proteins necessary for gene transcription. This interaction is mediated by a conserved motif, termed the NR box, found in many coregulators. Recent work has demonstrated that differentially assembled coregulator complexes can elicit specific biological responses. However, the mechanism for the selective assembly of these coregulator complexes has yet to be elucidated. To further understand the principles underlying thyroid receptor-coregulator selectivity, we designed a high-throughput *in vitro* binding assay to measure the equilibrium affinity of thyroid receptor to a library of potential coregulators in the presence of different ligands including the endogenous thyroid hormone T3, synthetic thyroid receptor β -selective agonist GC-1, and antagonist NH-3. Using this homogenous method several coregulator NR boxes capable of associating with thyroid receptor at physiologically relevant concentrations were identified including ones found in traditional coactivating proteins such as SRC1, SRC2, TRAP220, TRBP, p300 and ARA70; and those in coregulators known to repress gene activation including RIP140 and DAX-1. In addition, it was discovered that the thyroid receptor-coregulator binding patterns vary with ligand and that this differential binding can be used to predict biological responses. Finally, it is

demonstrated that this is a general method that can be applied to other nuclear receptors and can be used to establish rules for nuclear receptor-coregulator selectivity.

INTRODUCTION

To date there has been no comprehensive study of the interactions of TR and natural coregulator NR boxes. To address this issue, we designed an in vitro binding assay (Chapter 3) to measure the equilibrium binding of TR β to a library of potential coregulators (Chapter 2) in a high-throughput manner using fluorescence polarization. With this method, binding constants for TR β to coregulator NR boxes were determined in a consistent format, including NR boxes from SRCs and 9 other known coregulators. In addition the TR β - coregulator binding patterns for three different ligands including T3, the synthetic TR β -selective agonist GC-1, and the T3 antagonist NH-3 were defined. This quantitative information can be used to establish rules for TR β coregulator selectivity and these rules can be used for predicting biological responses.

RESULTS

T3 Recruitment of Coregulators

We report here the first comprehensive investigation of coregulator recruitment to liganded TR β with 12 different coregulators and 34 unique NR boxes as well as

appropriate negative controls (LXXAA). Of the 34 coregulator peptides tested, 20 appear to interact with TR β in the presence of T3 with varying degrees of affinity. The strongest recruitment observed was with SRC2-2 which exhibited a K_d of $0.7 \mu\text{M} \pm 0.2$. This was followed by TRBP-1 ($K_d=1.8 \mu\text{M} \pm 0.1$), RIP140-5 ($K_d=2.5 \mu\text{M} \pm 0.4$), TRAP220-1 ($K_d=2.7 \mu\text{M} \pm 1.1$), DAX1-3 ($K_d=3.6 \mu\text{M} \pm 2.3$), SRC2-3 ($K_d=4.5 \mu\text{M} \pm 1.5$), SRC2-1 ($K_d=6.0 \mu\text{M} \pm 2.0$), and p300 ($K_d=9.2 \mu\text{M} \pm 2.8$). The coregulator peptides that clearly did not interact with T3 liganded TR β included ARA55, all of the TRAP100 peptides, and some of the RIP140 and DAX1 NR box peptides. The remaining coregulator peptides bound to TR β weakly with K_d values ranging from $10\text{-}30 \mu\text{M}$ or $> 30 \mu\text{M}$ (Figure 4-1).

The SRCs are a family of coregulators whose interaction with TR β have been extensively studied using non-quantitative methods [24], [47], [63], [64]. Our data are consistent with previously published work where it was determined that TR β has a strong preference for SRC2 NR box peptides with the overall observed preference being SRC2-2>SRC2-3>SRC2-1 [24]. The next family member, SRC1, bound to liganded TR β to a lesser extent with SRC1-2~SRC1-3>SRC1-1. Only weak interactions were observed for SRC3 where affinity has been reported as SRC3-2>SRC3-1=SRC3-3.

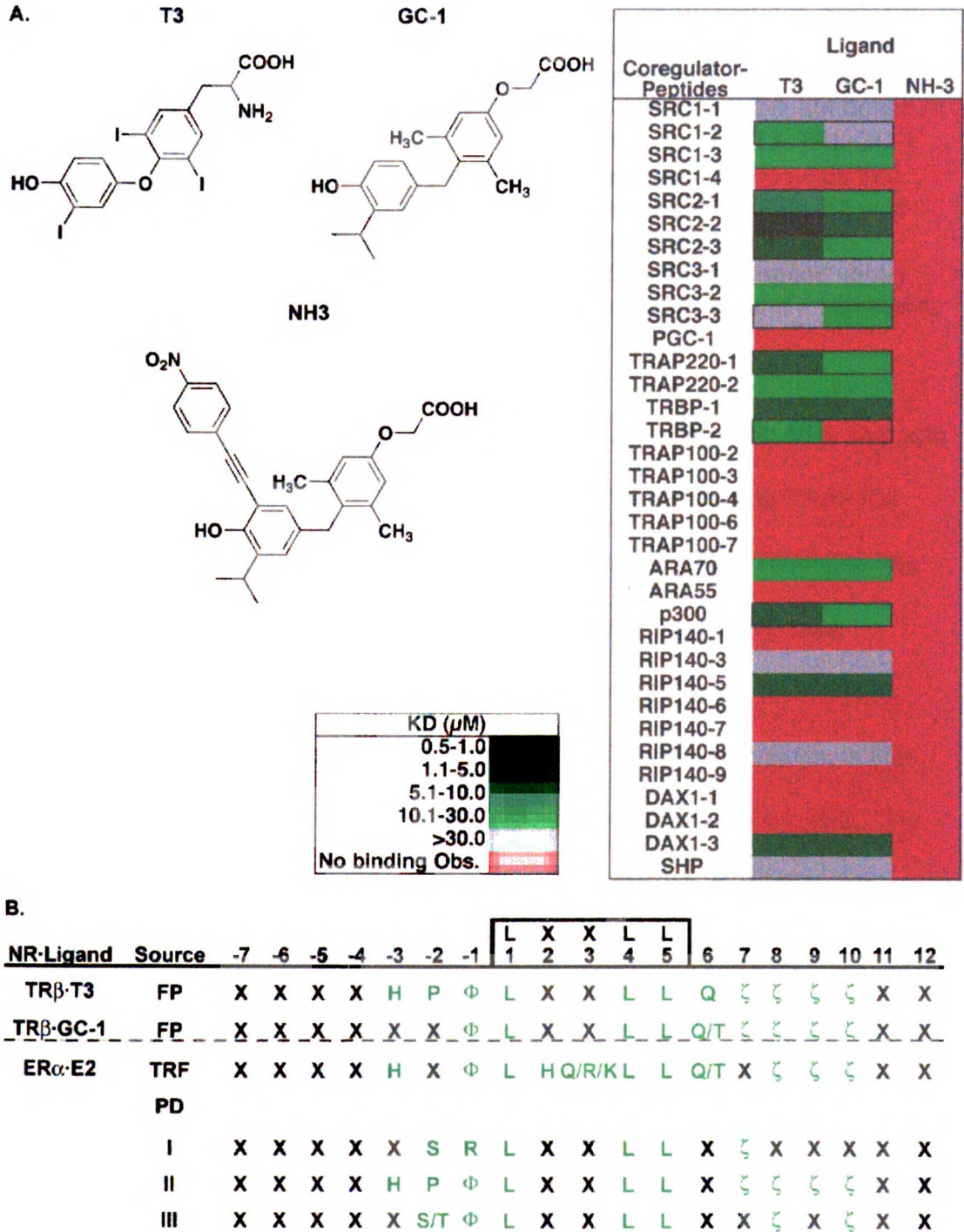


FIGURE 4-1. Coregulator Binding Patterns and Specificity Determinants.
 A. The structure of the TRβ ligands tested; endogenous thyroid hormone T3, synthetic TRβ-selective agonist GC-1, and T3 antagonist NH-3. The equilibrium binding constants for TRβ-coregulator NR boxes are reported for each ligand.

Accepted for publication
 10/22/04

The coregulator peptides are listed in the left column where SRC1-1, SRC1-2, SRC1-3, SRC1-4 represent the first, second, third, and fourth NR box in SRC1, respectively. Each color represents a unique K_D range as defined by the legend on the left. Significant differences between TR β ·T3 and TR β ·GC-1 are boxed in black. B. A representative coregulator peptide is listed for TR β ·T3, TR β ·GC-1, ER α ·E2 with amino acids highlighted in green representing amino acids that convey specificity for each NR·ligand state. The information for ER α ·E2 was extracted from two sources for comparative purposes 1) a time-resolved fluorescence assay conducted with SRCs [45] and 2) a phage peptide library screen with ER α ·E2 [44]. Φ denotes hydrophobic amino acids and ζ represents hydrophilic amino acids.

The TRAP coactivator complex has been shown to associate with NRs and help initiate transcription [29], [30]. Two single subunits TRAP220 and TRAP100 were investigated for their ability to interact with liganded TR β . TRAP220 has two NR boxes and in this report it was determined that the first NR box, TRAP220-1, interacted more strongly than the second NR box, TRAP220-2. This is the opposite of what has been reported for TR α , supporting the notion that TR isoforms can differentially recruit coactivator NR boxes [30], [65]. The TRAP100 protein contains 7 NR boxes, 5 of which were studied here. As previously reported, none of these NR boxes interact with liganded TR β [29].

Another coregulator that has been shown to interact with TR β is TRBP. This coactivator is ubiquitously expressed and appears to be a general coactivator that can associate with NR including TR, ER, PPAR, as well as other transcriptional proteins such as AP-1, CRE, and NF κ B-response element [35]. There are two LXXLL motifs in TRBP and both can interact with TR β . Our

studies indicate that TRBP-1 is preferentially recruited to TR β in the presence of T3.

RIP140 is a coregulator that contains 9 LXXLL motifs and has been shown to interact with many NRs including TR β . It has been suggested that RIP140 directly competes with other coregulators [33]. Unlike traditional coregulators, however, RIP140 represses transcription upon binding to NR [66-69]. Here we show liganded TR β has a clear preference for three of the NR boxes in RIP140, RIP140-3, RIP140-5, and RIP140-8. One NR box peptide in particular, RIP140-5, bound fairly tightly with a K_d of $2.5 \mu\text{M} \pm 0.4$.

Three additional coactivators, p300, ARA70, and DAX1, were also shown in this report to associate with TR β with varying degrees. ARA70 and DAX1 had not previously been investigated for their interaction with TR β .

Ligands Alter Coregulator Recruitment

To investigate ligand effects on coregulator recruitment, binding studies were performed in the presence of the TR β selective agonist, GC-1 provided by the Scanlan Laboratory. GC-1 is a halogen-free thyromimetic that is approximately 10-fold selective for binding to TR β vs. TR α [70]. It has been shown that the oxyacetic acid at the carbon-1 position (Figure 3A) is responsible for the selective TR β binding of GC-1 {Yoshihara, 2003 #48}. Additionally, crystallographic

studies have confirmed that the oxyacetic acid group participates in a hydrogen bonding network in the TR β LBD polar pocket [71]. We sought to determine how these interactions might alter coregulator specificity.

In the presence of GC-1 the coregulator peptides bound to TR β with varying degrees of affinity and all four binding modes were observed. Overall the coregulator binding patterns for GC-1 and T3 were similar in terms of which coregulator peptides were recruited. However, the degree to which they bound varied. In most cases, the coregulator peptides bound with similar or slightly lower affinity to TR β ·GC-1 than TR β ·T3. Several NR boxes, particularly those of the SRC family, exhibited significant differences in affinity to TR β ·GC-1 relative to TR β ·T3. All of the SRC2 NR boxes bound TR β ·T3 in a measurable K_d range, whereas in the presence of GC-1 a saturated binding curve was only observed for SRC2-2. Additionally, SRC1-2 appears to be much more strongly recruited by TR β ·T3, whereas the opposite is true for SRC3-3. Other notable differences between T3 and GC-1 were seen with TRAP220 and TRBP where recruitment decreased in the presence of GC-1.

In addition to studying agonist induced coregulator recruitment, we wanted to explore how antagonists may affect coregulator binding. The recently reported T3 antagonist NH-3 synthesized by Ngoc-Ha Nguyen in the Scanlan Laboratory (Figure 4-1) was tested against the entire coregulator peptide library [72]. In the

presence of saturating concentrations of NH-3, no coregulators from the library were recruited to the TR β -NH-3 complex (Figure 4-1A).

DISCUSSION AND CONCLUSION

Nuclear receptors are transcription factors that regulate a diverse set of biological events including cell proliferation, differentiation, reproduction, and development. A complex protein network consisting of NR, ligand, and coregulators controls regulation of important genes that mediate these events. Recent work has shown that the precise assembly of these complexes can signal specific biological responses [42]. However, the mechanism for the selective assembly of these complexes has yet to be elucidated. We sought to further understand the rules governing NR-coregulator selectivity.

There are several factors that may influence coregulator recruitment to NR. First, it has been shown that NRs show a clear preference for particular NR boxes and that this specificity stems from the amino acid residues immediately flanking the NR box [24], [43], [45], [46], [47]. In addition, it has been recently shown that the shape and electrostatics of the coactivator binding pocket varies with different NR, including NR isoforms, providing another level of coactivator discrimination [46]. Most of the literature reports regarding NR-coregulator specificity have focused on individual coregulators or the p160/SRC coregulator family [24], [29], [33], [35], [47], [63], [64], [65], [73]. To expand our understanding of coregulator

recruitment, we investigated the ability of TR β to bind to a library of known coregulator NR boxes using a homogenous equilibrium binding assay. While some of the interactions observed have been previously reported, no comprehensive atlas has been built using a single quantitative assay. The results from this screen demonstrate that the coregulator binding pattern for TR β is distinct from other NR (ER α , ER β , AR, data not shown) and new TR β - coregulator peptide interactions, including RIP140-5 ($K_d=2.5 \mu\text{M}$), ARA70 ($K_d=10\text{-}30 \mu\text{M}$), and DAX1-3 ($K_d=3.6 \mu\text{M}$) were identified. NR isoform distinctions were also observed. Literature reports indicate that TR α preferentially binds TRAP220-2, however in this study it was determined that TR β has a stronger affinity for TRAP220-1 [30], [65]. Based on the NR box peptides that interacted with TR β , amino acid residues that act as specificity determinants were identified. Consistent with predictions made from coactivator mimetic peptides, there is a high propensity for hydrophobic groups at the -1 position and for proline at the -2 position as seen in TRAP220 and TRBP-1 [30], [65]. Additional trends such as histidine at -3, glutamine at +6, and the presence of a serine at carboxy-terminal positions +7-+10 were also observed (Figure 4-1B).

Ligands are another factor that can impact the recruitment of coregulators to NR. Our group, along with several other laboratories, has reported that ligands allosterically modulate the coactivator binding pocket [45], [74], [47], [75]. Specifically, it was demonstrated that ER is able to selectively bind unique SRC2

peptidomimetics in the presence of different agonists. In this study, the ability of both agonists and antagonists to modulate the coactivator binding pocket of TR β were investigated. As predicted, the NR box binding patterns for TR β ·T3 and TR β ·GC-1 were different, and no coregulators were recruited in the presence of the T3 antagonist NH-3. Based on the differential NR box recruitment observed for the GC-1 ligand, specificity determinants that are distinct from T3 can be defined. While there is still a high propensity for hydrophobic amino acids at the -1 position and for serine at positions +7-+10, proline at -2 and histidine at -3 do not seem to be important for specificity in the presence of GC-1 (Figure 4-1B). In addition, the specificity determinants for TR β ·T3 and TR β ·GC-1 are distinct from those observed for the estrogen receptor with its cognate ligand (ER α ·E2). The specificity determinants for ER α ·E2 were extracted from two sources. The first sequence listed in Figure 3B for ER α ·E2 was constructed from binding data with SRCs using a time-resolved fluorescence assay and therefore amino acids are limited to SRC sequences [45]. The second source is a phage peptide screen with ER α ·E2 where three classes of peptides were identified [44]. Importantly there are differences between TR β and ER α as seen at position -2 and in the NR box at +4 and +5. The phage display studies also demonstrated that TR β had a clear preference for class II peptides containing a conserved proline at the -2 position and histidine at -3, similar to our findings.

The differential binding patterns for TR β ·T3, TR β ·GC-1, and TR β ·NH-3 may be used to predict biological responses. In hypothyroid and euthyroid hypercholesterolemic mice, GC-1 behaves like T3 to potently reduce serum cholesterol [76]. Additionally, while T3 potently induces positive inotropic and chronotropic cardiac effects, GC-1 is devoid of significant cardiac effects through a wide dose range. Although these observations may be partially explained by the selective binding of GC-1 to TR β as well as preferential liver vs. heart uptake [76], coregulator selectivity may also play a role. In the presence of T3 there is a stronger preference for the recruitment of SRC1 and SRC2 coregulator peptides to TR β , whereas SRC2 and SRC3 NR boxes are more strongly recruited to TR β ·GC-1. Recent investigations focusing on SRC1's role in regulating T3 responsive genes have revealed that SRC1 is important for the pituitary-hypothalamus-thyroid axis and for T3 effects in the heart but not for regulation of hepatic genes that regulate cholesterol levels [77-79]. This suggests that SRC2 and SRC3 regulate cholesterol modulating genes in the liver. In support of this argument, studies have shown that SRC2 and SRC3 liver expression is increased in hypothyroid mice while there is a slight decrease in SRC1 expression [80]. Other notable coregulator recruitment differences observed for GC-1 are the decrease in TRAP220 and TRBP binding. TRAP220 and TRBP appear to act as general coactivators, and their lack of interaction with TR β ·GC-1 may inhibit activation of certain genes, suggesting a possible role for these coactivators in the heart.

Studies utilizing cDNA microarrays have revealed that thyroid hormone can both positively and negatively regulate genes [17]. The mechanism for T3-dependent negative regulation of genes has yet to be fully elucidated. One mechanism may involve the T3-dependent interaction of TR with coregulators that repress gene transcription, such as RIP140 and DAX1. In our studies we find that both TR β ·T3 and TR β ·GC-1 strongly interact with RIP140-5 and DAX1-3, but TR β ·NH-3 fails to recruit these coregulators. From these observations, it can be predicted that T3 and GC-1 can repress gene transcription but NH-3 lacks this ability. Thus NH-3 treatment may result in partial activation of genes that are normally repressed by TR β ·T3. If this is the case, then NH-3 would display unique pharmacology by blocking ligand activation of positively regulated T3-responsive genes and causing derepression of negatively regulated T3-responsive genes.

Differential tissue distribution of NR and coregulators is another critical factor affecting NR-coregulator interactions. Studies using in situ hybridization and data generated from mice deficient in individual SRC family members and TRAP220 have demonstrated that these coregulators have differential tissue distribution [39], [40], [80], [81], [82]. These knock-out mice also exhibit distinct phenotypes. Mice deficient in SRC1 are resistant to thyroid hormone, whereas, mice deficient in SRC2 have normal responses to T3. This is particularly intriguing as our results indicate that SRC2 NR boxes have a stronger affinity for

TR β than for any of the SRC1 NR boxes, emphasizing the potential importance of local tissue concentrations of coregulators. SRC1 is expressed in many tissues containing T3-responsive genes including pituitary, heart, and liver. However, recent reports have demonstrated that SRC1 does not regulate all T3 responsive genes in those tissues. For instance in the liver, SRC1 is linked to spot 14 (S14) regulation, but does not seem to be required for malic enzyme activation [77]. These observations suggest there may also be zonal or temporal expression differences between coregulators.

Presumably there are additional factors that influence NR recruitment of coregulators such as post-translational modifications, structural determinants arising from specific DNA response elements, cooperativity, cellular environment, and additional interaction surfaces on the NR and coregulator proteins. To fully dissect NR-coregulator interactions, more complex models will need to be developed. The use of full-length molecules for determining NR-coregulator binding affinities has been employed with the estrogen receptors and members of the SRC family [83]. Although this work demonstrated that the binding affinities are 3-5 fold higher than predicted with coregulator peptides and NR-LBD, the overall selectivity of ER isoforms for SRC members was consistent with previous investigations. This emphasizes the utility of a simple affinity model as a first step for establishing rules of NR-coregulator selectivity.

NR signaling is a multivariant complex process that utilizes differences in NR, NR isoforms, a diverse set of coregulators, ligands, tissue variability, and unique DNA response elements. It remains unclear how this protein network can potentiate signals for specific biological responses. However one point of regulation may derive from specific NR-coregulator interactions. Using an equilibrium binding assay, the binding affinities of TR β for a large set of NR boxes in the presence of multiple ligands were quantitatively determined and some rules were defined that account for the specificity of these interactions. Additionally, it was shown that these binding patterns could be used to predict biological responses. Finally, we believe that this method may be generalized to other nuclear receptors to establish patterns of NR-coregulator selectivity.

Table 4-1. Dissociation Constants for NR box peptides for TR β

The dissociation constants for each NR box peptide are reported at each TR β ligand state. NB stands for no binding observed.

Coregulator-Peptides	K_d (μ M) \pm standard deviation		
	Ligand		
	T3	GC-1	NH-3
SRC1-1	> 30	> 30	NB
SRC1-2	10.1-30	> 30	NB
SRC1-3	10.1-30	10.1-30	NB
SRC1-4	NB	NB	NB
SRC2-1	6.0 \pm 2.0	10.1-30	NB
SRC2-2	0.7 \pm 0.2	3.8 \pm 0.1	NB
SRC2-3	4.5 \pm 1.5	10.1-30	NB
SRC3-1	> 30	> 30	NB
SRC3-2	10.1-30	10.1-30	NB
SRC3-3	> 30	10.1-30	NB
PGC-1	NB	NB	NB
TRAP220-1	2.7 \pm 1.1	10.1-30	NB

TRAP220-2	10.1-30	10.1-30	NB
TRBP-1	1.8 ± 0.1	2.7 ± 0.1	NB
TRBP-2	10.1-30	NB	NB
TRAP100-2	NB	NB	NB
TRAP100-3	NB	NB	NB
TRAP100-4	NB	NB	NB
TRAP100-6	NB	NB	NB
TRAP100-7	NB	NB	NB
ARA70	10.1-30	10.1-30	NB
ARA55	NB	NB	NB
p300	9.2 ± 2.8	10.1-30	NB
RIP140-1	NB	NB	NB
RIP140-3	> 30	> 30	NB
RIP140-5	2.5 ± 0.4	4.1 ± 0.1	NB
RIP140-6	NB	NB	NB
RIP140-7	NB	NB	NB
RIP140-8	> 30	> 30	NB
RIP140-9	NB	NB	NB
DAX1-1	NB	NB	NB
DAX1-2	NB	NB	NB
DAX1-3	3.6 ± 2.3	3.4 ± 0.9	NB
SHP	> 30	> 30	NB

METHODS

Ligand Synthesis -GC-1 and NH-3 were synthesized as previously described [70], [72].

Protein Expression and Purification- Human TR β LBD (His6; residues E202-D461) was expressed from a pET28a construct (Novagen) in BL21(DE3) (20°C, 0.5 mM IPTG added at OD600 = 0.6) as previously described [24]. Cells were harvested, resuspended in sonication buffer (20 mM Tris, 300 mM NaCl, 0.025%

tween, protease inhibitors, 10 mg lysozyme, pH 7.5, 30 minutes on ice), and sonicated for 3x3 minutes on ice. The lysed cells were centrifuged at 100,000 x g for 1 hr and the supernatant was loaded onto Talon resin (Clontech). Liganded-protein was eluted with 500 mM imidazole plus ligand (3,3',5-triiodo-L-thyronine, Sigma; GC-1; or NH-3;). Protein purity was assessed by SDS-PAGE and HPSEC and protein concentration measured by coomassie protein assay.

Peptide Library Synthesis – (Appendix A) Coregulator peptides consisting of 20 amino acids with the general motif of **CXXXXXXXXLXXL/AL/AXXXXXXXXX** were constructed, where C is cysteine, L is leucine, A is alanine, and X is any amino acid. The sequences of all the coregulator peptides were obtained from human isoform candidate genes (SRC1/AAC50305, SRC2/Q15596, SRC3/Q9Y6Q9, PGC-1/AAF19083, TRAP220/Q15648, TRBP/Q14686, TRAP100/Q75448, ARA70/Q13772, ARA55/NP_057011, p300/Q92831, RIP140/P48552, DAX-1/P51843, SHP/Q15466). The peptides were synthesized in parallel using standard fluorenylmethoxycarbonyl (Fmoc) chemistry in 48 well synthesis blocks (FlexChem System, Robbins) [57]. Preloaded Wang (Novagen) resin was deprotected with 20% piperidine in dimethylformamide. The next amino acid was then coupled using 2-(1H-Benzotriazole-1-yl)-1,1,3,3-tetramethyluronium hexafluorophosphate (2.38 equiv. wt.), Fmoc-protected amino acid (2.5 equiv. wt.), and diisopropylethylamine (5 equiv.wt.) in anhydrous dimethylformamide. Coupling efficiency was monitored by the Kaiser Test. Synthesis then proceeded

through a cycle of deprotection and coupling steps until the peptides were completely synthesized. The completed peptides were cleaved from the resin with concomitant side chain deprotection (81% TFA, 5% phenol, 5% thioanisole, 2.5% ethanedithiol, 3% water, 2% dimethylsulphide, 1.5% ammonium iodide) and crude product was dried down using a speedvac (GeneVac). Reversed-phase chromatography followed by mass spectrometry (MALDI-TOF/ESI) were used to purify the peptides. The purified peptides were lyophilized. A thiol reactive fluorophore, 5-iodoacetamidofluorescein (Molecular Probes), was then coupled to the amino terminal cysteine following the manufacturer's protocol. Labeled peptide was isolated using reversed-phase chromatography and mass spectrometry. Peptides were quantified using UV spectroscopy. Purity was assessed using LCMS (Supplemental Information).

Direct Binding Assay- (Appendix B) In 96 well plates, hTR β -LBD was serially diluted from 70 μ M to 0.002 μ M in binding buffer (50 mM Sodium Phosphate, 150 mM NaCl, pH 7.2, 1 mM DTT, 1 mM EDTA, 0.01% NP40, 10% glycerol) containing 140 μ M ligand (T3, GC-1, or NH-3). Then 10 μ L of diluted protein was added to 10 μ L of fluorescent coregulator peptide (20 nM) in 384 well plates yielding final protein concentrations of 35-0.001 μ M and 10 nM fluorescent peptide concentration. The samples were allowed to equilibrate for 30 minutes. Binding was then measured using fluorescence polarization (excitation λ 485 nm, emission λ 530 nm) on an Analyst AD (Molecular Devices). Two independent

experiments were assayed for each state in quadruplicate. Data were analyzed using SigmaPlot 8.0 (SPSS, Chicago, IL) and the K_d values were obtained by fitting data to the following equation ($y = \text{min} + (\text{max} - \text{min}) / (1 + (x/K_d)^{\text{Hillslope}})$).

ACKNOWLEDGMENTS

The authors wish to thank the DOD (DAMD17-01-1-0188), the Sandler Research Foundation, and the NIH (DK-52798 and DK-58390) for financial support.

Chapter 5

The Mechanism of Ligand Dependent Transactivation by the Androgen Receptor

Eva Estébanez-Perpiñá, Jamie Moore, Ellena Mar, Phuong Nguyen, Edson Delgado Rodrigues, John D. Baxter, Benjamin M. Buehrer, Paul Webb, Robert J. Fletterick, and R. Kiplin Guy: The Mechanism of Ligand Dependent Transactivation by the Androgen Receptor, Submitted to JBC June 2004

Copyright © 2004 by the American Society for Biochemistry and Molecular Biology

SUMMARY

Androgens drive sex differentiation, bone and muscle development, and promote growth of hormone dependent cancers by binding the nuclear androgen receptor (AR), which recruits coactivators to responsive genes. Most nuclear receptors recruit steroid receptor coactivators (SRCs) to their ligand binding domain (LBD) using a leucine rich motif (LXXLL). AR is believed to recruit unique coactivators to its LBD using an aromatic rich motif (FXXLF) while recruiting SRCs to its amino terminal domain (NTD) through an alternate mechanism. To investigate AR ability to recruit different coregulators, we looked at AR binding to our library of coregulator peptides. We determined that the AR-LBD interacts with both FXXLF motifs and a subset of LXXLL motifs including ones found in SRC2 and SRC3. In collaboration with the Paul Webb and Robert Fletcher laboratories, we were able to further confirm *in vivo* and structurally that both LXXLL and FXXLF motifs interact with AR-LBD. The Webb laboratory demonstrated that contacts with LXXLL motifs in SRC2 are both necessary and sufficient for SRC mediated AR regulation of transcription. Crystal structures, solved in the Fletcher Laboratory, of the activated AR in complex with both recruitment motifs reveal that side chains unique to the AR-LBD rearrange to bind either the bulky FXXLF motifs or the more compact LXXLL motifs, and that AR utilizes subsidiary contacts with LXXLL flanking sequences to discriminate between LXXLL motifs.

INTRODUCTION

The cellular effects of the hormone 5- α -dihydrotestosterone (DHT) are mediated by the androgen receptor (AR), a member of the nuclear hormone receptor superfamily [84]. AR is absolutely required for normal male development, plays a variety of important roles in metabolism and homeostasis in adult men and women, [85], [86] and is required for prostate cancer growth. Consequently, AR is a major target for pharmaceutical development and the recognized target for existing prostate cancer therapies, including androgen withdrawal and antiandrogens [84], [86], [87], [88]. It is nonetheless desirable to obtain new antiandrogens that spare patients from harmful side effects and inhibit AR action in secondary hormone resistant prostate cancer, where AR action becomes sensitized to low levels of androgens or existing antiandrogens (Santos, 2004 #147), [89]. Improved understanding of AR signaling pathways will facilitate development of these compounds.

Like most nuclear receptors (NRs), AR activity depends on interactions with members of steroid receptor coactivator (SRC) family [84], [90], [91]. Several lines of evidence indicate that AR contacts with SRCs are important in prostate cancer. First, androgens promote SRC recruitment to the androgen-regulated prostate specific antigen promoter and this event is inhibited by the antiandrogen flutamide [92]. Second, exogenous SRC2 (GRIP1/TIF2) promotes the androgen-dependent progression from the G1 to S phase in LNCaP prostate tumor cells, in

a manner that requires specific AR contact [92]. Third, SRCs often become expressed at high levels in prostate cancers [87]. Finally, AR contacts with SRCs

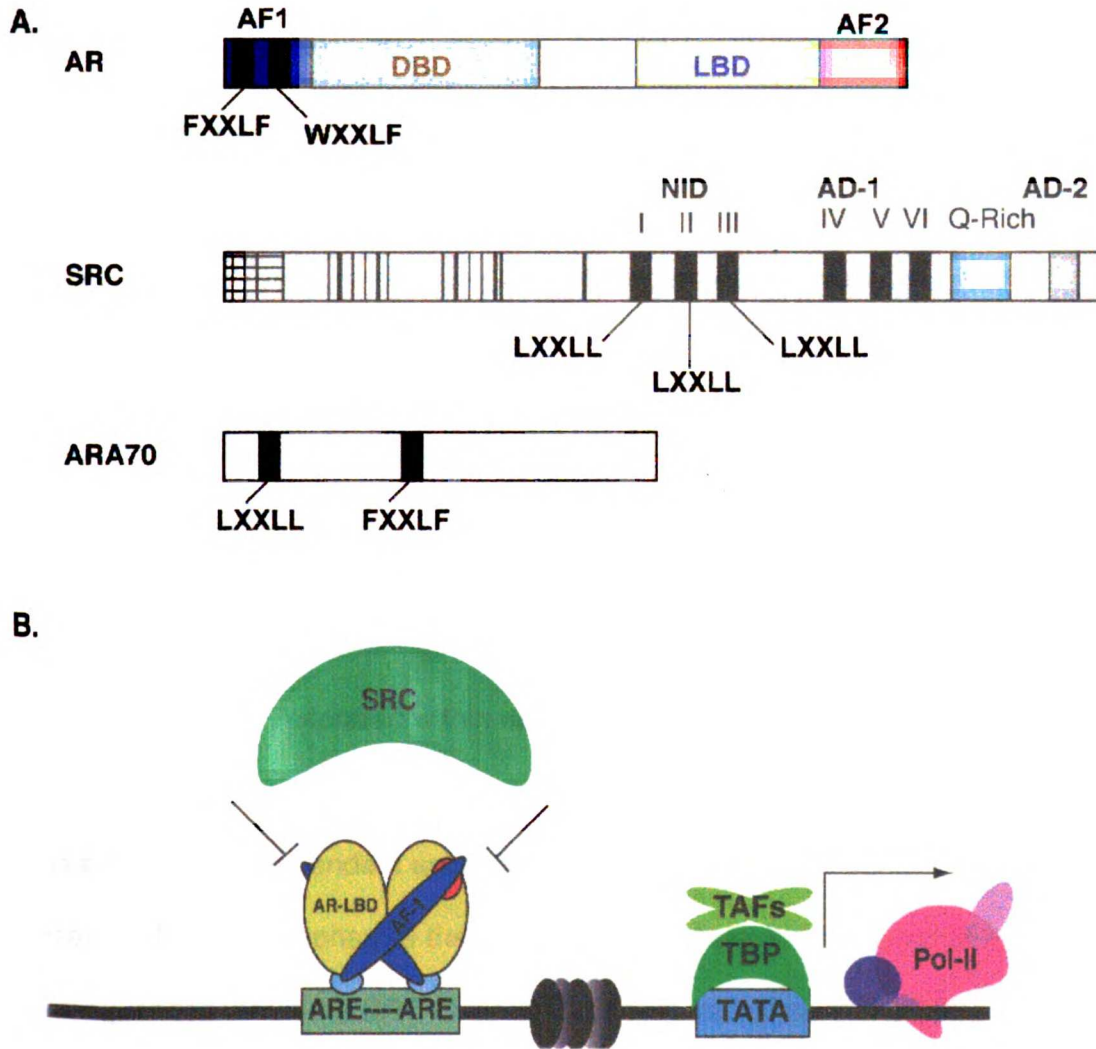


FIGURE 5-1. AR Model of Activation

A. The primary structure for the androgen receptor (AR), steroid receptor coactivator (SRC), and androgen receptor activator 70 (ARA70) are shown. AR has **two** activation function domains, AF-1 and AF-2. AF-1 is a ligand independent activation function and contains two interaction motifs, FXXLF and WXXLF, that are believed to interact with the AF-2 of AR either intra- or intermolecularly. SRCs contain three interaction motifs with the consensus sequence, LXXLL, in the nuclear interaction domain (NID) that are known to interact with the AF-2 of nuclear receptors. ARA70 is an AR specific coactivator

that contains both LXXLL and FXXLF interaction motifs capable of interacting with the AF-2 of AR. B. The current model for AR activation is shown. The current model suggests that FXXLF and WXXLF motifs make intramolecular interactions with the AF-2 of AR, therefore forming head-to-tail dimers. This dimer formation prevents AR from interacting with traditional LXXLL containing coactivators via its AF-2 and instead it is believed that the glutamine rich domains found in SRCs may be recruited.

mediate hormone-independent AR signaling in conditions that resemble secondary prostate cancer [93], [94]. Thus, strategies to inhibit AR contacts with SRCs could represent useful strategies to block prostate cancer cell growth.

For many NRs, overall transcriptional activity stems mostly from the hormone-dependent activation function (AF-2) within the NRs ligand binding domain (LBD), and involves interaction between a conserved hydrophobic cleft on the surface of the LBD and short leucine rich hydrophobic motifs (NR boxes, consensus LXXLL) reiterated within each SRC [95], [22]. (Figure 5-1A). In contrast, current models of AR action generally suggest that AR activity derives from a hormone independent activation function, AF-1, within the AR's N-terminal domain (NTD) and emphasize the role of contacts between NTD and glutamine rich sequences within the SRC C-terminus in SRC recruitment [96], [97], [98], [99], [100] (Figure 5-1).

The AR-LBD is proposed to bind LXXLL motifs weakly, and instead bind to aromatic rich motifs (FXXLF) that are found both within the AR-NTD and AR specific coactivators such as ARA70 (Figure 5-1A) [97], [101], [102], [103], [104].

Further, intramolecular interactions between the LBD and the NTD FXXLF motif promote formation of head to tail dimers, which render the AF-2 surface unavailable for direct cofactor contacts [101] (Figure 5-1B). It is believed that this dimer formation stabilizes the overall structure of AR to slow ligand dissociation and maintain AR in an active conformation. Together, both lines of evidence have suggested that AR AF-2 does not play an active role in SRC recruitment.

In this collaborative study with the Paul Webb and Robert Fletcher Laboratories, we examine AR AF-2 interactions with target coregulators using three different approaches. We first investigated the ability of AR-LBD to interact with our library of coregulator peptides using our *in vitro* fluorescence polarization binding assay. Our studies confirm that AR AF-2 binds FXXLF motifs, but also show that AR AF-2 binds a subset of SRC LXXLL motifs with higher affinity. These AR coregulator binding patterns were confirmed *in vivo* by the Webb laboratory and demonstrate that specific LXXLL motifs are required to mediate AR AF-2 activity. Finally, the Fletcher Laboratory provides crystallographic evidence that AR-LBD can form complexes with both native FXXLF and LXXLL peptides. These crystal structures reveal the structural basis for the unusual coactivator binding preferences, and may suggest new approaches to drug design.

RESULTS AND DISCUSSION

To understand the unusual spectrum of AR AF-2 coactivator interactions, we measured binding of the AR-LBD to a library composed of NR boxes from known

coactivating proteins including traditional LXXLL coregulators and AR specific coactivators with the FXXLF motif. However, initial testing with a GST AR-LBD construct proved to be unsuccessful (Figure 5-2) and no binding was observed independent of binding buffer conditions. After protein expression and purification were optimized, we tested AR-LBD with the entire coregulator peptide library and observed saturable binding with some coregulator peptides (Figure 5-2 and Figure 5-3, Figure 5-4A). As expected, AR-LBD bound FXXLF sequences present in ARA70 and the AR-NTD [101], [105]. Surprisingly, AR also recognized a subset of NR boxes from the SRC family [106]. Specifically, peptides of the first (SRC2-1) and third (SRC2-3) NR boxes of SRC2 (GRIP1/TiF-2/N-CoA-2) and the third NR box of SRC3 bind strongly to AR, followed in affinity by FXXLF motifs. In addition, we observed weak interactions with the following coregulator peptides: NR boxes from SRC1, SRC2-2, SRC3-1, SRC3-3, TRAP220-2, RIP140-5, and some NR boxes from DAX-1. We also observed weak interactions with TRAP100-2. This is intriguing as we have yet to see any other NR (TR, ER, SF-1, LRH) interact at any level with the TRAP100 NR boxes. Most of these coregulator interactions with AR have not previously been reported. Although some literature indicates that AR may weakly interact with SRC2 NR boxes[91], most reports suggest that the glutamine rich domain in SRC2 may be more important for AR contacts [96], [97], [98], [99], [100]. Phage display libraries containing LXXLL peptides predicted that AR would only bind to a small subset of LXXLL peptides with the consensus sequence SSRLSSLLM [107]. Our

results contradict this, as we identified very different LXXLL motifs. Our coregulator peptide libraries also contained control peptides where sequences in LXXLL or FXXLF had been converted to LXXAA or FXXAA confirming the binding was dependent upon the intact triad of hydrophobic amino acids (Figure 5-2).

Confirmation of AR-coregulator binding patterns were carried out in Paul Webb's Laboratory demonstrating that the AR-LBD bound SRC coactivators relatively strongly compared to similar preparations of other NR-LBDs and did so in a manner that was dependent upon LXXLL motifs (not shown). Thus, AR-LBD binds FXXLF motifs, but also binds a subset of classic NR box peptides with comparable or higher affinities. Moreover, the preference of AR for individual LXXLL motifs is different from that observed with other NRs, such as the estrogen receptor (ER) and thyroid receptors (TRs), which bind box 2 in each of the three SRCs with high affinity [108], [109], [24], [110] (Figure 5-3).

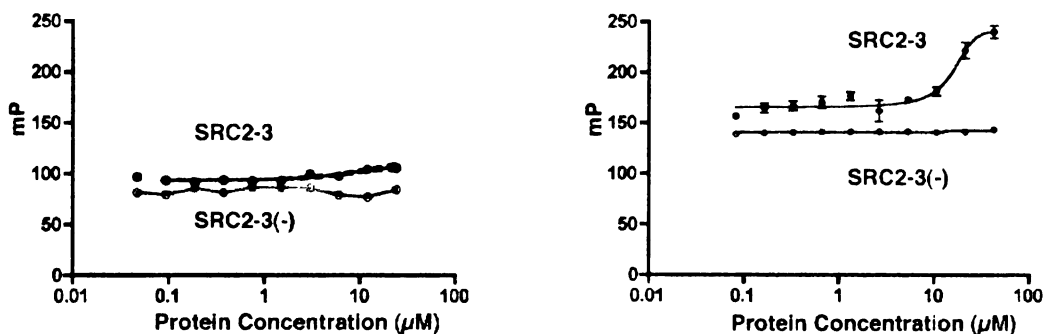


FIGURE 5-2. AR-LBD Coregulator Interactions

Binding isotherms for AR-LBD and SRC2-3 are shown. The binding isotherm on the left was constructed with GST protein (646-919) prior to optimization of protein expression and purification. No coregulator binding was observed for this

protein. After production of stable protein, saturable binding isotherms were observed for SRC2-3. The green solid circles and lines represent SRC2-3 (LXXLL), the red open circles and solid lines represent SRC2-3(-) negative controls (LXXAA).

Paul Webb's laboratory went on to demonstrate that signaling of full length AR acting at an androgen sensitive promoter was enhanced by exogenous expression of SRC2, in accordance with previous results (Figure 5-4B) [98]. This result confirms the functional consequences of the binding of SRC2 to full length AR. This was a surprising result given that current models of AR action suggest that SRCs enhance AR activity by binding to the AR-NTD and enhancing AR AF-1 activity, [98], [99], [100], [111]. This enhancement of signaling was lessened when the third NR box (SRC2-3) was mutated to LXXAA, consistent with in vitro binding results (Figure 5-4A). Thus, NR box SRC2-3, which interacts with AR AF-2 and not AR AF-1, seems to be sufficient and required to provide co-activation of AR by SRC2. The Webb laboratory also confirmed that AR-LBD (amino acids 646-919) confers androgen-dependent transcriptional activity on a reporter gene (Figure 5-5). The AR AF-2 induced transcriptional activity more potently than AR AF-1 in HeLa and DU145 prostate cancer cells and was about 20-30% as potent as that induced by TR and ER α LBDs that bind a wider range of SRCs (not shown). Thus, our results are consistent with the notion that AR AF-2 is potent [112], [113] and contradict the notion that AR AF-2 has little or no intrinsic activity. Further, AR AF-2 was inhibited by anti androgens such as flutamide and RU486 (not shown), confirming the requirement for functional LBD.

Simultaneous expression of SRC2 and the AR LBD strongly enhances transcriptional activity – more strongly than full length AR (Figure 5-5). Mutation of individual SRC2 NR boxes revealed a requirement for boxes 1 and 3 to provide full AR AF-2 activity. Thus, in the context of an isolated AR LBD, there is exact congruence between coactivator affinity and transactivation. Control experiments confirmed that, in contrast, SRC2-2 is required to mediate thyroid hormone receptor (TR β) AF-2, consistent with our own determinations, which show that this NR box motif exhibits high affinity for TR β [90], [24] (Figure 5-3). Finally, each mutant SRC retains the property of enhancing the activity of the CBP SRC binding region (AD2) [90] with comparable activity to wild type SRC2, confirming that NR box mutations do not affect other elements of SRC2 activity. Thus, AR AF-2 can bind FXXLF motifs, providing hormone dependent activation, but the fact that SRC2 coactivation of AR is dependent upon LXXLL motifs indicates that AR can also activate transcription using the same mechanism as other NRs. While the requirement for SRC2 LXXLL motifs in AR coactivation has not been previously documented, SRC2 does enhance the androgen-dependent G1 to S transition in LNCaP prostate tumor cells in a manner that is dependent upon the SRC2 NR box region (which binds AF-2) and independent of the SRC2 C-terminus (which binds AR AF-1) [92]. Thus, AR AF-2 contacts with SRC LXXLL motifs may be relevant for androgen-dependent cell cycle progression.

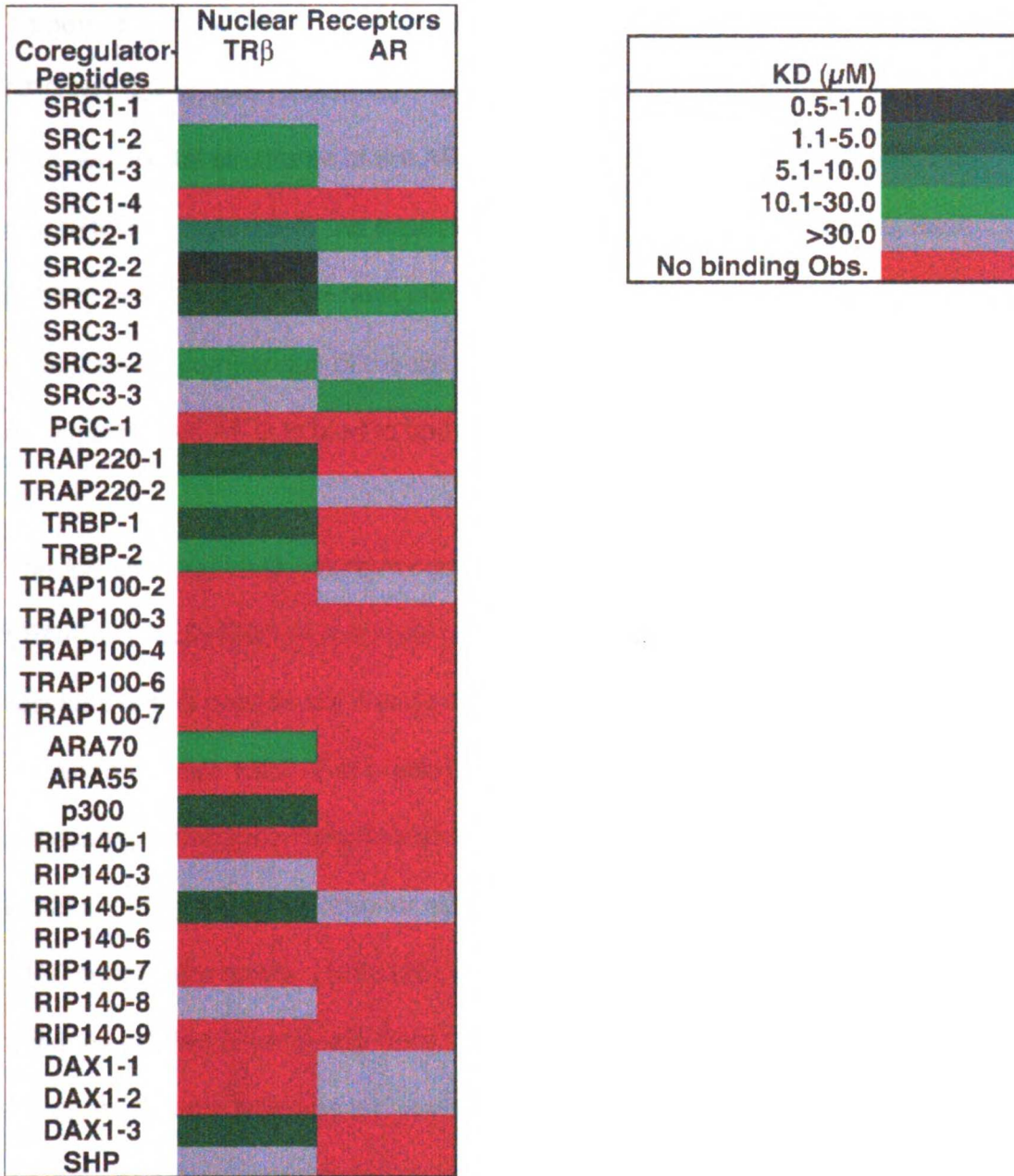


FIGURE 5-3. Comparison of AR and TR NCOA Recruitment

The equilibrium binding constants for TR β -coregulator and AR-coregulator NR boxes are reported. The coregulator peptides are listed in the left column where SRC1-1, SRC1-2, SRC1-3, SRC1-4 represent the first, second, third, and fourth NR box in SRC1, respectively. Each color represents a unique K_d range as defined by the legend on the right.

To determine how AR binds aromatic rich coactivator domains and the subset of SRC NR boxes, Eva Estébanez-Perpiñá in the Robert Fletterick Laboratory obtained crystal structures of the AR-LBD in complex with ARA70-2, SRC2-2, and SRC2-3 (Figure 5-6). As expected by analogy with other NR AF-2s, each peptide binds as a short α -helix into the L-shaped hydrophobic cleft.

Nonetheless, comparison of the structures also reveals features that explain the ability of the AR AF-2 to bind to both LXXLL and FXXLF motifs.

The AR LBD crystal structure in complex with the SRC2-3 peptide KENALLRYLLDKDD (14 mer) has been solved to 2.07 Å resolution. Thirteen residues of this peptide are clearly defined in the electron density, and the interaction buries 1322 Å² of predominantly hydrophobic surface area from both molecules. Estébanez-Perpiñá's structure shows that SRC2-3 hydrophobic motif binds in nearly the same manner as previously stated in other NRs with LXXLL p160 coactivator motifs [108], [26], [114], [115], [26, 108, 114, 115]. The residues located N-terminally from the first Leu residue (residue +1) are termed -1, -2, and so on, whereas the residues C-terminal from Leu+1, are termed +2, +3, etc. The core hydrophobic motif of the peptide (residues +1 to +5) forms a short α -helix that binds in the groove formed by helices 3, 4, 5, and 12. The LBD interacts primarily with the hydrophobic face of the SRC2-3 peptide α -helix formed by the side chains of the three LXXLL motif leucines (Leu923, Leu926

and Leu927). The side chain of Leu923 is embedded within the groove and forms van der Waals contacts with

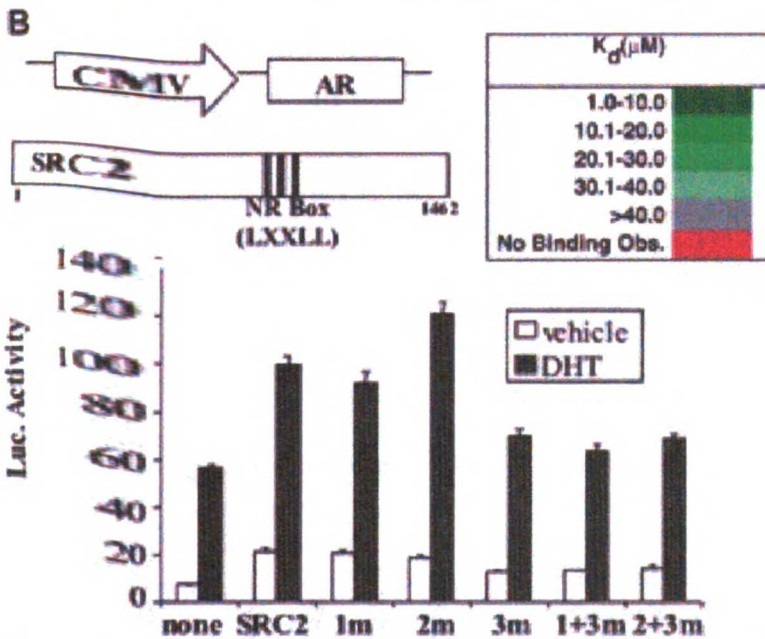
A

Coregulators	Sequence	AR	
		AR	AR (E897Q)
		1	2
SRC1-1	CYSQTSHKLVQLLTTTAEQQ	Dark Blue	Dark Blue
SRC1-2	CLTARHKILHRLLOEGSPSD	Dark Blue	Dark Blue
SRC1-3	CESKDHQLLRYLLOKDEKDL	Dark Blue	Dark Blue
SRC2-1	CDSKGQTKLLQLLTTKSDQM	Green	Dark Blue
SRC2-2	CLKEKHKILHRLLODSSSPV	Green	Dark Blue
SRC2-3	CKKKENALLRYLLODKDDTKD	Green	Dark Blue
SRC3-1	CESKGHKLLQLLTCSSDDR	Dark Blue	Dark Blue
SRC3-2	CLOEKHRI LHKLLONGNSPA	Dark Blue	Dark Blue
SRC3-3	CKKENALLRYLLODDPSPD	Dark Blue	Dark Blue
ARA70-1	CLOQQAQQLYSLLGQFNCLT	Red	Dark Blue
ARA70-2	CSRETSEKFKLLFQSYNVND	Green	Dark Blue
NTD-1	CTYRAGAFONLFQSVR	Green	Dark Blue
NTD-2	CAAASSWHTLFTAAE	Dark Blue	Dark Blue

FIGURE 5-4. AR Interacts with LXXLL and FXXLF Coregulator NR Boxes

The androgen receptor ligand binding domain (AR-LBD) binds a subset of steroid receptor coactivator (SRC) nuclear receptor interaction motifs (NR Boxes) and this interaction is sufficient and required for achieving of full length AR transactivation by the SRC. Panel A:

Sequences of relevant NR Boxes and relative equilibrium affinities of these NR boxes for binding to AR LBD and a mutant AR LBD in which one charge clamp residue has been neutralized. The binding affinities were determined using fluorescence polarization with fluorescently labeled NR box peptides. The coregulator peptides are



listed in the left column where SRC1-1, SRC1-2, SRC1-3, represent the first, second, and third NR box in SRC1, respectively. Each color represents a unique K_d range as defined by the legend in the bottom right-hand corner. (B) Transcriptional activation of an androgen response element (ARE) driven luciferase reporter construct cotransfected with a CMV driven full length androgen receptor in the presence or absence of exogenous wild type SRC2 and

SRC2 with mutationally inactivated NR boxes (1m implies LXXLL mutated to LXXAA for NR box SRC2-1, and so on).

the side chains of Val716, Met734, and Asn738. The side chain of Leu927 is also isolated within the groove and makes van der Waals contacts with the side chains of Gln733 and Met734. The side chain of the second NR box 3 leucine, (Leu926), makes van der Waals contacts with the side chains of Val716 and Met894. The LBD residues implicated in hydrophobic contacts with the peptide are valines 716, 730, and 901, methionines 734, 894, glutamines 733 and 738, Ile898, and the non-polar parts of Asp731 and Glu 893 and 897.

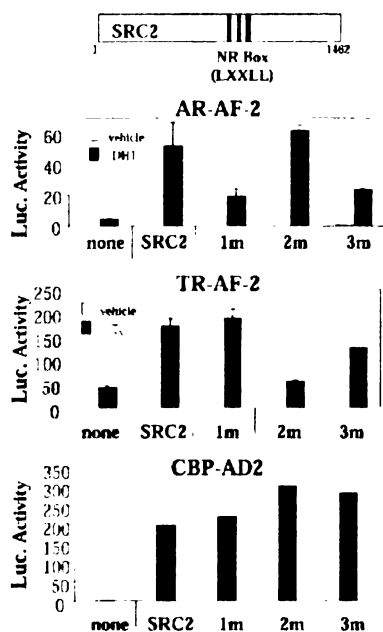


FIGURE 5-5. AR-LBD Confers AF-2 Activity

The effects of mutation of SRC2 NR boxes 1 through 2 upon signaling by GAL4-AR and GAL4-TR LBD constructs from a GAL driven luciferase reporter. Mutation of SRC2-1 and SRC2-3 both significantly reduce potentiation of transactivation by AR while not affecting transactivation by TR. Contra wise, Mutation of SRC2-2 significantly reduces transactivation by TR but not by AR. These mutational effects correlate with the observed relative affinities of the NR boxes for the respective receptors. As expected, none of the mutations significantly reduces transactivation by CBP, which interacts with a distinct locus on the SRC2 molecule, C-terminal to the LXXLL motifs.

The main chain carbonyl groups of residues Leu927, Asp930 and Asp931 from the SRC2-3 peptide also interact with Lys720, which is highly conserved in NRs and comprises the upper part of a charge clamp that stabilizes the α -helical NR box peptide conformation. However, contrary to predictions made on the basis of mutagenic analysis of AR surface residues[116] and comparisons with a glucocorticoid receptor (GR)/SRC2-3 structure [114], the SRC2-3 peptide does not form any hydrogen bonds to the second highly conserved charge clamp residue, Glu897 on Helix 12. Instead, the peptide engages in hydrophobic contacts with Glu897, and the distance to the three unpaired amide NH of the peptide helix is 5Å, so electrostatic stabilization is not possible. The peptide also engages in hydrogen bonding to seven water molecules in its vicinity. Residue Asp928 located at position +6 adopts two different conformations. However, neither Asp928 (+6) nor Arg924 (+2) interact with charged residues on the AR surface that comprise a second charge clamp, again contrary to predictions made on the basis of a GR/SRC2-3 structure[114]. Nonetheless, the SRC2-3 peptide displays clear electron density in the current structure for five residues N-terminal to the core hydrophobic motif and for four more residues C-terminal to the same motif, therefore displaying significantly greater electron density than any other NR box peptide in complex with a NR LBD to date.

Except for three N-terminal residues that are disordered, the position and interactions of the ARA70 FXXLF peptide with the AR surface more closely

recapitulate the binding mode observed in structures of ternary complexes of SRC LXXLL motifs with hormone bound NR LBDs (Figure 5-6A and 5-6C) [114] [108], [26], [115]. The triad of aromatic side chains (FXXLF) that forms the hydrophobic face of the coactivator helix fits tightly into a deep narrow pocket. In addition, charged residues at either end of the cleft, Glu897 and Lys720, cap the helix (the “charge clamp”). The fully engaged interaction is manifested in the tight binding of this coactivator and its strong transactivation.

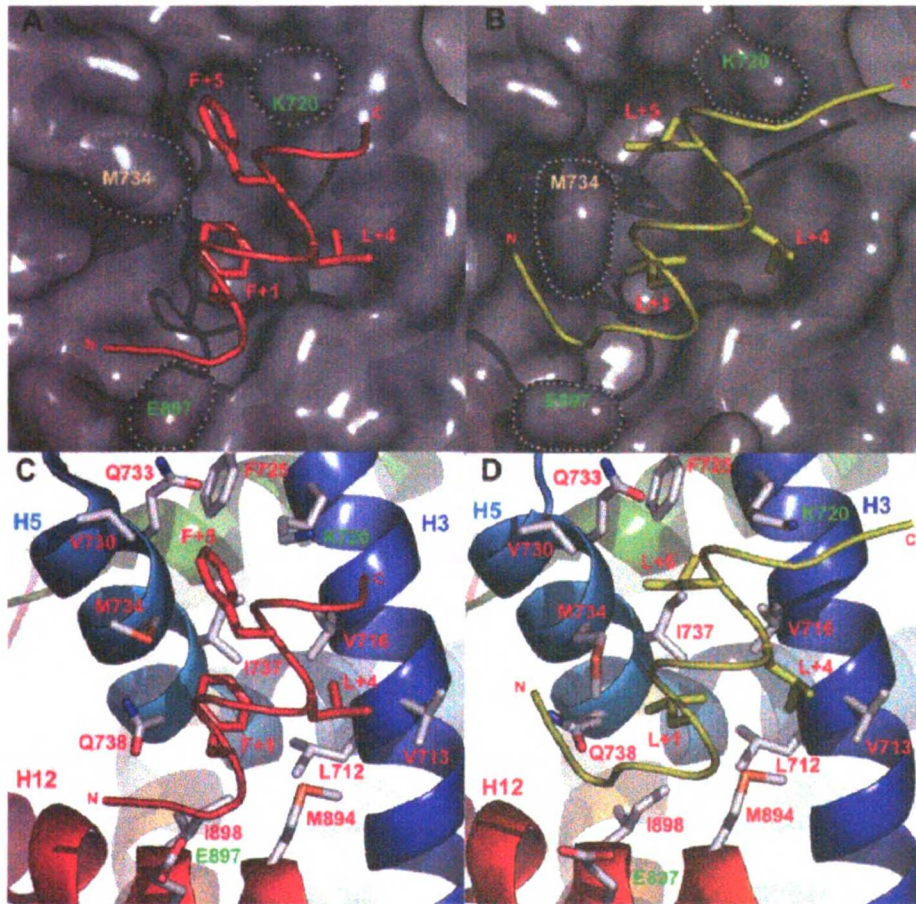


FIGURE 5-6. AR-LBD Structures with ARA70-2 and SRC2-3.

Associations of the AR-LBD with coactivator domains determined by X-ray crystallography. Close-up views of the interaction between ARA70, and SRC2-3 peptides with AR LBD AF2. The nuclear receptor AF-2 transactivation function is ascribed to a surface exposed hydrophobic cleft comprised of residues from helices 3 (H3), 5 (H5) and 12 (H12). A. The helix backbone of peptides from ARA70 (RETSEKFKLLFQSYN) (left red) and SRC2-3 (KENALLRYLLDKDD) (right yellow). AR LBD is represented by a solid semi-transparent surface (grey) on the top figures. The side chains of the motif hydrophobic residues Phe+1/Leu+1, Leu+4 and Phe+5/Leu+5 of the peptides are shown as stick models. Helix 12 is shown in red, with its Glu897 side chain stabilizing the N-terminus of the ARA70 peptide, but not the SRC2-3 peptide. On helix 3 (dark blue), the side chain of K720 is shown capping the C-terminus of both peptides. B. The side chains of the AR LBD residues contacting the peptides are depicted as stick models. ARA70: The triad of aromatic side chains (FXXLF) fits tightly into a deep narrow pocket comprised of Val 716 and Val730, Met734, Ile737, and the hydrophobic segment of Glu893. The Leu side chains of SRC2-3 fits loosely into a flat hydrophobic pocket comprised of the side chains of three valines, 716, 730, and 901, methionines 734, 894, glutamines 733 and 738, and Asp731 and Glu897. The accommodation of the bulkier Phe residues of ARA70 is accompanied by the rearrangements of Met734, Glu897, and Lys720 predominantly (indicated by grey dots on the AR's surface representation). All the figures were generated with Pymol [117].

To understand the apparent discrepancy between the reported requirement for Glu897 in AR AF-2 activity and its lack of contact with the LXXLL motif of SRC2-3 in the crystal structure, we examined effects of mutations in the AR-coactivator binding interface (Figure 5-6). Mutations that eliminated the upper charge clamp residue (Lys720Ala) inhibited AR AF-2 activity, as did introduction of positive charge at Glu 897 (Glu897Lys, Glu897Arg) [116], [113]. However, mutations that neutralized or lessened electrostatic potential at Glu897 (Glu897Ala, Glu897Gln) retained significant AF-2 activity (Figure 5-7A) [91]. The same mutations failed to disrupt AR interactions with SRC2 in binding assays with both peptides (Figure 5-4A) and full length SRC2 (Figure 5-7C). However, these mutations disrupt

binding with ARA 70 and AR-NTD FXXLF peptides (Figure 5-3A) and the AR NTD in pulldown assays (Figure 5-6B). Thus, the lower charge clamp residue is dispensable for SRC2 binding but required for ARA70 binding, exactly paralleling the requirement for E897 observed in both of our crystal structures.

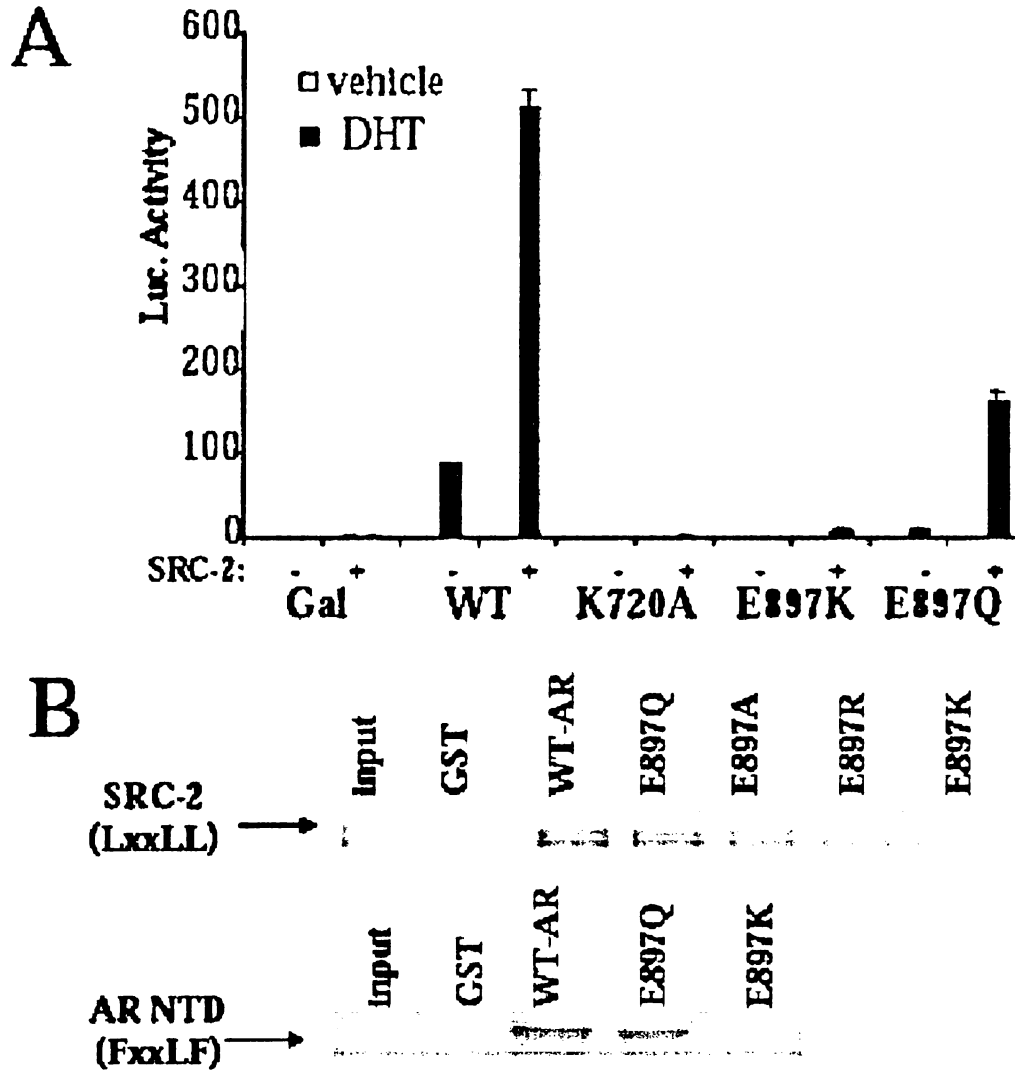


FIGURE 5-7. Effects of AR-LBD Mutations
 Role of the binding pocket and charge clamp residues of the AR-LBD AF-2 in potentiation of transcriptional activation by a GAL4-AR LBD construct. Panel A. Removing the charge at K720 or reversing the charge at E897 (the positive and

negative ends of the “charge clamp” that stabilizes helix dipole for the NR box) strongly reduces transcriptional activation by the AR-LBD. Panel B. The same mutations that effect AR-LBD transactivation also similarly effect potentiation of transcriptional activation by SRC2. Neutralization of charge at E897 is much less penetrant than similar mutations at K720. However, as would be expected from the binding data, there is no additional reduction in transcriptional activation due to failure to bind SRC 2.

Comparisons of each of the ternary complexes with each other, and with our own structures of AR in the absence of an associated peptide (not shown), reveal features that explain the ability of AR to bind both types of motif. The ability of AR AF-2 to accommodate both FXXLF and LXXLL motifs appears to derive from a striking rearrangement of the AF-2 surface. Movements of Lys720, Met734, and Glu897 create the deeper pockets and enhanced electrostatics allowing the binding of ARA70 (Figure 5-5).

The SRC2-3 LXXLL motif, by contrast to the ARA70 FXXLF motif and a variety of NR box peptides in complex with a variety of NR-LBDs is translated by about 2Å in the cleft, towards helix 3. This unusual positioning disrupts the electrostatic stabilization characteristic of most NR/NR box interactions, likely explaining reduced AR binding to most LXXLL motifs. However, for SRC2-3, the high degree of negative charge in the four residues following the motif (sequence DKDD) interacts with positively charged patches on the receptor surface. In fact, these portions of the structure are better ordered than in all previous NR-coactivator complexes, and are not visible in AR-LBD structures with the SRC2-2 *peptide* (not shown), which binds the AR-LBD with lower affinity. This influence

offsets suboptimal electrostatics and explains the selective binding of AR AF-2 to SRC2-3.

CONCLUSION

In conclusion, AR has a potent AF-2 that drives the cell's expression program by binding FXXLF motifs and selected LXXLL motifs. The receptor uses the same general coactivator binding mechanisms as other NRs, by providing a dimorphic cleft that facilitates interaction with aromatic amino acids in addition to leucines. The ability of the AR surface to rearrange to interact with FXXLF motifs is unique among transcription factors and represents a gain of function relative to other structurally defined interactions in the family. Most NRs are unable to accommodate bulky sidechains in the binding domains of the coactivators, and the dyadic recognition of AR has enabled development of more complex control mechanisms involving the NTD and the use of specialized subsets of coactivators. Most importantly, the new function *does not* come at the cost of a loss of ability to interact productively with SRCs. AR AF-2 interactions with SRCs are likely to be physiologically relevant, particularly in certain forms of prostate cancer.

METHODS

Construction of AR Mutants

Gal-AR LBD and GST AR LBD contained amino acids 646-919. AR sequences were amplified from AR coding sequences with standard PCR methodology and

cloned into the pM GAL4 vector (Clontech) or PGEX 5X-1 vector (Stratagene), respectively. Mutations were created using the QuickChange XL Site-Directed Mutagenesis Kit (Stratagene). Mutation of target sequences was verified by automated DNA sequence (Elim Biopharmaceuticals, Inc., Hayward, CA). GRIP1 NR box mutations were obtained similarly.

Protein Expression and Purification

AR-LBD (residues 663-919) has been expressed in *E. coli* and purified to homogeneity. We used a GST-fusion expression system using a modified version of protocols previously published [118]. Bacterial cell preparations are grown at ambient or lower temperatures to high OD at 600nm (>1.00) in 2XLB supplemented with DHT. AR-LBD protein is expressed by induction with IPTG for 14-16 hours at 15°C before harvest and cell lysis by freeze-thawing and mild sonication. Purification involves an initial affinity chromatography step using a glutathione Sepharose column, followed by thrombin cleavage of the GST affinity tag. We finally use cation exchange chromatography with Sepharose SP. Our procedures differ from published work in that we use Sepharose SP for the second purification step instead of Fractogel SO₃, which does not retain AR in our experiments.

Peptide Library Synthesis

Coregulator peptides consisting of 20 amino acids with the general motif of **CXXXXXXXXLXXL/AL/AXXXXXXXXX** were constructed, where C is cysteine, L is leucine, A is alanine, and X is any amino acid. The sequences of all the coregulator peptides were obtained from human isoform candidate genes (SRC1/AAC50305, SRC2/Q15596, SRC3/Q9Y6Q9, PGC-1/AAF19083, TRAP220/Q15648, TRBP/Q14686, TRAP100/Q75448, ARA70/Q13772, ARA55/NP_057011, p300/Q92831, RIP140/P48552, DAX-1/P51843, SHP/Q15466). The peptides were synthesized in parallel using standard fluorenylmethoxycarbonyl (Fmoc) chemistry in 48 well synthesis blocks (FlexChem System, Robbins) [57]. Preloaded Wang (Novagen) resin was deprotected with 20% piperidine in dimethylformamide. The next amino acid was then coupled using 2-(1H-Benzotriazole-1-yl)-1,1,3,3-tetramethyluronium hexafluorophosphate (2.38 equiv. wt.), Fmoc-protected amino acid (2.5 equiv. wt.), and diisopropylethylamine (5 equiv.wt.) in anhydrous dimethylformamide. Coupling efficiency was monitored by the Kaiser Test. Synthesis then proceeded through a cycle of deprotection and coupling steps until the peptides were completely synthesized. The completed peptides were cleaved from the resin with concomitant side chain deprotection (81% TFA, 5% phenol, 5% thioanisole, 2.5% ethanedithiol, 3% water, 2% dimethylsulphide, 1.5% ammonium iodide) and crude product was dried down using a speedvac (GeneVac). Reversed-phase chromatography followed by mass spectrometry (MALDI-TOF/ESI) were used to purify the peptides. The purified peptides were lyophilized. A thiol reactive

fluorophore, 5-iodoacetamidofluorescein (Molecular Probes), was then coupled to the amino terminal cysteine following the manufacturer's protocol. Labeled peptide was isolated using reversed-phase chromatography and mass spectrometry. Peptides were quantified using UV spectroscopy. Purity was assessed using LCMS.

Peptide Binding Assay

Using a BiomekFX in the Center for Advanced Technology (CAT), AR-LBD was serially diluted from 70 μM to 0.002 μM in binding buffer (50 mM Sodium Phosphate, 150 mM NaCl, pH 7.2, 1 mM DTT, 1 mM EDTA, 0.01% NP40, 10% glycerol) containing 140 μM ligand (dihydroxytestosterone) in 96 well plates. Then 10 μL of diluted protein was added to 10 μL of fluorescent coregulator peptide (20 nM) in 384 well plates yielding final protein concentrations of 35-0.001 μM and 10 nM fluorescent peptide concentration. The samples were allowed to equilibrate for 30 minutes. Binding was then measured using fluorescence polarization (excitation | 485 nm, emission | 530 nm) on an Analyst AD (Molecular Devices). Two independent experiments were assayed for each state in quadruplicate. Data were analyzed using SigmaPlot 8.0 (SPSS, Chicago, IL) and the K_d values were obtained by fitting data to the following equation ($y = \text{min} + (\text{max} - \text{min}) / (1 + (x / K_d)^{\text{Hillslope}})$).

GST Pull-Down Assays

Full-length SRC-2 (amino acids 1-1462) and AR NTD-DBD (amino acids 1-660) was expressed in a coupled transcription/translation system (TNT, Promega). AR LBD (amino acids 646-919), or AR LBD mutants, were expressed in *Escherichia coli* strain BL21 as a glutathione S-transferase (GST) fusion protein and attached to glutathione beads according to manufacturer's protocol (Amersham Pharmacia Biotech). Binding assays were performed by mixing glutathione-linked Sepharose beads containing 4 mg of GST fusion protein (estimated by Coomassie Plus protein assay reagent, Pierce) with 2 ml of ³⁵S-labeled SRC-2 or AR NTD-DBD in 20 mM HEPES, 150 mM KCl, 25 mM MgCl₂, 10% glycerol, 1 mM dithiothreitol, 0.2 mM phenylmethylsulfonyl fluoride, 20 mg/ml bovine serum albumin and protease inhibitors containing to a final volume of 150 ml. The bead mix was shaken at 4°C for 1.5 h, washed three times in 200 ml of binding buffer. The bound proteins were resuspended in SDS-PAGE loading buffer and were separated using 10% SDS-polyacrylamide gel electrophoresis and visualized by autoradiography.

Cell Culture and Transfection Assays

HeLa cells were maintained in DME H-21 4.5 g/l glucose, containing 10% steroid depleted fetal bovine serum (Gibco), 2 mM glutamine, 50 units/ml penicillin, and 50 mg/ml streptomycin. For transfection, cells were collected and resuspended in Dulbecco's phosphate-buffered saline (0.5 ml/4.5 x10⁷ cells) containing 0.1% dextrose, and typically 4 mg of luciferase reporter plasmid, 1 mg of AR

expression vector or empty vector control, and 2 mg of pCMV-b-galactosidase. Cells were electroporated at 240V and 960 microfarads, transferred to fresh media, and plated into 12-well plates. After incubation for 24 h at 37°C with androgen or vehicle, cells were collected and pellets were lysed by addition of 150 μ l of 100 mM Tris-HCl, pH 7.8 containing 0.1% Triton X-100.

For transfections with full length AR, the reporter gene utilized the Mouse Mammary Tumor Virus promoter fused to luciferase. For transfections with GAL-AR LBD, GAL-TR LBD and GAL-CBP fusions the reporter contained five GAL 4 response elements upstream of a minimal promoter. LUC and b-galactosidase activities were measured by using the Luciferase Assay System (Promega) and Galacto-Light Plus beta-Galactosidase Reporter Gene Assay System (Applied Biosystems), according to the manufacturer's instructions.

Crystallization, Structure Determination and Refinement

The complexes of peptide and AR LBD were prepared by mixing at 0°C for 2 hr, variable ratios of peptide (3 to 10 mM) and protein (at about 4.5 mg/ml). Crystals were obtained by vapor diffusion methods (sitting-drop technique) using crystal screens from Hampton. The protein-peptide complex solution was mixed with the reservoir solution (0.8M Na-Citrate, 0.1 M Tris pH=7.5 or pH=8.0), and concentrated against 300 μ l of the reservoir. Crystals appeared after one day and grew to maximal dimensions after four days. After four days these crystals started to crack so new crystallization trials were necessary to find additives that

stabilize the crystals. NaCl, LiCl₂, and EDTA used as additives, stabilize the crystals for months at room temperature.

Crystals for either AR-DHT or AR-DHT-peptide were transferred to a new drop containing 10% (v/v) of glycerol for cryoprotection. The crystals were then flash-cooled using liquid nitrogen and measured using the synchrotron radiation at the 8.3.1 beam line at ALS (Berkeley). Crystals containing SRC2-3 diffracted to 2.07 Å. Co-crystals of ARA70 peptide with AR LBD were also grown and a complete data set was obtained at 2.3 Å resolution. All the crystals belong to space group P2₁2₁2₁ (orthorhombic) and contain one molecule per asymmetric unit.

The diffraction data were integrated and scaled using ELVES (Holton, 2004).

Molecular replacement solutions for all AR LBD peptide structures were obtained using rotation and translation functions from CNS (Brunger, Adams *et al.* 1998).

The first electron maps calculated after the rigid body refinement that followed the molecular replacement displayed clear electron density for the peptides.

During the improvement of the protein model, the Fourier maps revealed better electron density for more flanking residues of the peptides. The electron density for the peptide was always modeled as a short α -helix. A composite omit map not including the peptides was calculated in the last steps of refinement for overcoming phase bias for each one of the complexes. This map was calculated omitting 5% of the total model allowing a better tracing of the peptide and also permitted to visualize more residues that were not visible in the 2Fo-Fc map.

Model building was done on a Silicon graphics indigo 2 workstation using the

program QUANTA monitored using the free-R factor. Calculation of the electron density maps and crystallographic refinement was performed with CNS using the target parameters of Engh and Huber. Several cycles of model building, conjugate gradient minimization and simulated annealing using CNS resulted in structures with good stereochemistry. A Ramachandran plot calculated using the program PROCHECK shows that most of the residues fall into the most favored or additionally favored regions. The statistics for data collection and refinement of each one of the data sets can be found in table 1.

The structures have been deposited with the PDB and assigned the following ID numbers: AR•DHT•SRC2-3; PDB 1T63, RCSB RCSB022358; AR•DHT•ARA70; PDB 1T5Z, RCSB RCSB022354.

ACKNOWLEDEMENTS

We thank Eugene Hur, Luke M. Rice, and Maia Vinogradova, for graphical assistance and useful discussions. James Holton and the staff at ALS beamline 8.3.1 for assistance in data collection and processing, as well as Corie Ralston at beamlines 8.2.2 and 8.2.1. The Prostate Cancer Foundation, NIH (DK58080, RJF and RKG and DK51281, JDB), the Department of Defense (DAMD17-01-1-0188, JRM and PC030607, PW) and a UCSF Prostate Cancer Postdoctoral Fellowship (SPORE NCI CA8952, EEP) supported this work.

Chapter 6

Ligand Affects on the Recruitment of Coregulators to Estrogen Receptor α

SUMMARY

The estrogen receptor (ER) regulates growth, differentiation, and development of reproductive tissues, bone, the cardiovascular system, and the central nervous system. A complex signaling network regulates these genes. The details of this network have yet to be fully elucidated but some of the important signaling players have been identified including, heat-shock proteins, estrogen, estrogen mimetics and selective estrogen modulators (SERMs), ER response elements (ERE), and coregulator proteins. In the absence of estrogen, the estrogen receptor is associated with heat-shock proteins in the cytoplasm. Upon binding of hormone, the chaperones are released and the estrogen receptor undergoes a conformational change, an event which promotes homodimer formation. This complex then recognizes specific DNA sequences within ER-responsive genes. Further interaction with coregulator proteins is required to regulate gene expression. The first step in this signaling pathway, binding of ligand, can influence subsequent steps. Different ligands alter the conformational change that takes place and therefore alters the coregulator binding pocket. To explore the ligand affects on coregulator binding further, we determined the binding affinities of coregulator peptides to ER α in the presence of endogenous 17 β -estradiol, the synthetic nonsteroidal estrogen diethylstilbestrol, the phytoestrogen genistein, and several SERMs (4-hydroxytamoxifen, NC13, NC-14, and NC15). The results confirm that coregulator binding patterns do change as a function of ligand and are consistent with previous reports. In addition, the differential

coregulator binding patterns provide information on specificity determinants.

Although we did not discover any significant new findings with this study, we do demonstrate that our *in vitro* coregulator binding assay reproduces literature reports and is a useful tool for studying ligand affects.

INTRODUCTION

Estrogens exert a wide range of biological effects on growth, development, and differentiation including regulatory functions in the reproductive system of both male and females, maintenance of bone density, anti-atherosclerotic in the cardiovascular system, and regulation of the central nervous system and hypothalamic-gonadal axis. Estrogen mediates these activities by binding two genetically distinct estrogen receptors (ER), ER α and ER β . These two receptors have different expression profiles and function [119], [120]. Upon binding of estrogen, heat-shock proteins are released and the estrogen receptor undergoes a conformational change leading to the formation of either ER α /ER α heterodimers or homodimers depending on the cell type. Activated ER can then regulate genes by several different signaling pathways (Figure 6-1) [Turgeon, 2004 #72]. In the nucleus, activated ER can regulate gene expression by either directly binding specific high-affinity estrogen response elements (ERE) within promoters in a process similar to other nuclear receptors or indirectly through protein-protein interactions with transcription factors such as AP1 or NF- κ B [120], [121], [122]. In addition, it is believed that activated ER may also participate in extranuclear signaling networks in the cytosol and caveoli at cell membranes ([123], [124]). The details of ER extranuclear signaling have not been fully elucidated, but several possible scenarios are presented in Figure 6-1.

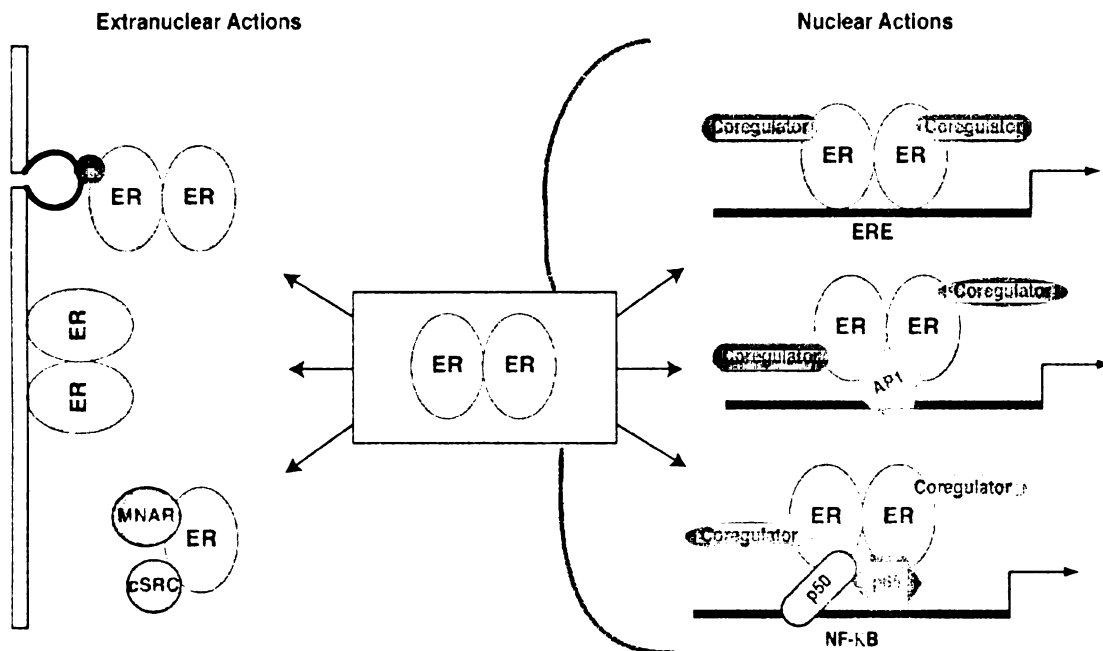


FIGURE 6-1. Pathways Regulated by Activated ER

Upon binding ligand, the estrogen receptor forms a homo- or hetero-dimer and can activate several different pathways both in the nucleus and cytosol depending on the cell type and availability of interacting partners. In the nucleus, the ER dimer can directly bind estrogen response elements (ERE) and recruit coregulator proteins necessary for regulating transcription. The ER dimer complex can also indirectly interact with DNA via AP1 or NF-κB to control transcription. Extranuclear actions occur in the cytoplasm or in caveoli at the cell membrane. It has been demonstrated that ER can induce endothelial nitric oxide synthase by interacting with caveolar membranes. ER can also insert into the cell membrane to mediate other responses such as estrogen-induced calcium transients. Finally ER can activate mitogen-activated protein kinase through interactions with cSRC and MNAR [125] [126].

The first step in the activation of ER signaling is binding of ligand. This step influences the direction of subsequent signaling steps. Although agonists such as 17 β -estradiol (E2) and the synthetic nonsteroidal estrogen diethylstilbestrol (DES) can bind ER and activate gene expression, there are many other ligands that can act as both agonist and antagonist depending on the cell type [127]. These types of ligands have been termed selective estrogen receptor modulators (SERMs). In addition, it has been shown by several groups that ligands can allosterically modulate the ligand binding domain of ER and therefore modify the interaction surface available for coregulator proteins, proteins required for regulating gene transcription [45], [46], [47]. This can be seen in Figure 6-2, where in the presence of DES ER interacts with the SRC2 coregulator, however in the presence of a SERM the coregulator binding surface is blocked. Further complexity in ER signaling arises from different coregulator complexes that have diverse functional activity regulated by the cell type, expression levels, and post-translational modifications. For example, overexpression of AIB1 (SRC3) has been linked to breast and ovarian cancer [128]. Therefore, the cellular response to a ligand arises from the conformation of the ER-ligand complex and the subsequent coregulator complex. In this study, we sought to define rules that govern ER-ligand coregulator selectivity.

There is a huge body of literature devoted to understanding coregulator recruitment to ER. These studies have both identified potential ER-coregulator

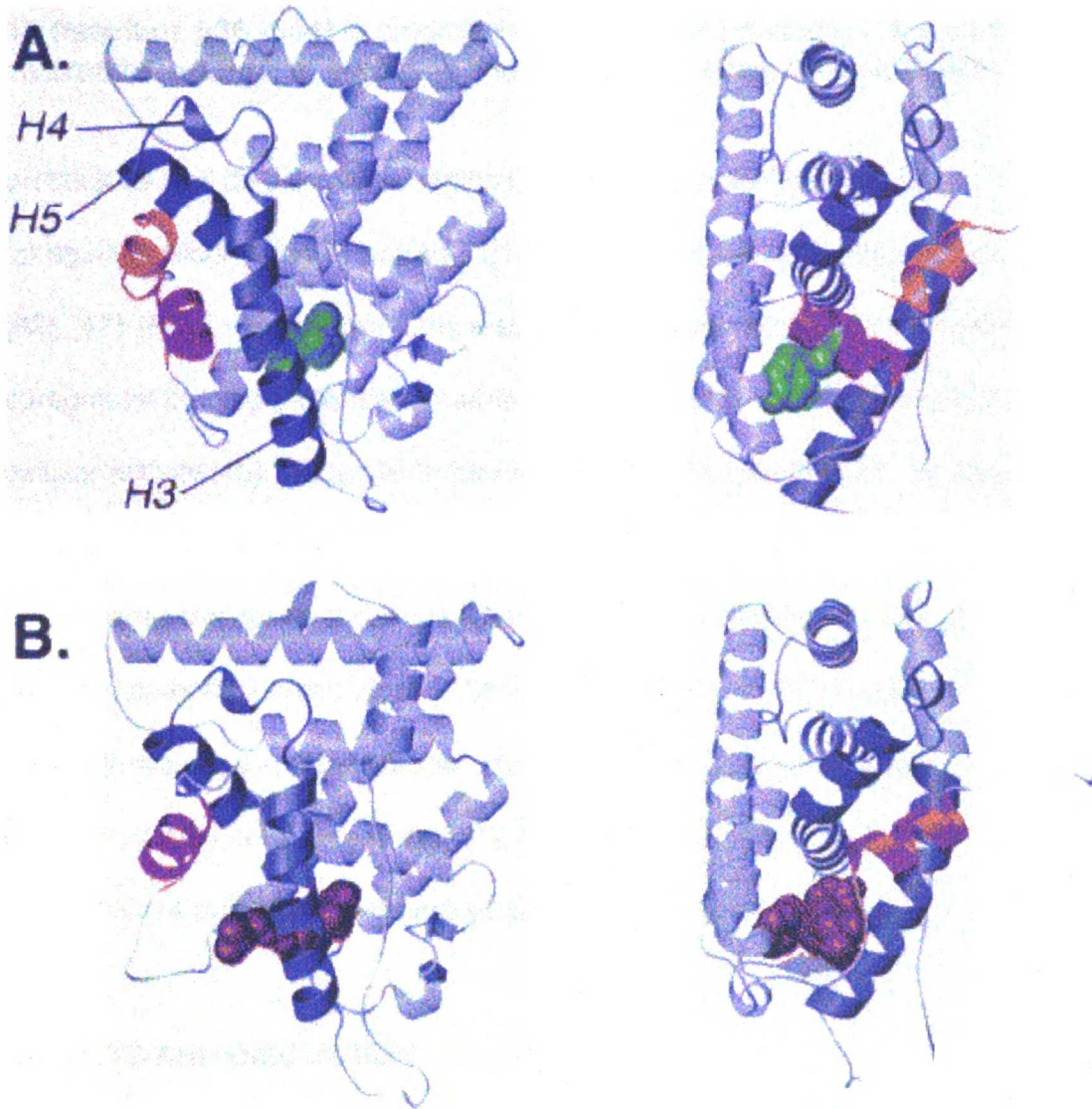


FIGURE 6-2. Structures of ER α -DES and ER α -OHT with SRC2-2

A) Two orthogonal views of the ER α -DES and SRC2-2 complex. SRC2-2 and ER α -LBD are shown as ribbon drawings. The SRC2-2 peptide is colored orange and helix 12 (residues 538–546) is colored magenta. Helices 3, 4, and 5 (labeled H3, H4, and H5, respectively) are colored blue. DES, colored green, is shown in space-filling representation. B) Two orthogonal views of the ER α -OHT complex. In the presence of OHT, helix 12 occupies the coregulator binding pocket preventing interaction with SRC2-2. The ER α -LBD is depicted as a ribbon drawing. As in (A), helix

12 (residues 536–544) is colored in magenta, and helices 3, 4, and 5 are colored blue. OHT, in purple, is shown in space-filling representation. [108]

proteins as well as discovered inhibitors capable of selectively blocking coregulator binding to ER isoforms ([129], [108], [46, 74], [45, 130], [131], [132], [83], [47], [81],). Recent work has also demonstrated that ligands can alter the coregulator binding pattern and that these binding patterns are predictive of cellular activity [45], [133]. To further contribute to the field of ER-coregulator recruitment, we investigated in collaboration with the Agard and Scanlan Laboratories the ability of various ligands to alter the binding affinities of ER to a library of potential coregulators. The ligands included endogenous 17 β -estradiol, the synthetic nonsteroidal estrogen diethylstilbestrol (DES), the phytoestrogen genistein (GEN), and several SERMs such as 4-hydroxytamoxifen (OHT) and NC13, NC-14 and NC15 synthesized by Nicola Clegg in the Scanlan Laboratory.

RESULTS AND DISCUSSION

To expand our understanding of coregulator recruitment by the estrogen receptor, we determined the binding affinities of coregulator peptides for the ligand binding domain of the estrogen receptor α (ER α -LBD) using the *in vitro* steady state fluorescence polarization binding assay (Chapter 2-3) in the presence of estradiol (E2). In order to do this, a fairly large quantity of pure ER α -LBD was required, approximately 20 mg. A His-tagged ER α -LBD construct was expressed in *E. Coli* following standard procedures optimized by Dr. Timothy

Geistlinger (See Methods). Although expression proceeded smoothly, obtaining enough pure, stable protein was the challenging aspect. Without ligand, ER α -LBD is not very stable and is prone to precipitation. To overcome this issue, estradiol was added at the lysis step and the concentration of E2 was maintained throughout the remaining purification by adding it to all buffers used. Initially, purification only included one column step using a nickel column (Invitrogen pro-bond resin). An additional anion exchange purification using FPLC was also required, however, as ER α -LBD was not very stable and was prone to precipitation. Prior to anion exchange, the protein was dialyzed into binding buffer (30 mM NaCl, 10mM Tris, 0.1mM EDTA, 5mM BME, 10% glycerol) with 1M Urea added. It was shown that the urea helped remove some of the unwanted, unstable protein. Protein quality was assessed using SDS-PAGE and binding assays (Figure 6-3). Typical yields of pure ER α -LBD ranged from 3-6mg/L, and therefore 10L expressions were required to obtain enough good quality protein.

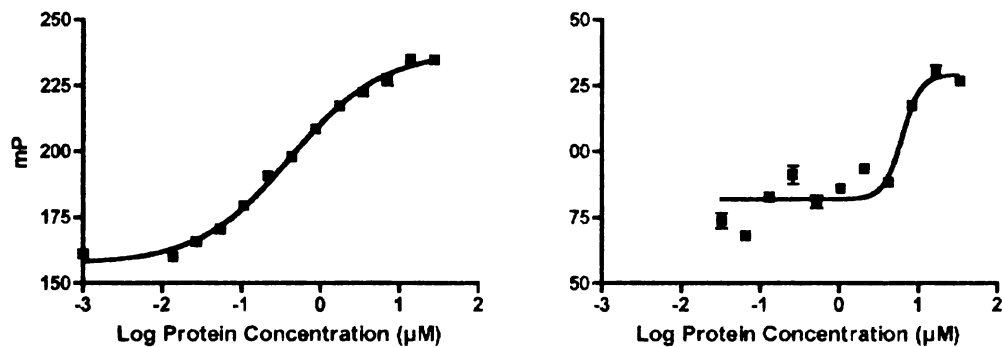


FIGURE 6-3. ER α -LBD Binding Curves

Displayed is the comparison of two different batches of ER α -LBD binding to SRC2-2. The y-axis represents milli-polarization (mP) and the x-axis is the log

concentration of ER α -LBD. The SRC2-2 peptide is held constant at 10 nM. The curve on the left was constructed with a good quality ER α -LBD protein with a measured K_d of 300 nM for the SRC2-2 peptide, consistent with literature reports. The curve on the right was constructed with un-pure ER α -LBD, as a consequence the K_d is shifted to > 6 μ M.

E2 Recruitment of Coregulators

Once we obtained enough pure ER α -LBD, we were able to quantitatively determine binding affinities for the entire coregulator peptide library in the presence of estradiol. The coregulator binding pattern for ER α -LBD is shown in Figure 6-4. Of the 32 coregulator peptides tested, 17 appear to interact with ER α -LBD in the presence of E2 with varying degrees of affinity. The strongest recruitment observed was with SRC1-2 which exhibited a K_d of $0.290 \mu\text{M} \pm 0.06$. This was followed by PGC-1 ($K_d= 0.29 \mu\text{M}$), SRC2-2 ($K_d= 0.313 \mu\text{M} \pm 0.09$), SRC3-1 ($K_d=0.330 \mu\text{M} \pm 0.04$), SRC3-2 ($K_d=0.350 \mu\text{M} \pm 0.09$), SRC2-1 ($K_d=0.915 \mu\text{M} \pm 0.001$), , SRC1-1 ($K_d=1.4 \mu\text{M} \pm 0.3$), TRBP-1 ($K_d=? \mu\text{M} \pm 2.8$), RIP140-8 ($K_d=? \mu\text{M} \pm 2.8$), DAX1-3 ($K_d= 4.2 \mu\text{M}$), SRC2-3 ($K_d=5.1 \mu\text{M} \pm 2.8$), TRAP220-2

($K_d = 9.5 \mu\text{M}$), and RIP140-5 ($K_d = ? \mu\text{M} \pm 2.8$). The coregulators

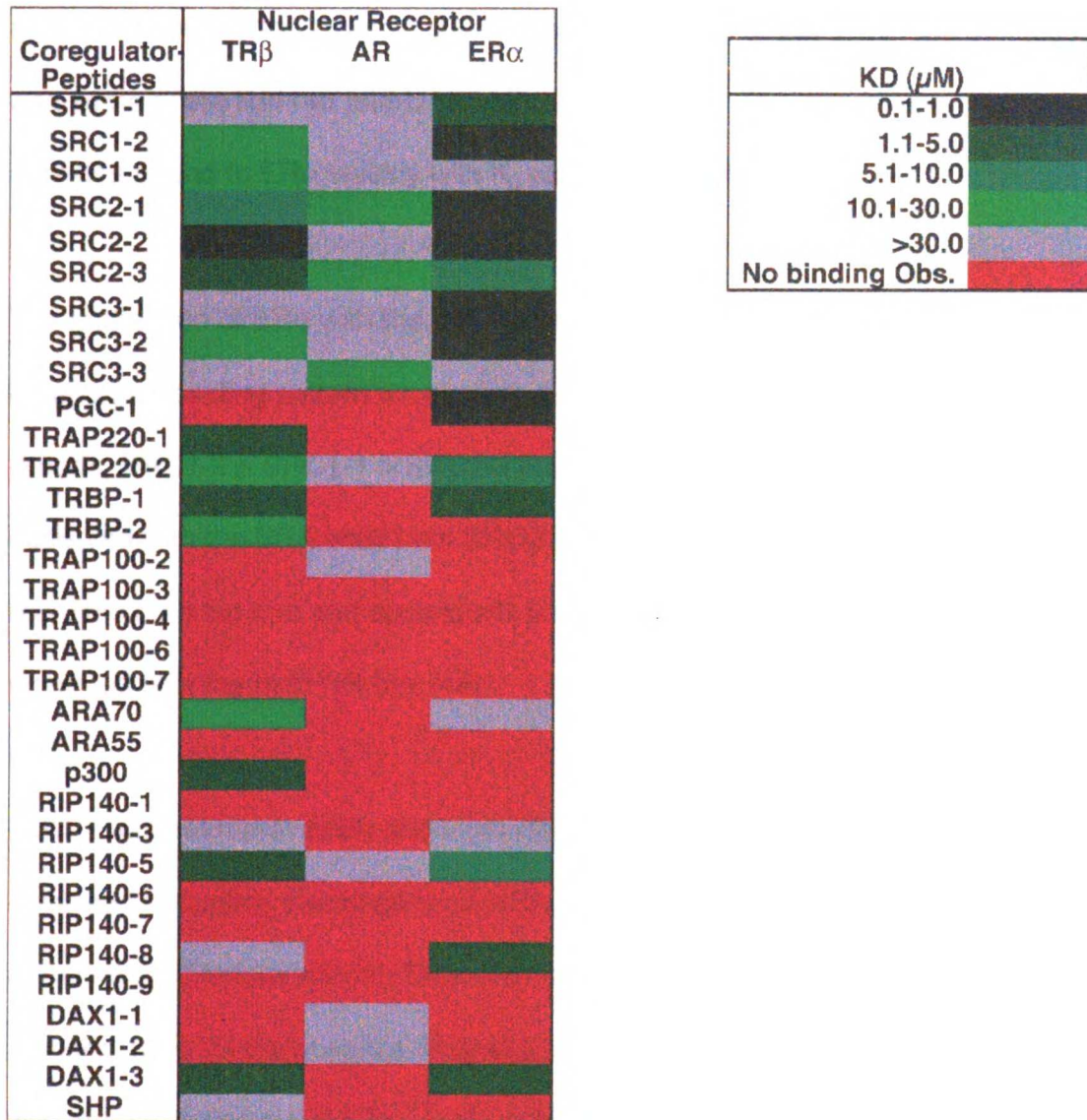


FIGURE 6-4. Coregulator Binding Patterns for Nuclear Receptor

The equilibrium binding constants for TRβ-coregulator, AR-coregulator and ERα-coregulator NR boxes are reported. The coregulator peptides are listed in the left column where SRC1-1, SRC1-2, SRC1-3, SRC1-4 represent the first, second, third, and fourth NR box in SRC1, respectively. Each color represents a unique K_d range as defined by the legend on the right.

The coregulator peptides that clearly did not interact with E2 liganded ER α included TRAP220-1, TRBP-1, ARA55, p300, SHP, all of the TRAP100 peptides, and some of the RIP140 and DAX1 NR box peptides. The remaining coregulator peptides bound to ER α weakly with K_d values $> 30 \mu\text{M}$.

The interaction of ER α with the SRC family has been extensively studied. The coregulator binding pattern we observed for SRC is consistent with previous reports, SRC1-2 $>$ SRC1-1 $>$ SRC1-3 [45], [47]. A similar binding pattern was observed with the NR boxes from SRC2 [45]. For SRC3 NR boxes, ER α strongly recruited both the first and second NR boxes and only weak interactions were observed with the third NR box [45].

PGC-1 has been previously shown to interact with PPAR γ to upregulate enzymes involved in adaptive thermogenesis [134]. It has also been recently demonstrated to interact with ER α in a ligand-independent and ligand-dependent manner [135]. In the absence of ligand, the carboxyl terminus of PGC-1 interacts with the hinge domain of ER α . In the presence of agonist, it is believed that ER α interacts with the LXXLL motif of PGC-1. Our results confirm this supposition.

TRAP220 and TRBP are other general coregulators with two LXXLL motifs that have been shown to interact with ER. In our binding studies we show that ER α has a strong preference for the second NR box of TRAP220 with little to no

binding observed with NR box 1. Although reports in the literature suggest that TRAP220 may be more important for ER β activation, there is evidence that ER α can interact weakly with TRAP220-2 [136]. Consistent with binding results in this study, it has been illustrated that the first NR box of TRBP is critical for interacting with ER α , specifically it was shown that the serine at -3 position provided ER α specificity [137]. Interestingly, ER α did not interact to any measurable degree with TRBP-2.

Unlike traditional coregulators, RIP140 and DAX1 repress transcription upon binding to liganded NR [66], [67], [68], [69]. NR boxes from both of these coregulators interact with ER α . Specifically we observed that RIP140-5 and RIP140-8 and DAX1-3 were recruited to ER α . These results vary from a previous report where RIP140-6, RIP140-7 and RIP140-8 were shown to be more important for ER α binding. However, in that study the coregulator peptides only encompassed amino acids spanning from the -2 position to +6, and we suspect that they may have missed specificity determinants arising from amino acids outside of this region.

Specificity Determinants for ER α -E2

A comparison of nuclear receptor coregulator binding patterns can be seen in Figure 6-4, where TR β , AR, and ER α coregulator binding patterns are displayed.

The coregulator binding patterns for each nuclear receptor are unique and in some cases the nuclear receptors show different NR box preferences for the same coregulator protein. All of the SRCs appear to interact to varying degrees with all of the NR. However, ER α is the only NR to strongly interact with the SRC3 NR boxes. This is interesting as the dysregulation of SRC3 has been linked to breast cancer [128]. Additionally, ER α in general binds to the SRCs with comparatively tighter affinities. This could be due to the proposed plasticity of the ER α coregulator binding pocket [46]. Other significant differences between ER and TR are observed with TRAP220 and RIP140, where they display distinct NR box preferences.

Based on the NR box peptides that interacted with ER α , amino acid residues that act as specificity determinants were identified. It was determined that glutamic acid, histidine, and isoleucine or leucine are preferred at the -5, -3, -1, positions, respectively (Figure 6-5). In addition, serine appears to be important at the +9 position and hydrophilic amino acids at positions +7-+8. This is in contrast to specificity determinants identified for TR β in the presence of its cognate ligand T3. While histidine at the -3 position and hydrophilic amino acids at +7-+10 are required for TR β , glutamic acid and serine are not important and the -1 position can tolerate any hydrophobic amino acid. We also compared ER α specificity determinants from our experiment to ones identified from both a time-resolved fluorescence assay and a phage display library. Although, critical amino acids

identified here vary from the phage display results, they are consistent with the time-resolved fluorescence experiments that were conducted using physiologically relevant coregulator peptides.

NR-Ligand	Source	-7	-6	-5	-4	-3	-2	-1	L X X L L					6	7	8	9	10	11	12
									1	2	3	4	5							
TRβ·T3	FP	X	X	X	X	H	P	Φ	L	X	X	L	L	Q	ζ	ζ	ζ	ζ	X	X
ERα·E2	FP	X	X	E	X	H	X	I/L	L	X	X	L	L	ζ	ζ	X	S	X	X	X
ERα·E2	TRF	X	X	X	X	H	X	Φ	L	H	Q/R/K	L	L	Q/T	X	ζ	ζ	ζ	X	X
	PD																			
	I	X	X	X	X	X	S	R	L	X	X	L	L	X	ζ	X	X	X	X	X
	II	X	X	X	X	H	P	Φ	L	X	X	L	L	X	ζ	ζ	ζ	ζ	X	X
	III	X	X	X	X	X	S/T	Φ	L	X	X	L	L	X	X	ζ	X	ζ	X	X

FIGURE 6-5. Specificity Determinants

A representative coregulator peptide is listed for ERα·E2 and TRβ·T3 with amino acids highlighted in green representing amino acids that convey specificity for each NR·ligand state. In addition, specificity determinants for ERα·E2 from two other sources are displayed below the dashed line for comparative purposes. This data was extracted from two sources 1) a time-resolved fluorescence assay conducted with SRCs [45] and 2) a phage peptide library screen with ERα·E2 [44]. Φ denotes hydrophobic amino acids and ζ represents hydrophilic amino acids.

Ligands Alter Coregulator Recruitment

To investigate ligand effects on coregulator recruitment, binding studies were performed in the presence of the synthetic nonsteroidal estrogen diethylstilbestrol (DES), the phytoestrogen genistein (GEN), and 4- hydroxytamoxifen (OHT).

These studies were conducted in collaboration with the Agard Laboratory. The results of this experiment are consistent with others and demonstrate that different ligands can significantly alter coregulator binding patterns (Bramlett) (Figure 6-6). Comparing the two agonists, E2 and DES, it was found that while ERα·DES can interact with all NR boxes from SRC1 and SRC2, only select

boxes from these coregulators interact with ER α ·E2. Additionally, ER α ·DES interacts weakly with SRC3 NR boxes in contrast to ER α ·E2. In the presence of GEN, fewer coregulator peptides are recruited to ER α , consistent with GEN acting as a partial agonist. Finally, in the presence of a SERM, OHT, no coregulators are recruited to ER α as predicted from the crystal structure (Figure 6-2).

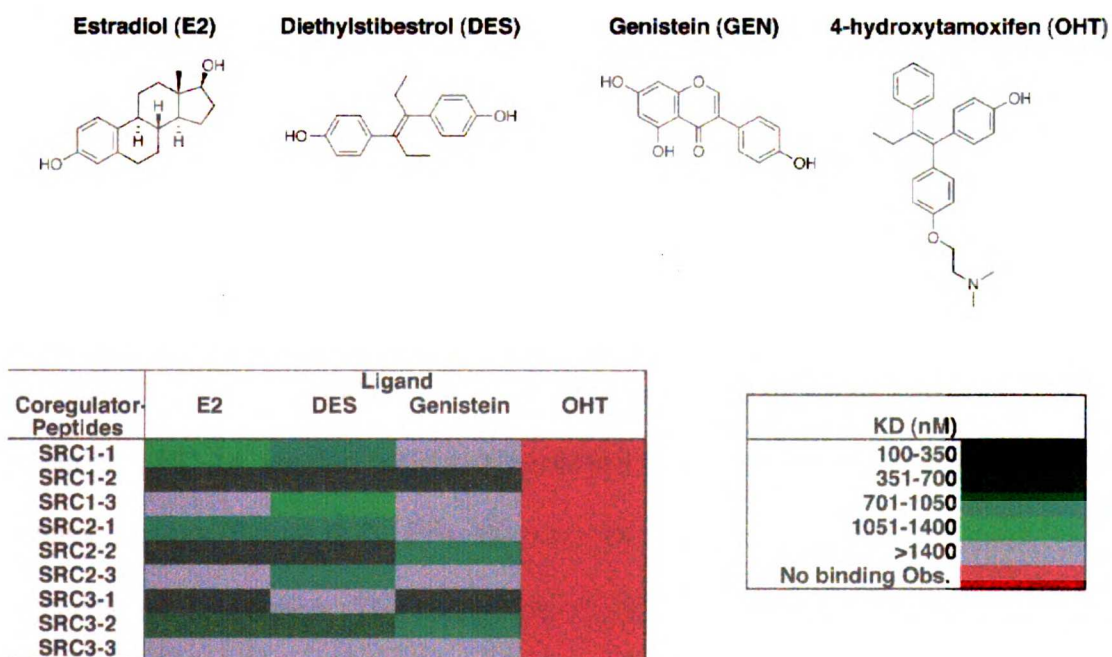


FIGURE 6-6. Ligand Affects on ER α -LBD Coregulator Recruitment
 The structure of the ER α ligands tested; endogenous estradiol (E2), synthetic agonist diethylstilbestrol (DES), partial agonist genistein (GEN), and selective estrogen modulator 4-hydroxytamoxifen (OHT). The equilibrium binding constants for ER α -coregulator NR boxes from the p160 family are reported for each ligand. The coregulator peptides are listed in the left column where SRC1-1, SRC1-2, SRC1-3, represent the first, second, and third NR box in SRC1, respectively. Each color represents a unique K_d range as defined by the legend on the right.

In collaboration with the Scanlan Laboratory, we further investigated the affects of SERMS by studying the coregulator binding affinity of 3 ligands synthesized by Nicola Clegg, NC-13, NC-14, NC-15. Based on studies conducted by Clegg, NC-13 and NC-15 are partial ER α agonists and ER β antagonists. NC-14 is an agonist and NC-19 is an antagonist for both ER isoforms. To conduct these studies modification of ER α expression was required. Typically ligand is added at the lysis step and maintained throughout the remaining purification as described above. However, in an attempt to limit the number of expressions, we omitted ligand until the IMAC column. Prior to adding the supernatant to the IMAC column, the supernatant was divided into 4 pools and E2, NC-13, NC-14, and NC-15 were added to the individual pools, respectively. Purification then proceeded following standard protocol and all of the pools, except the one containing NC-14, yielded good quality protein as assessed by SDS-PAGE and binding assays (Figure 6-7). ER α :NC-14, unfortunately precipitated just after the final column purification. The coregulator binding patterns for NC-13 and NC-15 are similar to GEN and are characteristic of partial agonists (Figure 6-7).

CONCLUSION

There is a complex interplay between activated ER and coregulators at the promoter regions of estrogen responsive genes that regulate transcriptional activity. Cellular expression levels of ligands, NRs, and coregulators, post-translational modifications of these proteins, and structural determinants arising

from the DNA facilitate regulation of this signaling cascade. There has been a plethora of work devoted to deciphering ER signaling and with each study the system becomes more complex. It is clear that one critical point in the network is the interaction between ligand and ER. The subsequent conformational change of ER dictates further interactions with coregulator proteins to elicit specific biological responses. In this report we show that distinct coregulator binding patterns are associated with ER α ligand states and we are able to define some rules that govern this differential binding. We hope that this information can be used to develop more complex *in vivo* models for investigating ER signaling.

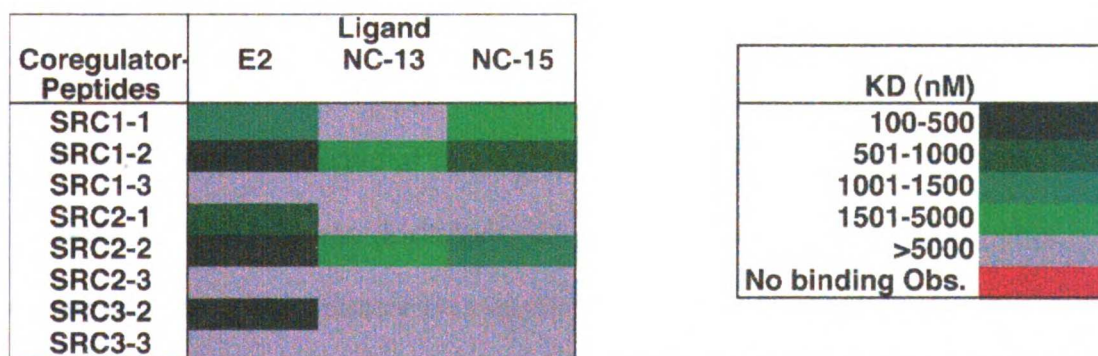
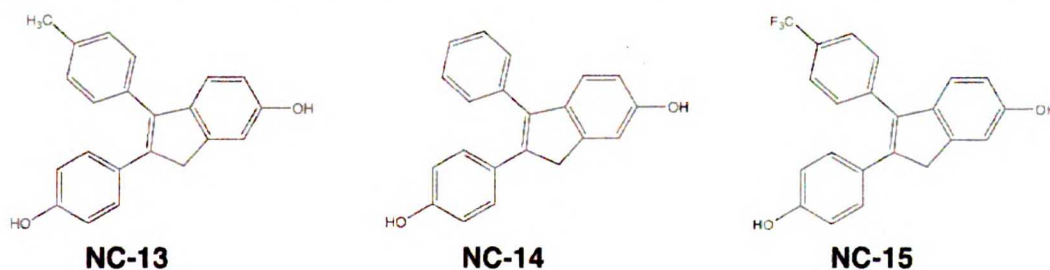


FIGURE 6-7. Affects of Indene Ligands on p160 Coregulator Binding to ER
 The structure of the ER α ligands generated by Nicola Clegg in the Scanlan Laboratory; endogenous estradiol (E2), ER α agonist and ER β antagonist NC-13, ER α agonist and ER β agonist NC-14, ER α partial agonist and ER β antagonist NC-15. The equilibrium binding constants for ER α -coregulator NR boxes from the p160 family are reported for each ligand.



METHODS

Ligands

Estradiol, diethylstilbestrol, and genistein were purchased from Sigma. 4-hydroxytamoxifen was obtained from the Agard Laboratory. NC13, NC14, and NC15 were synthesized by Nicola Clegg in the Scanlan Laboratory.

Protein Expression and Purification

Expressed and purified human ER α -LBD used for E2, DES, GEN, and OHT studies was obtained from Yoko Shibato in the Agard Laboratory. The remaining studies used the following protocol designed by Dr. Geistlinger to obtain ER α -LBD: Human ER α -LBD (His6; residues 297-595) was expressed from a pET15b construct (Novagen) in BL21De (3) pLys S (Stratagene) (23°C, 0.5 mM IPTG added at OD600 = 0.6). Cells were harvested, resuspended in sonication buffer (100 mM Tris, pH 8.0 at 4°C, 100 mM NaCl, 10% Glycerol, protease inhibitors, 10 mg/mL lysozyme, 30 minutes on ice), and sonicated for 3x3 minutes on ice. The lysed cells were centrifuged at 100,000 x g for 1 hr and the supernatant was loaded onto IMAC column (Invitrogen pro-bond resin). Liganded-protein was eluted with 500 mM imidazole plus ligand (E2, NC13-, NC-14, NC-15). The liganded ER α -LBD was then dialyzed against dialysis buffer (30 mM NaCl, 10 mM Tris pH 8 (4°C), 0.1 mM EDTA, 5 mM BME, 1M urea, 10% glycerol) and further purified by ion exchange chromatography (Mono Q, Pharmacia). Protein

purity was assessed by SDS-PAGE and protein concentration measured by coomassie protein assay.

Peptide Library Synthesis

(Appendix A) Coregulator peptides consisting of 20 amino acids with the general motif of **CXXXXXXXXLXXL/AL/AXXXXXXXXX** were constructed, where C is cysteine, L is leucine, A is alanine, and X is any amino acid. The sequences of all the coregulator peptides were obtained from human isoform candidate genes (SRC1/AAC50305, SRC2/Q15596, SRC3/Q9Y6Q9, PGC-1/AAF19083, TRAP220/Q15648, TRBP/Q14686, TRAP100/Q75448, ARA70/Q13772, ARA55/NP_057011, p300/Q92831, RIP140/P48552, DAX-1/P51843, SHP/Q15466). The peptides were synthesized in parallel using standard fluorenylmethoxycarbonyl (Fmoc) chemistry in 48 well synthesis blocks (FlexChem System, Robbins) [57]. Preloaded Wang (Novagen) resin was deprotected with 20% piperidine in dimethylformamide. The next amino acid was then coupled using 2-(1H-Benzotriazole-1-yl)-1,1,3,3-tetramethyluronium hexafluorophosphate (2.38 equiv. wt.), Fmoc-protected amino acid (2.5 equiv. wt.), and diisopropylethylamine (5 equiv.wt.) in anhydrous dimethylformamide. Coupling efficiency was monitored by the Kaiser Test. Synthesis then proceeded through a cycle of deprotection and coupling steps until the peptides were completely synthesized. The completed peptides were cleaved from the resin with concomitant side chain deprotection (81% TFA, 5% phenol, 5% thioanisole,

2.5% ethanedithiol, 3% water, 2% dimethylsulphide, 1.5% ammonium iodide) and crude product was dried down using a speedvac (GeneVac). Reversed-phase chromatography followed by mass spectrometry (MALDI-TOF/ESI) were used to purify the peptides. The purified peptides were lyophilized. A thiol reactive fluorophore, 5-iodoacetamidofluorescein (Molecular Probes), was then coupled to the amino terminal cysteine following the manufacturer's protocol. Labeled peptide was isolated using reversed-phase chromatography and mass spectrometry. Peptides were quantified using UV spectroscopy. Purity was assessed using LCMS.

Peptide Binding Assay

(Appendix B) Using a BiomekFX in the Center for Advanced Technology (CAT), ER α -LBD was serially diluted from 70 μ M to 0.002 μ M in binding buffer (30 mM NaCl, 10 mM Tris pH 8 (at 4°C), 0.1 mM EDTA, 5 mM BME, 10% glycerol) containing 140 μ M ligand in 96 well plates. Then 10 μ L of diluted protein was added to 10 μ L of fluorescent coregulator peptide (20 nM) in 384 well plates yielding final protein concentrations of 35-0.001 μ M and 10 nM fluorescent peptide concentration. The samples were allowed to equilibrate for 30 minutes. Binding was then measured using fluorescence polarization (excitation | 485 nm, emission | 530 nm) on an Analyst AD (Molecular Devices). Two independent experiments were assayed for each state in quadruplicate. Data were analyzed

using SigmaPlot 8.0 (SPSS, Chicago, IL) and the K_0 values were obtained by fitting data to the following equation ($y = \min + (\max - \min) / (1 + (x/K_0)^{\text{Hillslope}})$).

ACKNOWLEDGEMENTS

We would like to thank Dr. Timothy Geistlinger and Dr. Wenchen Luo for optimizing ER α -LBD expression and providing valuable technical advice. We would also like to acknowledge Yoko Shibato (ER α -E2 ER α -DES, ER α -GEN, and ER α -OHT) and Andrea McReynolds (ER α -E2 ER α -NC13, ER α -NC14 and ER α -15) who carried out the majority of ER α -LBD expression and purification. NC13, NC14, and NC15 were synthesized and characterized by Nicola Clegg. JMRM was funded by Department of Defense Breast Cancer Research Fund #DAMD17-01-1-0188. Additional financial support came from the Sandler Research Foundation, and the NIH (DK-52798 and DK-58390).

CHAPTER 7

Biophysical Characterization of AF-2 activation of SF-1 and LRH-1

SUMMARY

Liver receptor homolog-1 (LRH-1) and Steroidogenic factor-1 (SF-1) regulate genes involved in bile acid/cholesterol and steroid homeostasis, respectively. They are highly homologous orphan nuclear hormone receptors with 53% identity in their ligand binding domains and 90% identity in their DNA-binding domains. Unlike other members of the nuclear hormones receptors, they bind to specific DNA response elements as monomers. Although the biological roles for LRH-1 and SF-1 have been highly characterized, the precise mechanism for their regulation of gene expression has yet to be elucidated. To address this issue, we investigated the ability of LRH-1 and SF-1 to recruit coregulator peptides via their AF-2 domains. LRH-1 moderately interacted with several coregulators, including NR boxes from the SRC family, ARA70, RIP140, DAX1, and SHP. SF-1 interacted with a larger number of NR boxes with varying degrees including SRCs, PGC-1, p300, RIP140, DAX1, and SHP. To further investigate the direct link between LRH-1 and SF-1 with DAX1 and SHP, additional binding studies are being carried out using mouse DAX1 and SHP "LXXLL" like motifs. Preliminary studies with these mouse peptides resulted in a crystal structure of SF-1 complexed to NR box 1 of SHP. These additional studies should provide some mechanistic information on how LRH-1 and SF-1 regulate transcriptional activity.

INTRODUCTION

Liver receptor homolog-1 (LRH-1) and Steroidogenic factor-1 (SF-1) belong to one of the evolutionary oldest subfamilies of nuclear receptors, Ftz-F1 subfamily NR5A [138], [139]. Both LRH-1 and SF-1 are key players in early development and homeostasis. Although the precise developmental roles for LRH-1 have yet to be defined, both LRH-1 and SF-1 coordinately regulate genes involved in bile acid/cholesterol and steroid homeostasis, respectively [140], [141], [142]. LRH-1 has increased expression in the liver and intestine where it has been shown to regulate genes required for bile acid synthesis, such as Cyp7A and CYP8B1 [143] [144], and genes involved in cholesterol transport [145], [146]. On the other hand, SF-1 is highly expressed in the adrenals and gonads and is responsible for the regulation of steroidogenesis. In addition, SF-1 has been directly linked to sexual differentiation in mammals and is required for proper male sexual development [147] [148], [149], [150]. This was demonstrated in *SF-1* null mice, where it was found that these mice lack testes and adrenals, and are phenotypic females regardless of chromosomal sex [149], [150].

Although LRH-1 and SF-1 belong to the nuclear hormone receptor family (NR), the precise mechanism for their regulation of genes has yet to be elucidated. Contrary to other NR, LRH-1 and SF-1 both bind their specific DNA response elements as high affinity monomers. In addition, to date the existence of an obligatory endogenous LRH-1 or SF-1 ligand has not been demonstrated, hence

they have been termed orphan nuclear hormone receptors. It is possible that these receptors may be activated in the absence of ligand. Alternatively, it has been proposed that small lipophilic molecules may act as non-specific ubiquitous ligands[151]. It remains an open question as to whether or not LRH-1 and SF-1 are activated by a ligand-dependent, or by a ligand-independent mechanism. In an attempt to address this issue, we investigated the ability of LRH-1 and SF-1 to recruit coregulator peptides in the absence of ligand. This project was conducted in collaboration with the Holly Ingraham Laboratory.

RESULTS AND DISCUSSION

The ability of SF-1 and LRH to interact with coregulator peptides was investigated and the coregulator binding patterns for each receptor were

determined (Figure 7-1).

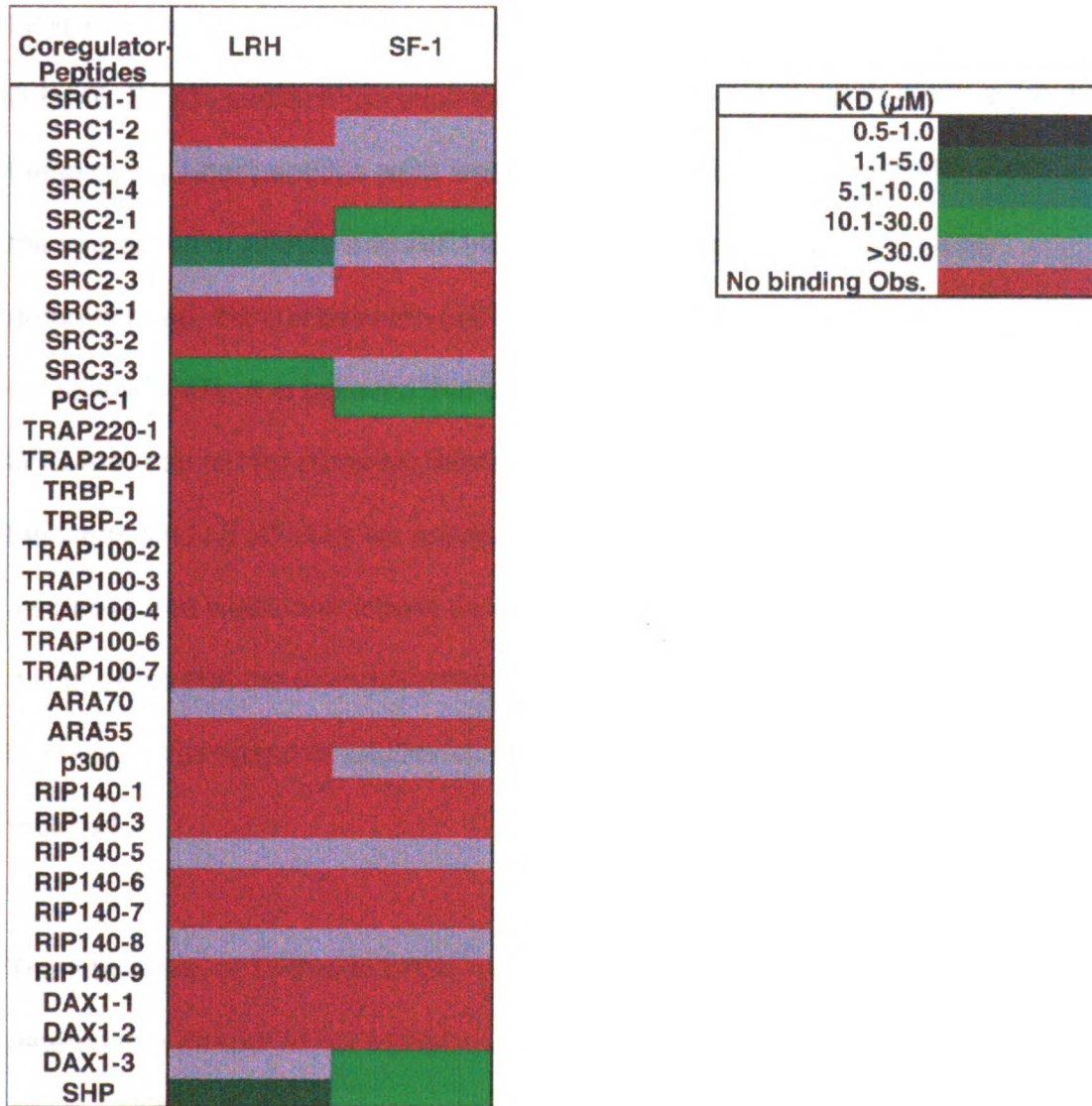


Figure 7-1. LRH-1 and SF-1 Coregulator Binding Patterns

The equilibrium binding constants for LRH-1-coregulator and SF-1-coregulator NR boxes are reported. The coregulator peptides are listed in the left column where SRC1-1, SRC1-2, SRC1-3, SRC1-4 represent the first, second, third, and fourth NR box in SRC1, respectively. The sequences of these peptides were derived from human proteins. Each color represents a unique K_d range as defined by the legend on the right.

Both NR recruited only a small subset of coregulator peptides in comparison to TR and ER.

LRH-1 Coregulator Binding Pattern

LRH-1 interacted with some NR boxes from the SRC family, ARA70, and RIP140, DAX1, and SHP coregulator proteins. The binding affinities for most of these coregulator peptides were weaker in comparison to liganded NR. Although the interaction of ARA70 and RIP140 with LRH-1 has not been previously demonstrated, the link between LRH-1 with SRC, DAX-1 and SHP has been established [37]. It is believed that additional segments outside of the NR box of SRC are required for complete interaction with LRH-1 [152]. This may explain the weak binding affinities we observed for the SRC coregulator peptides. We also observed weak interactions between LRH-1 and the third NR box of DAX-1. It is possible that the strength of this interaction would increase in the presence of endogenous ligand or additional motifs beside the LXXLL box may also be required.

The interaction of SHP with LRH-1 has been well documented. SHP, small heterodimer partner, is an orphan nuclear receptor that lacks the highly conserved DNA binding domain. It is believed that SHP can interact with a variety of NR to repress transcriptional activity [153], [154]. SHP exerts its inhibitory affect through a two-step mechanism [155]. The first step is direct interaction of SHP with AF-2 of NR where it has been shown to compete with coregulator proteins. The final step requires the autonomous repression function of SHP. Work in the David Moore laboratory has shown that LRH-1 can

transactivate the SHP promoter [156]. Further studies demonstrated the existence of a negative feedback regulation of SHP expression by LRH-1 in bile acid metabolism whereby excessive bile acids upregulate SHP, via activation of the bile acid receptor FXR and this ultimately leads to LRH-1 and SHP repression[142]. In the dual mechanism for repression, the first step of repression is the interaction SHP with the AF-2 domain of LRH-1 [155]. Our results suggest that this interaction is via an LXXLL motif in SHP. Then the C-terminal autonomous repression function is then required for full inhibition [155].

SF-1 Coregulator Binding Pattern

SF-1 appears to interact with a wider range of coregulator peptides in comparison to LRH-1. Although most of these interactions are fairly weak, SF-1 does strongly recruit NR boxes from SRC2, PGC-1, DAX1, and SHP.

The interaction of SF-1 and SRC family members has been investigated in the past. Most reports have shown that this interaction is fairly weak in comparison to other liganded NR, consistent with our results.

The interaction of PGC-1 and SF-1 has not been previously reported. It is unclear if this interaction is physiologically relevant. PGC-1 expression is fairly limited and at this point the presence of PGC-1 in cells that express SF-1 has not been demonstrated.

The interaction of DAX1 with SF-1 has been extensively studied. DAX1 (dosage-sensitive sex reversal-adrenal hypoplasia congenital critical region of the X chromosome gene) is similar to SHP as it is an orphan nuclear receptor also lacking a traditional DNA binding domain. DAX1 co-localizes with SF-1 in many cell types, and its mutations in humans cause disgenesis and dysfunction of adreno-gonadal tissues that are reminiscent of *SF-1* null mice and SF-1 human mutants, therefore suggesting DAX-1 co-function with SF-1[157]. However, the precise interaction of DAX-1 and SF-1 has yet to be elucidated. In our binding studies it appears that the third NR box of DAX-1 may be important for this interaction. However, the coregulator peptides used in our binding studies contain sequences from the human DAX1 peptides, whereas the SF-1 protein is a mouse construct. Although mouse and human DAX1 peptides are similar (Table 7-1), to fully investigate the interaction of mouse DAX1 with mouse SF-1 we conducted binding studies with mouse coregulator peptides (Figure 7-2). For SF-1, it appears that the mouse DAX1-3 is more strongly recruited than the human DAX1-3. There are only 3 amino acids that differ between the human and mouse sequences suggesting that serine at -2, alanine at +8, and glutamine at +9 may be important specificity determinants. Interestingly, the serine at -2 is present in the human sequences, however during our library synthesis we found that gly-ser was prone to cleaving and therefore we mutated that serine to alanine. It appears that the serine at -2 is important. There were no other major

differences observed between mouse and human coregulator peptide

recruitment.

Table 7-1. Comparison of Mouse and Human “LXXLL” Sequences for DAX1 and SHP.

The peptides are listed in the far left column, where h represents the human sequences, and m denotes mouse sequences. Similarities between mouse and human sequences are highlighted in green.

PEPTIDE	-7	-6	-5	-4	-3	-2	-1	1	2	3	4	5	6	7	8	9	10	11	12
hDAX1-1	H	Q	W	Q	G	A	I	L	Y	N	M	L	M	S	A	K	Q	T	R
hDAX1-2	H	P	R	Q	G	A	I	L	Y	S	M	L	T	S	A	K	Q	T	Y
hDAX1-3	H	P	R	Q	G	A	I	L	Y	S	L	L	T	S	S	K	Q	T	H
mDAX1-3				Q	G	A	I	L	Y	S	L	L	T	S	A	Q	Q		
mDAX1-4			E	C	T	N	T	T	Q	E	M	L	T	T	R	R	Q		
hSHP-1	A	A	S	R	P	A	I	L	Y	A	L	L	S	S	S	L	K	A	V
mSHP-1				R	P	T	I	L	Y	A	L	L	S	P	S	P	R		
mSHP-2				V	P	S	I	L	K	K	I	L	L	E	E	A	S		
mSHP-3				S	Q	G	R	L	A	R	I	L	L	M	A	S	T		
mSHP-Helix 12	D	V	D	I	T	E	L	L	E	D	M	L	L	L	R				

In our coregulator binding studies, we observed a fairly strong interaction of SHP coregulator peptide with SF-1. Although, it has been shown that SF-1 can transactivate the SHP promoter [156], a direct interaction between SF-1 and SHP proteins has not been established. Given that SF-1 and LRH-1 are so similar (53% identity in the ligand-binding domain and 90% identity in the DNA-binding domain), it is possible that SF-1 may also regulate the expression of SHP through a negative feedback loop. To further investigate this interaction, mouse SHP “LXXLL” like sequences are being

Coregulator-Peptides	LRH-1	SF-1
hDAX1-3		
mDAX1-3		
mDAX1-4		
hSHP-1		
mSHP-1		
mSHP-2		
mSHP-3		
mSHP-Helix 12		

KD (μM)	
0.5-1.0	
1.1-5.0	
5.1-10.0	
10.1-30.0	
>30.0	
No binding Obs.	

Figure 7-2. Comparison of Mouse and Human Coregulator Recruitment to LRH-1 and SF-1.

There were no detectable differences observed for LRH-1 recruitment of human and mouse coregulators peptides from either DAX-1 or SHP. Interestingly, LRH-1 does strongly recruit the second NR box from SHP. For SF-1, it appears that mouse DAX1-3 is more strongly recruited than human DAX1-3. No other major differences were observed.

synthesized and binding studies will be conducted in collaboration with the Ingraham laboratory. In addition, crystal trays were set-up with mouse SHP box one and mouse SF-1 ligand binding domains. A preliminary crystal structure of these two proteins has been solved at 2.0Å (Figure 7-3, Figure 7-4). Further refinement is in process in the Fletterick laboratory and attempts to biological link SHP and SF-1 are underway in the Ingraham laboratory.

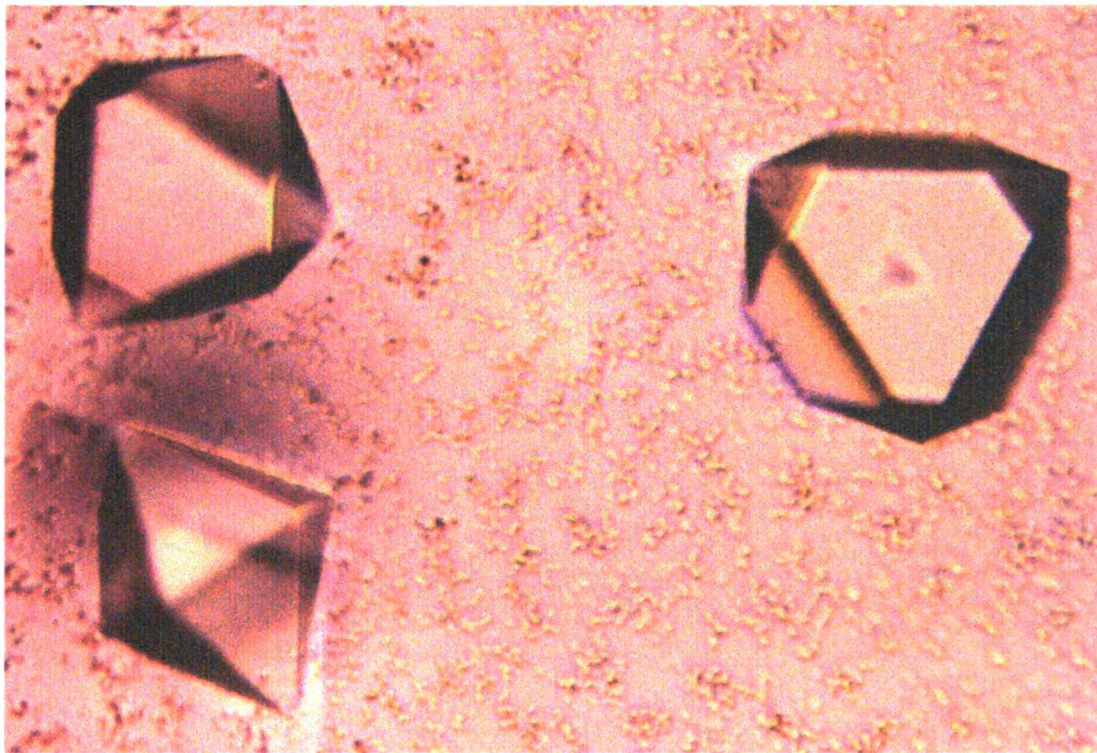


Figure 7-3. Crystals obtained with mouse SF-1 ligand binding domain and box 1 of mouse SHP.

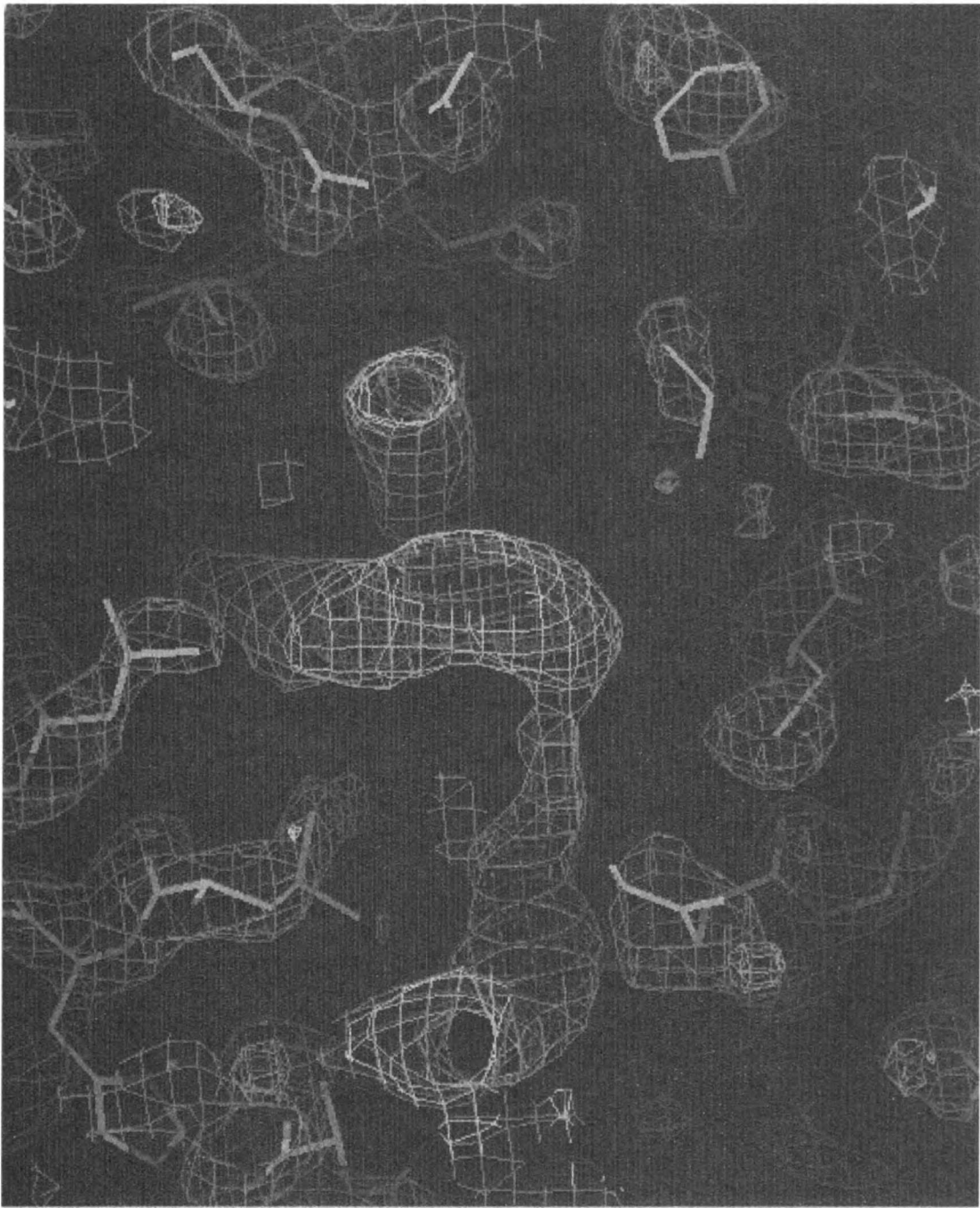


Figure 7-4. SF-1 with SHP box 1 in Coregulator Binding Pocket.

CONCLUSION

In this study we demonstrate that both LRH-1 and SF-1 are able to selectively recruit coregulator peptides and despite their similarity each nuclear receptor has a unique coregulator binding pattern. Interestingly though, both LRH-1 and SF-1 strongly recruited SHP. Although the existence of a negative feedback regulation of SHP expression has been established for LRH-1, no such link has been made with SF-1. Preliminary studies in the Ingraham and Fletterick laboratory have solved a crystal structure of SF-1 complexed to box one of SHP. Further studies hope to elucidate the biological role of this interaction and shed some light on the mechanistic role of SF-1 in gene regulation.

METHODS

Protein Expression

LRH-1 and SF-1 were obtained from Irina Krylova in the Holly Ingraham Laboratory.

Peptide Library Synthesis

Coregulator peptides consisting of 20 amino acids with the general motif of **CXXXXXXXXLXXL/AL/AXXXXXXX** were constructed, where C is cysteine, L is leucine, A is alanine, and X is any amino acid. The sequences of all the coregulator peptides were obtained from human isoform candidate genes (SRC1/AAC50305, SRC2/Q15596, SRC3/Q9Y6Q9, PGC-1/AAF19083, TRAP220/Q15648, TRBP/Q14686, TRAP100/Q75448, ARA70/Q13772, ARA55/NP_057011, p300/Q92831, RIP140/P48552, DAX-1/P51843,

SHP/Q15466). The peptides were synthesized in parallel using standard fluorenylmethoxycarbonyl (Fmoc) chemistry in 48 well synthesis blocks (FlexChem System, Robbins) [57]. Preloaded Wang (Novagen) resin was deprotected with 20% piperidine in dimethylformamide. The next amino acid was then coupled using 2-(1H-Benzotriazole-1-yl)-1,1,3,3-tetramethyluronium hexafluorophosphate (2.38 equiv. wt.), Fmoc-protected amino acid (2.5 equiv. wt.), and diisopropylethylamine (5 equiv.wt.) in anhydrous dimethylformamide. Coupling efficiency was monitored by the Kaiser Test. Synthesis then proceeded through a cycle of deprotection and coupling steps until the peptides were completely synthesized. The completed peptides were cleaved from the resin with concomitant side chain deprotection (81% TFA, 5% phenol, 5% thioanisole, 2.5% ethanedithiol, 3% water, 2% dimethylsulphide, 1.5% ammonium iodide) and crude product was dried down using a speedvac (GeneVac). Reversed-phase chromatography followed by mass spectrometry (MALDI-TOF/ESI) were used to purify the peptides. The purified peptides were lyophilized. A thiol reactive fluorophore, 5-iodoacetamidofluorescein (Molecular Probes), was then coupled to the amino terminal cysteine following the manufacturer's protocol. Labeled peptide was isolated using reversed-phase chromatography and mass spectrometry. Peptides were quantified using UV spectroscopy. Purity was assessed using LCMS.

Direct Binding Assay

In 96 well plates, SF-1-LBD or LRH-1 was serially diluted from 150 μM to 0.002 μM in binding buffer (50 mM Sodium Phosphate, 150 mM NaCl, pH 7.2, 1 mM DTT, 1 mM EDTA, 0.01% NP40, 10% glycerol). Then 10 μL of diluted protein was added to 10 μL of fluorescent coregulator peptide (20 nM) in 384 well plates yielding final protein concentrations of 75-0.001 μM and 10 nM fluorescent peptide concentration. The samples were allowed to equilibrate for 30 minutes. Binding was then measured using fluorescence polarization (excitation λ 485 nm, emission λ 530 nm) on an Analyst AD (Molecular Devices). Two independent experiments were assayed for each state in quadruplicate. Data were analyzed using SigmaPlot 8.0 (SPSS, Chicago, IL) and the K_d values were obtained by fitting data to the following equation ($y = \text{min} + (\text{max} - \text{min}) / (1 + (x/K_d)^{\text{Hillslope}})$).

ACKNOWLEDGEMENTS

This research project was conducted in collaboration with the Holly Ingraham laboratory. Specifically I would like to acknowledge Irina Krylova for all of her efforts in expressing SF-1 and LRH-1, obtaining crystals for both of these receptors, and providing technical assistance and intellectual insight. This project was funded by the NIH (PO1DK58390-01).

APPENDIX

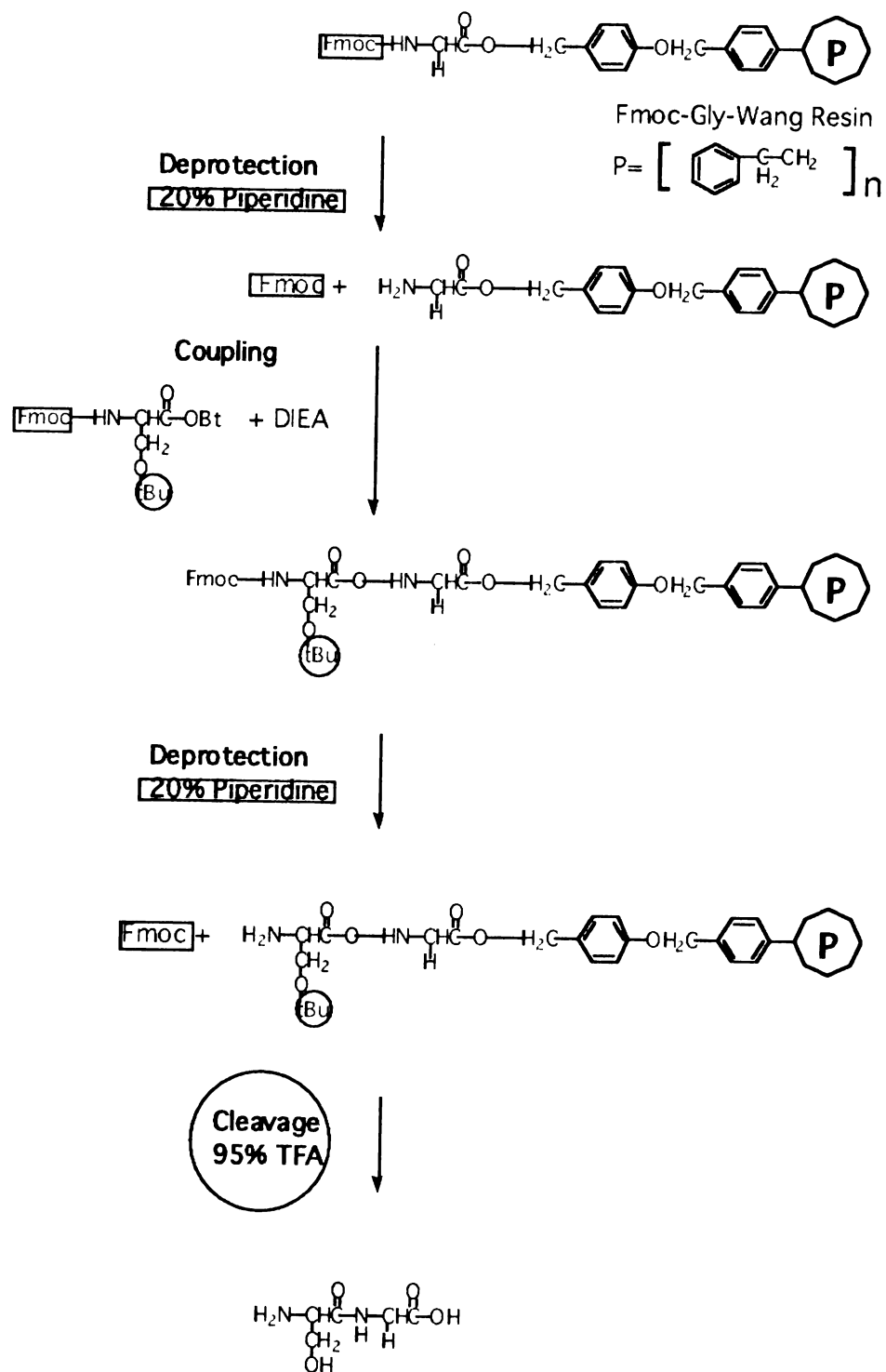
A. Protocol for Peptide Library Synthesis

.

OVERVIEW

Solid phase peptide synthesis consists of assembling amino acids from the C-terminal to the N-terminal. The α -carboxyl group is attached via an acid-labile linker to a solid support, "resin" (Figure 1). Resins commonly used are composed of polystyrene (**P**). The amino terminal end of the amino acid is protected by a base-labile Fmoc (9-fluorenylmethoxycarbonyl) protecting group while the side chains are protected by acid-labile groups such as tertiary-butyl (tBu). After the first amino acid is loaded onto the resin, the Fmoc group is removed using piperidine (Deprotection). A Kaiser test is then performed to confirm that all of the Fmoc protecting groups are removed. The next Fmoc-amino acid is then attached to the growing peptide by activation of its carboxyl group (Coupling). A Kaiser test is then performed to confirm that complete coupling has occurred on all the free amines on the resin. Synthesis then proceeds through a cycle of 1) deprotection of Fmoc amino terminus groups and 2) coupling of the next amino acid until the peptide is completely synthesized. The completely synthesized peptide is then cleaved from the resin and side chain protection groups are removed using trifluoroacetic acid (Cleavage).

Figure 1



Reagents

Acetic Anhydride
Acetonitrile
Alpha cyano 4-hydroxy cinnamic acid (alpha CHC acid), Agilent Technologies
Fmoc-Amino Acids (Table 1), Novabiochem or Advanced Chemtech
Ammonium iodide
Dichloromethane (CH₂Cl₂)
Diethylether
Anhydrous *N,N*-Dimethylformamide (DMF), J.T. Baker
Diisopropylethylamine (DIEA), Acros
Dimethylsulphide
2-(1H-Benzotriazole-1-yl)-1,1,3,3-tetramethyluronium hexafluorophosphate (HBTU), Quantum Biotech
Ethanedithiol (EDT)
Ethanol
5-iodoacetamido fluorescein (5-IAF), Molecular Probes
β-mercaptoethanol
1-(Mesitylene-2-sulfonyl)-3-nitro-1H-1,2,4-triazole (MSNT), Novabiochem
1-Methylimidazole
Ninhydrin
Phenol
Piperidine
Potassium cyanide
Pyridine
Thioanisole
Trifluoroacetic acid (TFA)
Wang Resin (100-200 mesh), Novabiochem
Wang Preloaded Resin (Table 2), Novabiochem

Note: Unless otherwise stated, reagents are purchased from Fisher.

Stock Solutions

20% Piperidine

20% piperidine in DMF (v/v)

Kaiser Test Solutions

A. Ninhydrin (5%, w/v) in ethanol

B. Phenol (4:1, w/v) in ethanol

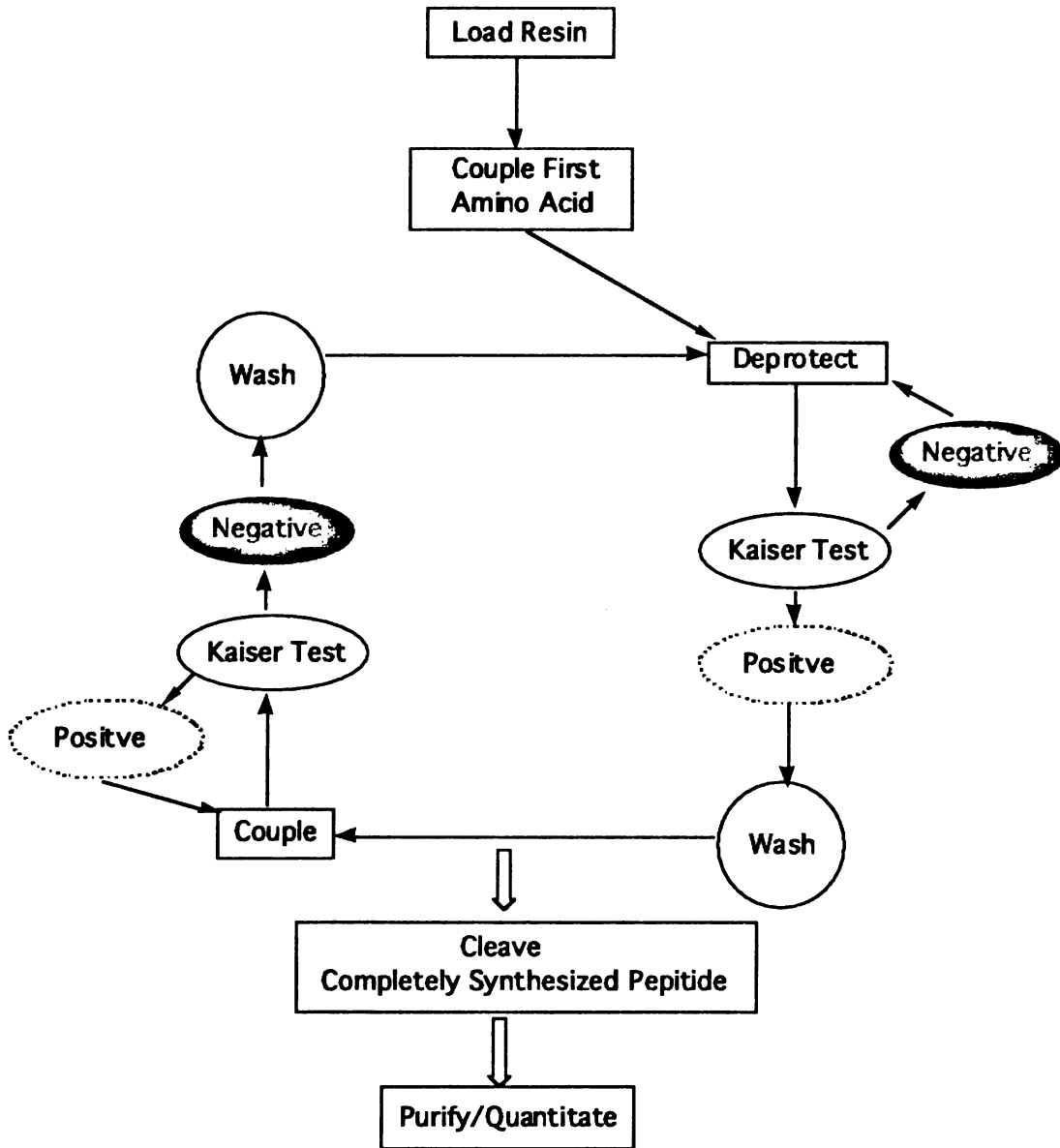
C. Potassium cyanide (2%, v/v, of a 1mmole/liter aqueous solution) in pyridine

Apparatus

Robbins Flexchem Reactor Block (48 or 96 well)

Sealing Covers (top-red, bottom-blue)
Rubber gasket (2)
Viton gasket (2)
Flexchem rotator
Robbins Resin Loader
Speed Vac (GeneVac HT-4 or Mega)
Deep well plates (48 or 96)
Preparatory HPLC (Biotage Parallax Flex)
MALDI-TOF (Perseptives Voyager)
Analytical HPLC (Waters Alliance 2695)
LCMS (Waters Micromass ZQ)
UV Spectrophotometer (Spectronic Genesys 5)

Peptide Synthesis Flow Chart



1. Loading of C-terminal Amino Acid to Wang Resin

(Skip to Step 3 if using preloaded Wang Resin)

- 1.1. Place appropriate amount of Wang resin in wells of reactor block (96 well: 50mg, 48 well: 100mg) either using the Robbins Resin loader or manually with weighing paper.
- 1.2. Mix 3.3 equivalents (eq.) of Fmoc-amino acid to be coupled with 0.1M MSNT in CH_2Cl_2 , and 2.25 eq. 1-Methylimidazole. Add to appropriate wells in the reactor block, place block on rotator, and allow to couple for at least 1 1/2 hours and maximally for 8 hours. (volume per well: 48 well, 2mL; 96 well, 1mL,).
- 1.3. Remove block from rotator. Manually invert block quickly then wait 1-2 minutes to allow resin to fall into solution. Remove bottom cover followed by top cover. This step is necessary to remove excess resin from the cover.
- 1.4. Allow the solution to drain and wash resin with DMF two times (2x 1mL).
- 1.5. Repeat steps 1.2-1.4 two times.
- 1.6. Wash thoroughly with DMF and CH_2Cl_2 . (See Step 2)
- 1.7. Add acetic anhydride to acetylate any remaining functional groups of the resin.
- 1.8. Wash thoroughly with DMF and CH_2Cl_2 . (See Step 2)
- 1.9. Proceed to Step 4.

2. Wash Step

- 2.1. First rinse with DMF along all four walls of the well.
- 2.2. Rinse again with DMF forcefully on the center of the well to agitate resin using approximately 1 mL. Rotate block. Pull off DMF completely.
- 2.3. Repeat 2.2 2-3 times.
- 2.4. Rinse with CH_2Cl_2 following the same procedure outlined in 2.1.
- 2.5. Rinse again with CH_2Cl_2 forcefully on the center of the well to agitate resin.
- 2.6. Repeat step 2.5 2-3 times.)
- 2.7. Rinse both top and bottom seal with CH_2Cl_2 making sure to remove any resin.

Note: When performing washes, the force of the reagent and the number of washes is more critical than the volume of reagent. In between washes, allow solutions to drain completely.

3. Preloaded Wang Resin

- 3.1. Place appropriate amount of Wang resin in wells of reactor block (96 well: 50mg, 48 well: 100mg) either using the Robbins Resin loader or manually with weighing paper.
- 3.2. Proceed to Step 4.

4. Deprotection - Removal of Fmoc Amino-Terminal Protecting Group

- 4.1. Add 20% piperidine in DMF (v/v) to each well. (volume per well: 48 well, 2mL; 96 well, 1mL,).
- 4.2. Rotate block on rotator and allow deprotection to proceed for 30 minutes.

- 4.3. Remove block from rotator. Manually invert block quickly then wait 1-2 minutes to allow resin to fall into solution. Remove bottom cover followed by top cover. This step is necessary to remove excess resin from the cover.
- 4.4. Allow the solution to drain completely.
- 4.5. Wash (Step 2).
- 4.6. Perform Kaiser Test (Step 5).
 - 4.6.1. Negative Kaiser Test: repeat steps 4.1-4.3.
 - 4.6.2. Positive Kaiser Test:
 - 4.6.2.1. If peptide is not completely synthesized proceed to coupling Step 6.
 - 4.6.2.2. If peptide is completely synthesized proceed to cleavage Step 7.

Note: Washing all of the piperidine out is crucial before proceeding to next step.

5. Kaiser Test

- 5.1. Make up three test solutions:
 - A. Ninhydrin (5% w/v) in ethanol
 - B. Phenol (4:1, w/v) in ethanol
 - C. Potassium cyanide (2%, v/v, of a 1 mmole/liter aqueous solution) in pyridine
- 5.2. The test is carried out by adding 2 drops of A, 1 drop of B and 1 drop of C to the test sample (usually 1-2 mg of resin, 10-20 resin particles) contained in a small glass test tube and then heating the tube for 2-5 minutes on a hot plate.
- 5.3. A blue coloration of the resin is a positive result indicating that there are free amines on the growing peptide ie: coupling is incomplete or deprotection is complete. Occasionally, some amino acid residues can give unusual coloration ranging from red to blue (Asn, Cys, Ser, Thr).
- 5.4. If the resin does not change color, this is a negative test ie: coupling is complete or deprotection is incomplete.

Note: The result of the Kaiser test is based on the color of the resin and not the color of the solution. If solution turns blue, it could be due the presence of DIEA, piperidine, or too much DMF.

6. Coupling - Peptide Bond Formation

- 6.1. Add in order 1) 3 eq. of Fmoc-amino acid, 2) 2.5 eq. of HBTU, and 3) DMF (volume per well: 48 well, 1.5 mL; 96 well, 1 mL) allow mixture to react for 2-3 minutes (agitation may be required to get Fmoc-amino acid into solution) Alternatively, a pre-made solution of HBTU in DMF can be made fresh each day and stored at 5°C, then added to Fmoc-amino acid.
 - 4) Add 5 eq. of DIEA after Fmoc-amino acid is in solution, mix.
- 6.2. Add mixture to appropriate wells.
- 6.3. Place reactor block on rotator and allow coupling to occur for a minimum of 1 1/2 hours and a maximum of 8 hours.

- 6.4. Remove block from rotator. Manually invert block quickly then wait 1-2 minutes to allow resin to fall into solution. Remove bottom cover followed by top cover. This step is necessary to remove excess resin from the cover.
- 6.5. Allow the solution to drain.
- 6.6. Wash (Step 2).
- 6.7. Perform Kaiser Test (Step 5).
 - 6.7.1. Negative Kaiser Test: proceed to deprotection Step 4.
 - 6.7.2. Positive Kaiser Test:
 - 6.7.2.1. Repeat Steps 6.1-6.2.
 - 6.7.2.2. Allow coupling to proceed for 30 minutes.
 - 6.7.2.3. Remove top cover, do not draw off solution, and perform Kaiser testing resin from at least 3 different wells.
 - 6.7.2.4. For negative Kaiser Test proceed to deprotection Step 4.
 - 6.7.2.5. For positive Kaiser Test, replace top cover and allow coupling to continue until a negative Kaiser test is obtained. If Kaiser Test remains positive after 8 hours, Repeat Step 6.7.2.
7. **Cleavage of Peptides from Resin**
 - 7.1. After performing the deprotection Step 4, further wash the resin with CH_2Cl_2 (3 times).
 - 7.2. Wash resin with methanol to shrink the resin.
 - 7.3. Allow the resin to dry under vacuum for at least four hours or overnight.
 - 7.4. Cleavage Cocktail
 - 7.4.1. For peptides containing methionine and cysteine: 81% TFA, 5% phenol, 5% thioanisole, 2.5% EDT, 3% water, 2% dimethylsulphide, 1.5% ammonium iodide (w/w).

Note: This is a very stinky solution!! Perform everything in the hood and wash everything this solution touches with bleach prior to removing from hood including gloves.
 - 7.4.2. For all other peptides: 95% TFA, 1% thioanisole, 2% phenol, 2% water.
 - 7.5. Add appropriate cleavage cocktail to wells (volume per well: 96 well, 1mL; 48 well, 1.5mL).
 - 7.6. Allow peptides to cleave for at least 2 hours up to 24 hours. Note: Peptides containing > 2 arginines require longer cleaving times to remove protecting groups.
 - 7.7. After cleavage time is complete, collect filtrate in deep well plates (46 or 96 well).
 - 7.8. Wash resin twice using TFA, collecting the filtrate.
 - 7.9. Remove TFA using Genvac.
 - 7.10. Dissolve the precipitate in < 50% ACN/water.
 - 7.11. Purify peptide using HPLC-MS.
8. **Purification by HPLC on Biotage**

- 8.1. Before using the Biotage, new peptides may require method optimization on an analytical HPLC system.
- 8.2. Before using the Biotage proper training is required.
- 8.3. Once a method has been established, place crude peptides in either 96 well or 48 deep well plates.
- 8.4. Run Biotage Method and follow current Biotage Protocols

8.4.1. For NCOA peptides use the following method:

UV detection: 214 and 280nm
 Injection volume: 1.8 mL
 Mobile Phase A: Water 0.05% TFA
 Mobile Phase B: Acetonitrile 0.05% TFA
 Flow Rate: 20mL/min
 Gradient:

	Mobile Phase A	Mobile Phase B	Time (minutes)
Equilibrate	90%	10%	3.0
Injection	90%	10%	0.6
Gradient	10%	90%	12.0
	10%	90%	1.0
Equilibrate	90%	10%	3.0

- 8.4.2. Collect fractions based on peak absorption at 214 and 280nm.
- 8.4.3. Identify fractions using MALDI-TOF.
 - 8.4.3.1. Add 0.5µL of sample to plate
 - 8.4.3.2. Add 0.5µL of matrix (alpha CHC Acid) on top of samples and allow to dry
 - 8.4.3.3. Detect samples on MALDI-TOF (training may be required).
- 8.4.4. Dry down selected samples on Genevac (Mega or HT-4) using the two step acetonitrile preprogrammed method.

9. Attaching a thiol reactive fluorophore (5-iodoacetamido fluorescein)

- 9.1. Dissolve 2-5mg of peptide (minimum 2 mg) in 2 Ml of phosphate buffer, (50 Mm sodium phosphate, 154 Mm NaCl, Ph 7.2). If peptide is very hydrophobic dissolve in DMF. Final concentration should be approximately 250µM.
- 9.2. Dissolve 100mg of 5-IAF in 1 Ml of DMF (194Mm)
- 9.3. Add 50µL to 2 Ml peptide solution (approximately 20-fold excess)
- 9.4. Allow reaction to proceed for at least 2 hours.
- 9.5. Quench with a an excess of β-mercaptoethanol, approximately 20 µL.
- 9.6. HPLC purify following step 8.0.

10. Quality Control Testing

- 10.1. Test the purity of the peptides samples using LCMS.
- 10.2. Dissolve peptides in 50:50 Acetonitrile:Water
- 10.3. LCMS methods may need to be optimized for individual peptides and libraries
- 10.4. For labeled NCOA peptides use the following method:

UV detection: Diode Array detection
 Injection volume: 10 μ L
 Mobile Phase A: Water 0.05% TFA
 Mobile Phase B: Acetonitrile 0.05% TFA
 Flow Rate: 0.2 MI/min
 Gradient:

	Mobile Phase A	Mobile Phase B	Time (minutes)
Equilibrate	90%	10%	1.0
Gradient	10%	90%	15.0
	10%	90%	1.0
	90%	10%	4.0
Equilibrate	90%	10%	5.0

MS Tune Conditions:

Capillary (kV)	3.0
Cone (V)	51
Extractor (V)	5
RF Lens	0
Source Temperature ($^{\circ}$ C)	100
Desolvation Temperature ($^{\circ}$ C)	250

11. Determination of Peptide Concentration for Labeled Peptides (5-IAF)

- 11.1. Dissolve peptides in DMSO.
- 11.2. Add 10 μ L of peptides from 11.1 into 1 mL Tris Buffer (20 mM Tris, pH 9.0).
- 11.3. Detect UV absorption at 492 nm.
- 11.4. Calculate concentration using the extinction coefficient of 78,000 $\text{cm}^{-1} \text{M}^{-1}$.

12. Storage of Peptides

- 12.1. The best storage conditions are in the dried state at -80° C. Alternatively, store stock solutions in DMSO at -80° C.
- 12.2. Working stock solutions can be made in buffer and stored at -80° C.

Table 1. List of common Fmoc-amino acids

Amino Acid	Fmoc Protected	g/mole
A	Fmoc-Ala-OH	311.30
R	Fmoc-Arg(Mtr)-OH	608.70
N	Fmoc-Asn(Trt)-OH	596.70
D	Fmoc-Asp(OtBu)-OH	411.50
C	Fmoc-Cys(trt)-OH	585.70
Q	Fmoc-Gln(Trt)-OH	610.70
E	Fmoc-Glu(OtBu)-OH	425.50
G	Fmoc-Gly-OH	297.30
H	Fmoc-His(Trt)-OH	619.70
I	Fmoc-Ile-OH	353.40
L	Fmoc-Leu-OH	353.40
K	Fmoc-Lys(Boc)-OH	468.55
M	Fmoc-Met-OH	371.50
F	Fmoc-Phe-OH	387.00
P	Fmoc-Pro-OH	337.40
S	Fmoc-Ser(tBu)-OH	383.40
T	Fmoc-Thr(tBu)-OH	397.50
W	Fmoc-Trp(Boc)-OH	526.60
Y	Fmoc-Tyr(tBu)-OH	466.00
V	Fmoc-Val-OH	339.40

Purchased from Novabiochem or Advanced Chemtech

Table 2. List of common Fmoc-amino acid wang resin

Amino Acid	Fmoc Amino Acid Resin	*Substitution (mmol/g)
A	Fmoc-Ala-Wang	0.69
R	Fmoc-Arg(Pbf)-Wang	0.35
N	Fmoc-Asn(Trt)-Wang	0.40
D	Fmoc-Asp(OtBu)-Wang	0.86
C	Fmoc-Cys(Trt)-Wang	0.45
Q	Fmoc-Gln(Trt)-Wang	0.71
E	Fmoc-Glu(OtBu)-Wang	0.51
G	Fmoc-Gly-Wang	1.00
H	Fmoc-His-(Trt)-Wang	0.39
I	Fmoc-Ile-Wang	0.81
L	Fmoc-Leu-Wang	0.88
K	Fmoc-Lys(Boc)-Wang	0.60
M	Fmoc-Met-Wang	0.43
F	Fmoc-Phe(4-1)-Wang	0.60
P	Fmoc-Pro-Wang	0.51
S	Fmoc-Ser(tBu)-Wang	0.94
T	Fmoc-Thr(tBu)-Wang	0.61
W	Fmoc-Trp-Wang	0.54
Y	Fmoc-Tyr(tBu)-Wang	0.88
V	Fmoc-Val-Wang	0.68

*Substitution may vary from lot to lot

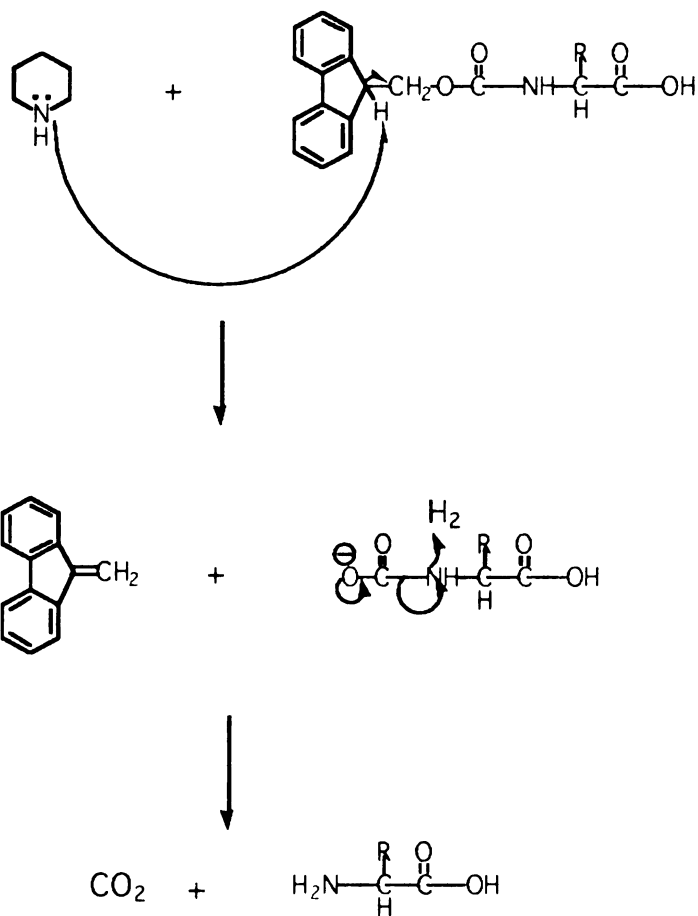
Purchased from Novabiochem or Advanced Chemtech

Table 3. Relevant Physical Properties

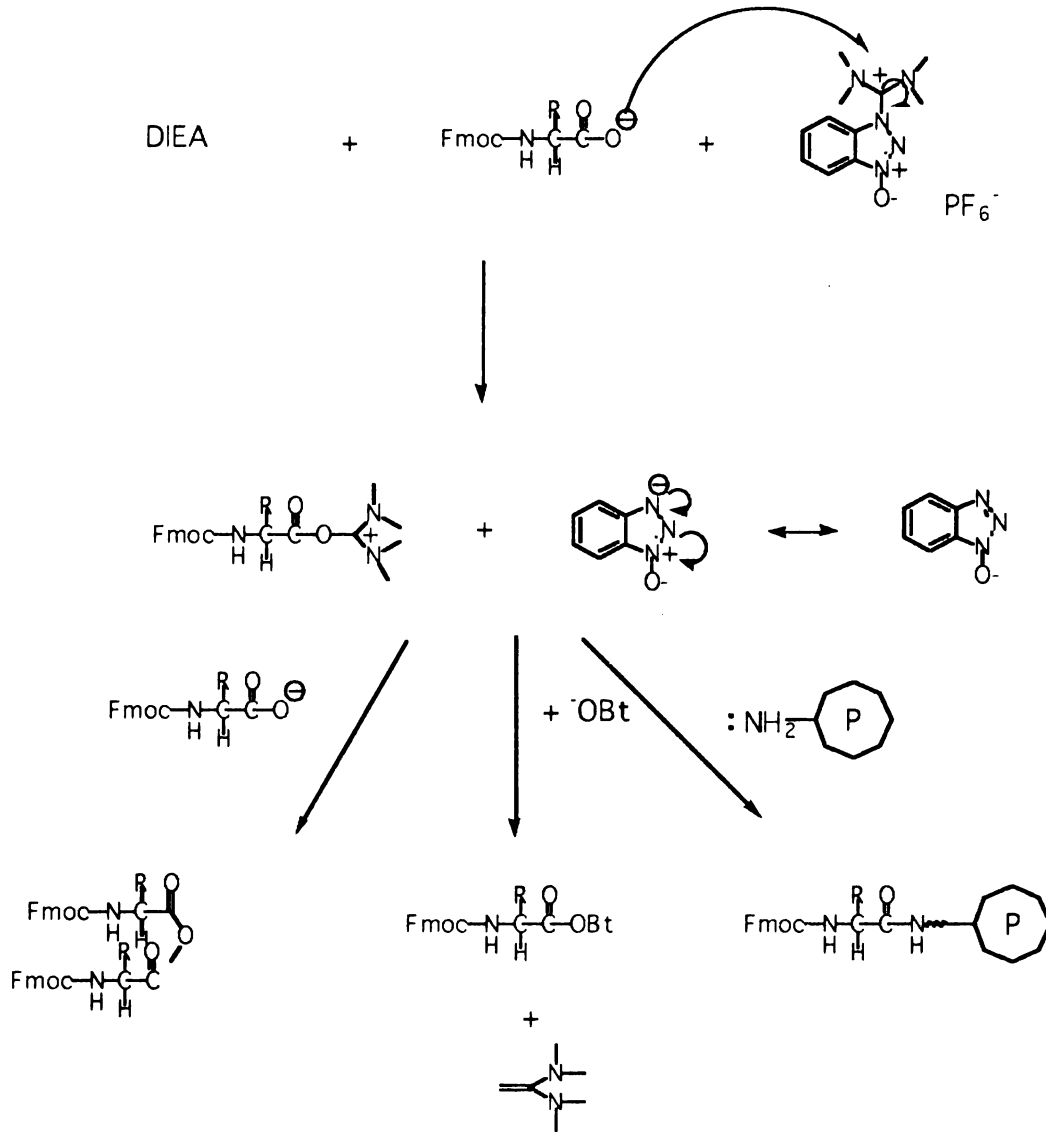
Reagent	Structure	Molecular Weight	pKa
DIEA		129.24	
Fmoc			
HBTU		379.3	
Piperidine		85.15	

Mechanisms

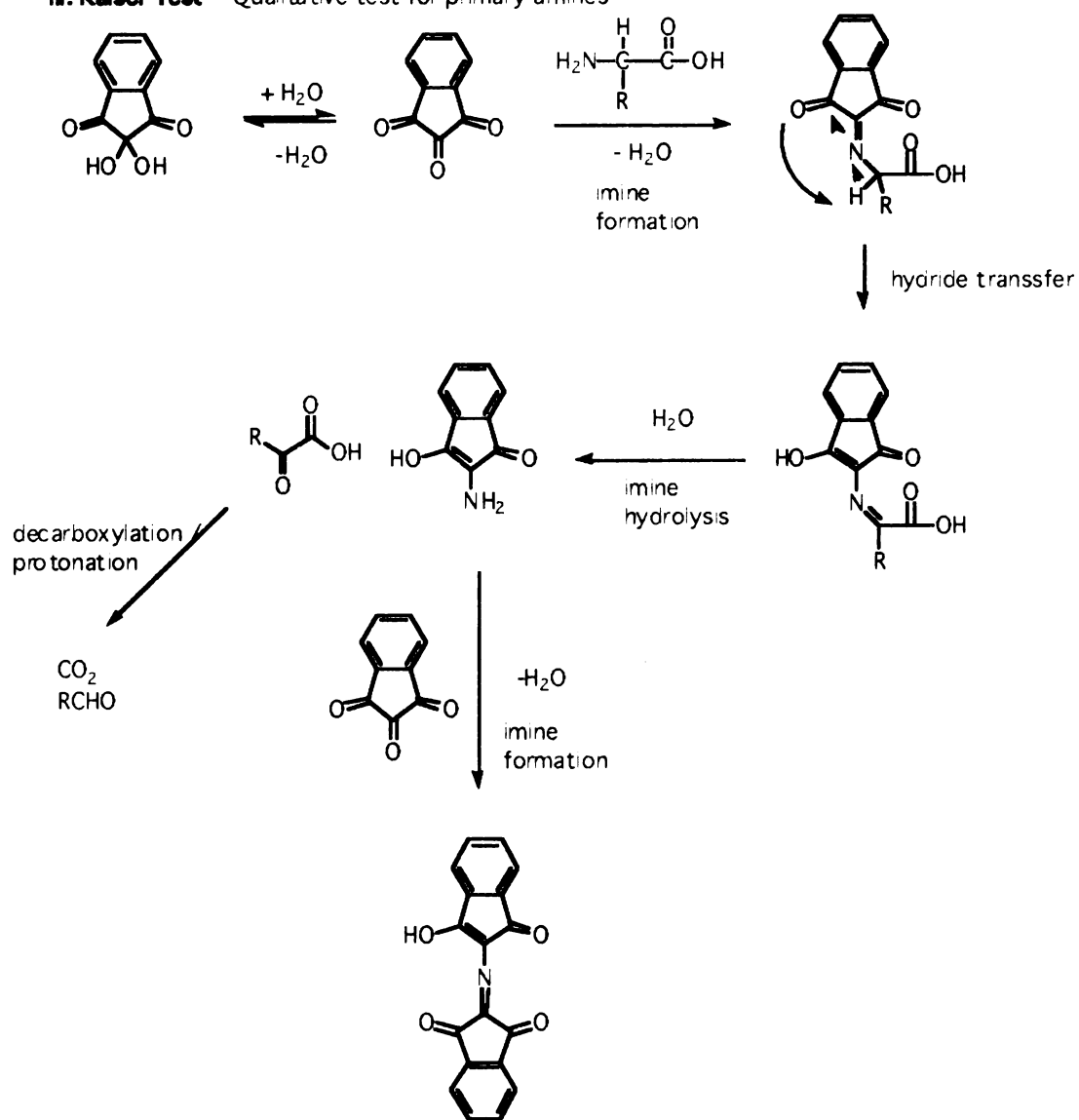
I. Deprotection - Removal of Fmoc group using piperidine



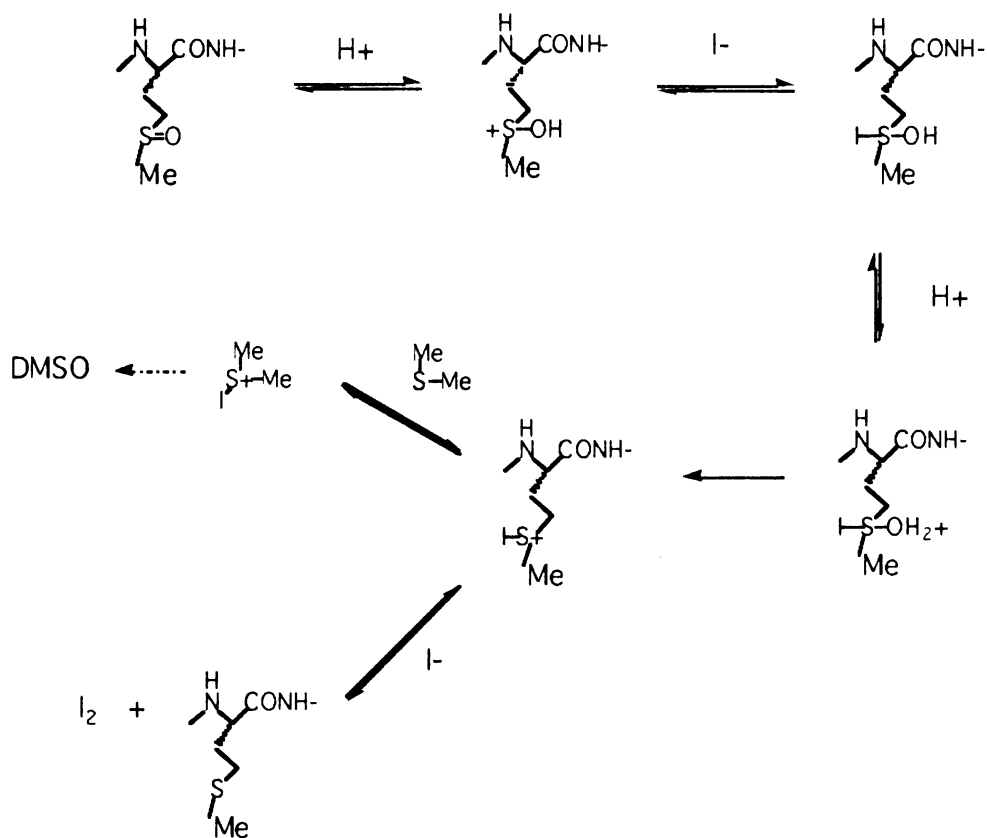
II. **Coupling Reaction** - Coupling of Fmoc-amino acid to growing peptide using HBTU



III. Kaiser Test - Qualitative test for primary amines



IV. Cleavage Reaction - Mechanism for the reduction of methionine sulphoxide to methionine with TFA, ammonium iodide, and dimethylsulphide



APPENDIX

B. Protocol for Measuring Binding Affinities of the Thyroid Receptor β to NCOA Peptide using Fluorescence Polarization

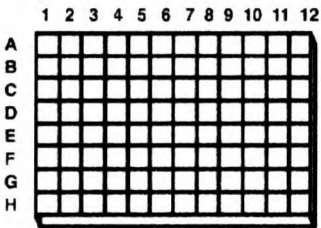
I. Overview.....	2
II. Reagents and Apparatus.....	3
III. Flow Chart.....	4
IV. Protocol.....	6

Overview

The direct binding of thyroid receptor b ligand binding domain (TR β -LBD) to fluorescent coregulator peptides can be measured using fluorescence polarization. In 96 well plates, TR β -LBD is serially diluted from 70 μ M to 0.002 μ M in binding buffer containing 140 μ M ligand (T3). Then 10 μ L of diluted protein is added to 10 μ L of fluorescent coregulator peptide (20 nM) in 384 well plates yielding final protein concentrations of 35-0.001 μ M and 10 nM fluorescent peptide concentration. The samples are allowed to equilibrate. Binding is then measured using fluorescence polarization (excitation λ 485 nm, emission λ 530 nm) on an Analyst AD (Molecular Devices). Two independent experiments are assayed for each state in quadruplicate. Data are analyzed using SigmaPlot 8.0 (SPSS, Chicago, IL) and the K_d values are obtained by fitting data to the following equation ($y = \text{min} + (\text{max} - \text{min}) / (1 + (x / K_d)^{\text{Hillslope}})$).

Flow Chart

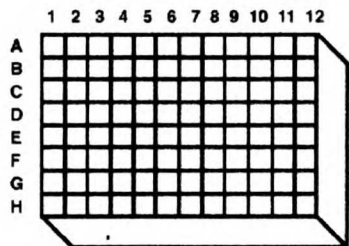
Preparation of Protein Plates:



Serial Dilution of TR β -LBD
70 μ M - 0.068 μ M

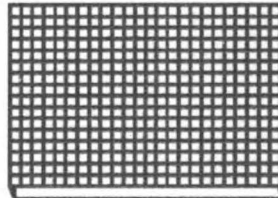
Protein Plates
96 well plates

Preparation of NCOA Plates:



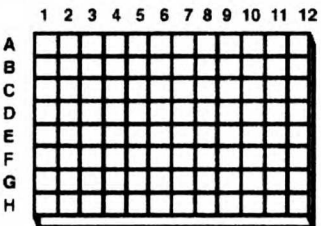
NCOA Working Stocks (20nM)
96 deep well plates

10 μ L
4x



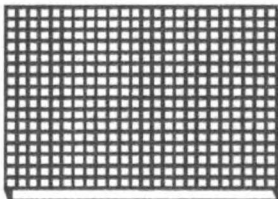
NCOA Assay Plates
384 well plates

Preparation of Assay Plates:



Protein Plates
96 well platse

10 μ L
Mixing
4x



NCOA Assay Plates
384 well plates
Final Concentrations:
10 nM NCOA Peptides
35-0.034 μ M TR β -LBD

Fluorescence
Polarization

Reagents

Dithiothreitol (DTT)
Ethanol
Ethylenedinitrilotetraaceticacid, free base (EDTA)
Fluorescent NCOA Peptides working plates (20nM)
Glycerol
Nonidet P-40 (NP-40)
Sodium Chloride
Sodium Phosphate, dibasic
Sodium Phosphate, monobasic
3,3'5-triiodo-Lthyronine, T3 (Sigma)
TR β -LBD – expressed and purified

Buffers and Stock Solutions

TR β -LBD Binding Buffer

50mM Sodium Phosphate, pH 7.2
154mM NaCl
1mM DTT
1mM EDTA
0.01 NP40 (w/v)
10% glycerol

10mM T3

Make stock solution in ethanol

Size Exclusion Chromatography (SEC) Mobile Phase

50mM Sodium Phosphate, pH 7.2
154mM NaCl

Material and Apparatus

Amicon Concentrators
Biomek
Fluorescence Polarization Plate Reader (Analyst AD, LJL Biosystem,
Molecular Devices)
G3000SW Column (TosoHaas)
HPLC (Waters Delta 600)
Multichannel Pipettor
Pipettors
SDS-PAGE Supplies
UV Spectrophotometer (Spectronic Genesys 5)
96 Well Plates (Costar)
384 Well Plate (Costar)

1. Preparation of TR β -LBD Plates

12.3. Obtain pure TR β -LBD (See Chapter 4)

12.3.1. Determine protein concentration following Coomassie BSA Protocol. Protein should be close to 2mg/mL (Approx. MW: 30,000daltons). If it is significantly below this concentration, concentrate using amicon. If it is above this concentration, then proceed to next step.

12.4. Set-up Plates

12.4.1. In 96 well plates use the following table for set-up:

Row Number	Final Protein Conc. (μ M)	Actual Protein Conc. (μ M)	Amount of Protein to Add (μ L)	Amount of Buffer to Add (μ L)
1	35.0	70.0	120	0
2	17.5	35.0	60	60
3	8.75	17.5	60	60
4	4.38	8.75	60	60
5	2.19	4.38	60	60
6	1.094	2.19	60	60
7	0.547	1.094	60	60
8	0.273	0.547	60	60
9	0.137	0.273	60	60
10	0.068	0.137	60	60
11	0.034	0.068	60	60
12	buffer	buffer	0	60

12.4.1.1. Place TR β -LBD binding buffer in a trough, then add 60 μ L to columns 2-12, row A using a multichannel pipettor. Repeat, for all rows (A-H).

12.4.1.2. Add 120 μ L of TR β -LBD to column 1 row A using a P200 pipettor. Repeat for all rows (A-H).

12.4.1.3. Perform serial dilutions using a multichannel pipettor by aspirating 60 μ L from column 1 and dispensing into column 2, mixing 3-5 times by gently aspirating and dispensing. Without dispensing pipette tips, continue dilutions by now aspirating from column 2 and dispensing into column 3 and mixing. Repeat serial dilutions until you reach column 11.

12.4.1.4. Repeat steps 1.2.1-1.2.1.3 for ten plates, labeling each plate 1-10. Ten plates are required for testing the complete NCOA library.

12.5. Quality Control Check of Protein

12.5.1. Run a sample on SDS-PAGE according to standard protocols.

12.5.2. Test a sample of TR β -LBD by Size Exclusion Chromatography (SEC).

12.5.2.1. Following HPLC protocols, using the following conditions:

Mobile Phase: TR β -LBD Mobile Phase

Flow Rate: 1mL/min

Injection Volume: 50 μ L

UV Detection: 280nm

Run time: 15 minutes

12.5.2.2. First inject TR β -LBD binding buffer and run HPLC conditions.

12.5.2.3. Repeat with TR β -LBD.

13. Preparation of NCOA Plates

13.1. The day before testing, thaw all ten working stock plates of NCOA fluorescent peptides at room temperature, protected from light. This can be done in a laboratory drawer or cabinet.

13.2. Using the Biomek FX, make daughter plates in 384 well plates.

13.2.1. Dispense 10 μ L from 20nM working stock plates (96 –deep well plates) into 384 well plates. Repeat 3 times, to make quadruplicate readings.

13.2.2. Repeat step 2.2.1 for each NCOA peptide stock plate (10 total plates).

14. Preparation of Assay Plates

(See Flow Chart)

14.1. Using the Biomek FX, prepare assay plates by dispensing 10 μ L from protein plate 1 into peptide 384 plate 1 and mix three times. Repeat 3 times, to make quadruplicate readings.

14.2. Repeat step 3.1 for remaining protein (plates 2-10) and peptide plates (plates 2-10).

15. Measuring Fluorescence Polarization

15.1. Test fluorescence polarization on Analyst AD enabling the plate stacker using the following method:

Parameters on Left

Lamp	Continuous
Plate Format	Corning 384 Square Opaque
Switch Polarization	By Well
Select Wells	High light appropriate wells
G Factor	0.8 (for fluorescein)
Z Height	2mm

Parameters on Right

Filters: Excitation	Fluorescein 485nm
Filters: Emission	Fluorescein 530nm
Reading per Well	3
Integration Time	100000

Parameters on Advanced Settings:

Dynamic Polarizer	Emission
State Polarizer	S
PMT	Set to digital

15.2. Measure fluorescence intensity on LJL enabling the plate stacker using the following method:

Lamp	Continuous
Plate Format	Corning 384 Square Opaque
Switch Polarization	By Well
Select Wells	High light appropriate wells
G Factor	0.8 (for fluorescein)
Z Height	2mm

Parameters on Right

Filters: Excitation	Fluorescein 485nm
Filters: Emission	Fluorescein 530nm
Reading per Well	3
Integration Time	100000

Parameters on Advanced Settings:

Dynamic Polarizer	None
State Polarizer	None
PMT	Set to digital

15.3.

16. Data Handling

16.1. Import data into a spreadsheet, such as excel. For example, data can be cut and paste into an excel spreadsheet.

16.2. Use Sigmaplot or Prism or equivalent program to determine Kd by fitting the data to the following equation:

$$y = \min + (\max - \min) / (1 + (x/K_d)^{\text{Hillslope}})$$

REFERENCES

1. Gloss, B., et al., *Cardiac ion channel expression and contractile function in mice with deletion of thyroid hormone receptor alpha or beta*. *Endocrinology*, 2001. **142**(2): p. 544-50.
2. Freake, H.C. and J.H. Oppenheimer, *Thermogenesis and thyroid function*. *Annu Rev Nutr*, 1995. **15**: p. 263-91.
3. Scanlan, T.S., et al., *3-Iodothyronamine is an endogenous and rapid-acting derivative of thyroid hormone*. *Nat Med*, 2004. **10**(6): p. 638-42.
4. Lazar, M.A. and W.W. Chin, *Nuclear thyroid hormone receptors*. *J Clin Invest*, 1990. **86**(6): p. 1777-82.
5. Lazar, M.A., *Thyroid hormone receptors: multiple forms, multiple possibilities*. *Endocr Rev*, 1993. **14**(2): p. 184-93.
6. Flamant, F. and J. Samarut, *Thyroid hormone receptors: lessons from knockout and knock-in mutant mice*. *Trends Endocrinol Metab*, 2003. **14**(2): p. 85-90.
7. Forrest, D., et al., *Recessive resistance to thyroid hormone in mice lacking thyroid hormone receptor beta: evidence for tissue-specific modulation of receptor function*. *Embo J*, 1996. **15**(12): p. 3006-15.
8. Forrest, D., et al., *Genetic analysis of thyroid hormone receptors in development and disease*. *Recent Prog Horm Res*, 1996. **51**: p. 1-22.
9. Fraichard, A., et al., *The T3R alpha gene encoding a thyroid hormone receptor is essential for post-natal development and thyroid hormone production*. *Embo J*, 1997. **16**(14): p. 4412-20.
10. Gauthier, K., et al., *Different functions for the thyroid hormone receptors TRalpha and TRbeta in the control of thyroid hormone production and post-natal development*. *Embo J*, 1999. **18**(3): p. 623-31.
11. Ng, L., et al., *A thyroid hormone receptor that is required for the development of green cone photoreceptors*. *Nat Genet*, 2001. **27**(1): p. 94-8.
12. Ogawa, K., et al., *Identification of a receptor tyrosine kinase involved in germ cell differentiation in planarians*. *Biochem Biophys Res Commun*, 1998. **248**(1): p. 204-9.
13. Umesonu, K., et al., *Direct repeats as selective response elements for the thyroid hormone, retinoic acid, and vitamin D3 receptors*. *Cell*, 1991. **65**(7): p. 1255-66.
14. Rastinejad, F., et al., *Structural determinants of nuclear receptor assembly on DNA direct repeats*. *Nature*, 1995. **375**(6528): p. 203-11.
15. Hu, X. and M.A. Lazar, *The CoRNR motif controls the recruitment of corepressors by nuclear hormone receptors*. *Nature*, 1999. **402**(6757): p. 93-6.
16. Mangelsdorf, D.J., et al., *The nuclear receptor superfamily: the second decade*. *Cell*, 1995. **83**(6): p. 835-9.
17. Feng, X., et al., *Thyroid hormone regulation of hepatic genes in vivo detected by complementary DNA microarray*. *Mol Endocrinol*, 2000. **14**(7): p. 947-55.
18. Sasaki, S., et al., *Ligand-induced recruitment of a histone deacetylase in the negative-feedback regulation of the thyrotropin beta gene*. *Embo J*, 1999. **18**(19): p. 5389-98.
19. Pfahl, M., *Nuclear receptor/AP-1 interaction*. *Endocr Rev*, 1993. **14**(5): p. 651-8.

20. Tagami, T., et al., *Nuclear receptor corepressors activate rather than suppress basal transcription of genes that are negatively regulated by thyroid hormone*. Mol Cell Biol, 1997. **17**(5): p. 2642-8.
21. Lazar, M.A., *Thyroid hormone action: a binding contract*. J Clin Invest, 2003. **112**(4): p. 497-9.
22. Leo, C. and J.D. Chen, *The SRC family of nuclear receptor coactivators*. Gene, 2000. **245**(1): p. 1-11.
23. Heery, D.M., et al., *A signature motif in transcriptional co-activators mediates binding to nuclear receptors*. Nature, 1997. **387**(6634): p. 733-6.
24. Darimont, B.D., et al., *Structure and specificity of nuclear receptor-coactivator interactions*. Genes Dev, 1998. **12**(21): p. 3343-56.
25. Wagner, R.L., et al., *A structural role for hormone in the thyroid hormone receptor*. Nature, 1995. **378**(6558): p. 690-7.
26. Shiau, A.K., et al., *Structural characterization of a subtype-selective ligand reveals a novel mode of estrogen receptor antagonism*. Nat Struct Biol, 2002. **9**(5): p. 359-64.
27. Chrivia, J.C., et al., *Phosphorylated CREB binds specifically to the nuclear protein CBP*. Nature, 1993. **365**(6449): p. 855-9.
28. Eckner, R., et al., *The adenovirus E1A-associated 300-kD protein exhibits properties of a transcriptional coactivator and belongs to an evolutionarily conserved family*. Cold Spring Harb Symp Quant Biol, 1994. **59**: p. 85-95.
29. Zhang, J. and J.D. Fondell, *Identification of mouse TRAP100: a transcriptional coregulatory factor for thyroid hormone and vitamin D receptors*. Mol Endocrinol, 1999. **13**(7): p. 1130-40.
30. Yuan, C.X., et al., *The TRAP220 component of a thyroid hormone receptor-associated protein (TRAP) coactivator complex interacts directly with nuclear receptors in a ligand-dependent fashion*. Proc Natl Acad Sci U S A, 1998. **95**(14): p. 7939-44.
31. Yeh, S., et al., *Functional analysis of androgen receptor N-terminal and ligand binding domain interacting coregulators in prostate cancer*. J Formos Med Assoc, 2000. **99**(12): p. 885-94.
32. Heinlein, C.A., et al., *Identification of ARA70 as a ligand-enhanced coactivator for the peroxisome proliferator-activated receptor gamma*. J Biol Chem, 1999. **274**(23): p. 16147-52.
33. Treuter, E., et al., *A regulatory role for RIP140 in nuclear receptor activation*. Mol Endocrinol, 1998. **12**(6): p. 864-81.
34. Esterbauer, H., et al., *Human peroxisome proliferator activated receptor gamma coactivator 1 (PPARGC1) gene: cDNA sequence, genomic organization, chromosomal localization, and tissue expression*. Genomics, 1999. **62**(1): p. 98-102.
35. Ko, L., G.R. Cardona, and W.W. Chin, *Thyroid hormone receptor-binding protein, an LXXLL motif-containing protein, functions as a general coactivator*. Proc Natl Acad Sci U S A, 2000. **97**(11): p. 6212-7.
36. Zhu, Y., et al., *Isolation and characterization of peroxisome proliferator-activated receptor (PPAR) interacting protein (PRIP) as a coactivator for PPAR*. J Biol Chem, 2000. **275**(18): p. 13510-6.

37. Suzuki, T., et al., *LXXLL-related motifs in Dax-1 have target specificity for the orphan nuclear receptors Ad4BP/SF-1 and LRH-1*. Mol Cell Biol, 2003. **23**(1): p. 238-49.
38. Johansson, L., et al., *The orphan nuclear receptor SHP utilizes conserved LXXLL-related motifs for interactions with ligand-activated estrogen receptors*. Mol Cell Biol, 2000. **20**(4): p. 1124-33.
39. Xu, J., et al., *The steroid receptor coactivator SRC-3 (p/CIP/RAC3/AIB1/ACTR/TRAM-1) is required for normal growth, puberty, female reproductive function, and mammary gland development*. Proc Natl Acad Sci U S A, 2000. **97**(12): p. 6379-84.
40. Weiss, R.E., et al., *Mice deficient in the steroid receptor co-activator 1 (SRC-1) are resistant to thyroid hormone*. Embo J, 1999. **18**(7): p. 1900-4.
41. Weiss, R.E., et al., *Thyroid function in mice with compound heterozygous and homozygous disruptions of SRC-1 and TIF-2 coactivators: evidence for haploinsufficiency*. Endocrinology, 2002. **143**(4): p. 1554-7.
42. Li, X., et al., *Progesterone and glucocorticoid receptors recruit distinct coactivator complexes and promote distinct patterns of local chromatin modification*. Mol Cell Biol, 2003. **23**(11): p. 3763-73.
43. Northrop, J.P., et al., *Selection of estrogen receptor beta- and thyroid hormone receptor beta-specific coactivator-mimetic peptides using recombinant peptide libraries*. Mol Endocrinol, 2000. **14**(5): p. 605-22.
44. Chang, C., et al., *Dissection of the LXXLL nuclear receptor-coactivator interaction motif using combinatorial peptide libraries: discovery of peptide antagonists of estrogen receptors alpha and beta*. Mol Cell Biol, 1999. **19**(12): p. 8226-39.
45. Bramlett, K.S., Y. Wu, and T.P. Burris, *Ligands specify coactivator nuclear receptor (NR) box affinity for estrogen receptor subtypes*. Mol Endocrinol, 2001. **15**(6): p. 909-22.
46. Geistlinger, T.R., McReynold, A. C., Guy, R. K., *Ligand Selective Inhibition of the Interaction of Steroid Receptor Coactivators and Estrogen Receptor Isoforms*. Chemistry and Biology, 2004. **In Press**.
47. McInerney, E.M., et al., *Determinants of coactivator LXXLL motif specificity in nuclear receptor transcriptional activation*. Genes Dev, 1998. **12**(21): p. 3357-68.
48. Coulthard, V.H., S. Matsuda, and D.M. Heery, *An extended LXXLL motif sequence determines the nuclear receptor binding specificity of TRAP220*. J Biol Chem, 2003. **278**(13): p. 10942-51.
49. Fischer, E., Ber. Dtsch. Chem. Ges., 1901. **34**: p. 2868.
50. Vigneaud, V.d., Ressler, C., Swan, J. M., Roberts, C. W., Katsoyannis, P. G., Gordon, S., J. Am. Chem. Soc., 1953. **75**: p. 4879.
51. Merrifield, R.B., J Am Chem Soc, 1963. **85**: p. 2149.
52. Merrifield, R.B., *Automated synthesis of peptides*. Science, 1965. **150**(693): p. 178-85.
53. Merrifield, R.B., *Solid-Phase Peptide Syntheses*. Endeavour, 1965. **24**: p. 3-7.
54. Merrifield, R.B. and J.M. Stewart, *Automated peptide synthesis*. Nature, 1965. **207**(996): p. 522-3.
55. Chang, C.D.a.M., J., Int. J. Pept. Protein Res., 1978. **11**: p. 246.

56. Atherton, E., Fox, H., Harkiss, D., Logan, C. J., Sheppard, R. C., and Williams, B. J., *J. Chem. Soc. Chem. Commun.*, 1978: p. 537.
57. Wellings, D.A. and E. Atherton, *Standard Fmoc protocols*. *Methods Enzymol*, 1997. **289**: p. 44-67.
58. Backes, B.J., et al., *Synthesis of positional-scanning libraries of fluorogenic peptide substrates to define the extended substrate specificity of plasmin and thrombin*. *Nat Biotechnol*, 2000. **18**(2): p. 187-93.
59. van Woerkom, W.J. and J.W. van Nispen, *Difficult couplings in stepwise solid phase peptide synthesis: predictable or just a guess?* *Int J Pept Protein Res*, 1991. **38**(2): p. 103-13.
60. Kent, S.a.C.-L., I, *Synthetic Peptides in Biology and Medicine*. 1985, Amsterdam: Elsevier Science Publishing, 29-57.
61. Luu, T., S. Pham, and S. Deshpande, *Automated multiple peptide synthesis: improvements in obtaining quality peptides*. *Int J Pept Protein Res*, 1996. **47**(1-2): p. 91-7.
62. Huang, H. and D.L. Rabenstein, *A cleavage cocktail for methionine-containing peptides*. *J Pept Res*, 1999. **53**(5): p. 548-53.
63. Takeshita, A., et al., *TRAM-1, A novel 160-kDa thyroid hormone receptor activator molecule, exhibits distinct properties from steroid receptor coactivator-1*. *J Biol Chem*, 1997. **272**(44): p. 27629-34.
64. Li, H., P.J. Gomes, and J.D. Chen, *RAC3, a steroid/nuclear receptor-associated coactivator that is related to SRC-1 and TIF2*. *Proc Natl Acad Sci U S A*, 1997. **94**(16): p. 8479-84.
65. Ren, Y., et al., *Specific structural motifs determine TRAP220 interactions with nuclear hormone receptors*. *Mol Cell Biol*, 2000. **20**(15): p. 5433-46.
66. Subramaniam, N., E. Treuter, and S. Okret, *Receptor interacting protein RIP140 inhibits both positive and negative gene regulation by glucocorticoids*. *J Biol Chem*, 1999. **274**(25): p. 18121-7.
67. Cavailles, V., et al., *Nuclear factor RIP140 modulates transcriptional activation by the estrogen receptor*. *Embo J*, 1995. **14**(15): p. 3741-51.
68. Mellgren, G., et al., *Characterization of receptor-interacting protein RIP140 in the regulation of SF-1 responsive target genes*. *Mol Cell Endocrinol*, 2003. **203**(1-2): p. 91-103.
69. Miyata, K.S., et al., *Receptor-interacting protein 140 interacts with and inhibits transactivation by, peroxisome proliferator-activated receptor alpha and liver-X-receptor alpha*. *Mol Cell Endocrinol*, 1998. **146**(1-2): p. 69-76.
70. Chiellini, G., et al., *A high-affinity subtype-selective agonist ligand for the thyroid hormone receptor*. *Chem Biol*, 1998. **5**(6): p. 299-306.
71. Wagner, R.L., et al., *Hormone selectivity in thyroid hormone receptors*. *Mol Endocrinol*, 2001. **15**(3): p. 398-410.
72. Nguyen, N.H., et al., *Rational design and synthesis of a novel thyroid hormone antagonist that blocks coactivator recruitment*. *J Med Chem*, 2002. **45**(15): p. 3310-20.
73. Wu, Y., et al., *Requirement of helix 1 and the AF-2 domain of the thyroid hormone receptor for coactivation by PGC-1*. *J Biol Chem*, 2002. **277**(11): p. 8898-905.

74. Geistlinger, T.R. and R.K. Guy, *Novel selective inhibitors of the interaction of individual nuclear hormone receptors with a mutually shared steroid receptor coactivator 2*. J Am Chem Soc, 2003. **125**(23): p. 6852-3.
75. Kodera, Y., et al., *Ligand type-specific interactions of peroxisome proliferator-activated receptor gamma with transcriptional coactivators*. J Biol Chem, 2000. **275**(43): p. 33201-4.
76. Trost, S.U., et al., *The thyroid hormone receptor-beta-selective agonist GC-1 differentially affects plasma lipids and cardiac activity*. Endocrinology, 2000. **141**(9): p. 3057-64.
77. Takeuchi, Y., et al., *Steroid receptor coactivator-1 deficiency causes variable alterations in the modulation of T(3)-regulated transcription of genes in vivo*. Endocrinology, 2002. **143**(4): p. 1346-52.
78. Sadow, P.M., et al., *Thyroid hormone receptor-specific interactions with steroid receptor coactivator-1 in the pituitary*. Mol Endocrinol, 2003. **17**(5): p. 882-94.
79. Sadow, P.M., et al., *Specificity of thyroid hormone receptor subtype and steroid receptor coactivator-1 on thyroid hormone action*. Am J Physiol Endocrinol Metab, 2003. **284**(1): p. E36-46.
80. Sadow, P.M., et al., *Regulation of expression of thyroid hormone receptor isoforms and coactivators in liver and heart by thyroid hormone*. Mol Cell Endocrinol, 2003. **203**(1-2): p. 65-75.
81. Puustinen, R., et al., *Localization of glucocorticoid receptor interacting protein 1 in murine tissues using two novel polyclonal antibodies*. Eur J Endocrinol, 2001. **145**(3): p. 323-33.
82. Meijer, O.C., P.J. Steenbergen, and E.R. De Kloet, *Differential expression and regional distribution of steroid receptor coactivators SRC-1 and SRC-2 in brain and pituitary*. Endocrinology, 2000. **141**(6): p. 2192-9.
83. Cheskis, B.J., et al., *Hierarchical affinities and a bipartite interaction model for estrogen receptor isoforms and full-length steroid receptor coactivator (SRC/p160) family members*. J Biol Chem, 2003. **278**(15): p. 13271-7.
84. Lee, H.J. and C. Chang, *Recent advances in androgen receptor action*. Cell Mol Life Sci, 2003. **60**(8): p. 1613-22.
85. Legros, J.J., et al., *Partial Androgen Deficiency of Aging Male (P.A.D.A.M.) might in part be due to excessive organochloride pesticide (OC) impregnation*. Ann Endocrinol (Paris), 2003. **64**(2): p. 136.
86. Gregory, C.W., et al., *A mechanism for androgen receptor-mediated prostate cancer recurrence after androgen deprivation therapy*. Cancer Res, 2001. **61**(11): p. 4315-9.
87. Culig, Z., et al., *Androgen receptors in prostate cancer*. Endocr Relat Cancer, 2002. **9**(3): p. 155-70.
88. Santos, A.F., H. Huang, and D.J. Tindall, *The androgen receptor: a potential target for therapy of prostate cancer*. Steroids, 2004. **69**(2): p. 79-85.
89. Balk, S.P., *Androgen receptor as a target in androgen-independent prostate cancer*. Urology, 2002. **60**(3 Suppl 1): p. 132-8; discussion 138-9.
90. Ding, X.F., et al., *Nuclear receptor-binding sites of coactivators glucocorticoid receptor interacting protein 1 (GRIP1) and steroid receptor coactivator 1 (SRC-*

- 1): *multiple motifs with different binding specificities*. Mol Endocrinol, 1998. **12**(2): p. 302-13.
91. Berrevoets, C.A., et al., *Functional interactions of the AF-2 activation domain core region of the human androgen receptor with the amino-terminal domain and with the transcriptional coactivator TIF2 (transcriptional intermediary factor2)*. Mol Endocrinol, 1998. **12**(8): p. 1172-83.
 92. Shang, Y., M. Myers, and M. Brown, *Formation of the androgen receptor transcription complex*. Mol Cell, 2002. **9**(3): p. 601-10.
 93. Gregory, C.W., et al., *Epidermal growth factor increases coactivation of the androgen receptor in recurrent prostate cancer*. J Biol Chem, 2004. **279**(8): p. 7119-30.
 94. Blaszczyk, N., et al., *Osteoblast-derived factors induce androgen-independent proliferation and expression of prostate-specific antigen in human prostate cancer cells*. Clin Cancer Res, 2004. **10**(5): p. 1860-9.
 95. Needham, M., et al., *Differential interaction of steroid hormone receptors with LXXLL motifs in SRC-1a depends on residues flanking the motif*. J Steroid Biochem Mol Biol, 2000. **72**(1-2): p. 35-46.
 96. Alen, P., et al., *Interaction of the putative androgen receptor-specific coactivator ARA70/ELE1alpha with multiple steroid receptors and identification of an internally deleted ELE1beta isoform*. Mol Endocrinol, 1999. **13**(1): p. 117-28.
 97. He, B., et al., *Dependence of selective gene activation on the androgen receptor NH2- and COOH-terminal interaction*. J Biol Chem, 2002. **277**(28): p. 25631-9.
 98. Ma, H., et al., *Multiple signal input and output domains of the 160-kilodalton nuclear receptor coactivator proteins*. Mol Cell Biol, 1999. **19**(9): p. 6164-73.
 99. Christiaens, V., et al., *Characterization of the two coactivator-interacting surfaces of the androgen receptor and their relative role in transcriptional control*. J Biol Chem, 2002. **277**(51): p. 49230-7.
 100. Powell, S.M., et al., *Mechanisms of androgen receptor signalling via steroid receptor coactivator-1 in prostate*. Endocr Relat Cancer, 2004. **11**(1): p. 117-30.
 101. He, B. and E.M. Wilson, *The NH(2)-terminal and carboxyl-terminal interaction in the human androgen receptor*. Mol Genet Metab, 2002. **75**(4): p. 293-8.
 102. He, B., et al., *The FXXLF motif mediates androgen receptor-specific interactions with coregulators*. J Biol Chem, 2002. **277**(12): p. 10226-35.
 103. Zhou, Z.X., et al., *Domain interactions between coregulator ARA(70) and the androgen receptor (AR)*. Mol Endocrinol, 2002. **16**(2): p. 287-300.
 104. He, B., J.A. Kempainen, and E.M. Wilson, *FXXLF and WXXLF sequences mediate the NH2-terminal interaction with the ligand binding domain of the androgen receptor*. J Biol Chem, 2000. **275**(30): p. 22986-94.
 105. Bourguet, W., et al., *Heterodimeric complex of RAR and RXR nuclear receptor ligand-binding domains: purification, crystallization, and preliminary X-ray diffraction analysis*. Protein Expr Purif, 2000. **19**(2): p. 284-8.
 106. Wilson, E.M., B. He, and E. Langley, *Methods for detecting domain interactions in nuclear receptors*. Methods Enzymol, 2003. **364**: p. 142-52.
 107. Chang, C.Y. and D.P. McDonnell, *Evaluation of ligand-dependent changes in AR structure using peptide probes*. Mol Endocrinol, 2002. **16**(4): p. 647-60.

108. Shiau, A.K., et al., *The structural basis of estrogen receptor/coactivator recognition and the antagonism of this interaction by tamoxifen*. Cell, 1998. **95**(7): p. 927-37.
109. Ribeiro, R.C., et al., *The molecular biology of thyroid hormone action*. Ann N Y Acad Sci, 1995. **758**: p. 366-89.
110. Moore, J.M., et al., *Quantitative proteomics of the thyroid hormone receptor-coregulator interactions*. J Biol Chem, 2004. **279**(26): p. 27584-90.
111. Bevan, C.L., et al., *The AF1 and AF2 domains of the androgen receptor interact with distinct regions of SRC1*. Mol Cell Biol, 1999. **19**(12): p. 8383-92.
112. Wang, Q., J. Lu, and E.L. Yong, *Ligand- and coactivator-mediated transactivation function (AF2) of the androgen receptor ligand-binding domain is inhibited by the cognate hinge region*. J Biol Chem, 2001. **276**(10): p. 7493-9.
113. Slagsvold, T., et al., *Mutational analysis of the androgen receptor AF-2 (activation function 2) core domain reveals functional and mechanistic differences of conserved residues compared with other nuclear receptors*. Mol Endocrinol, 2000. **14**(10): p. 1603-17.
114. Bledsoe, R.K., et al., *Crystal structure of the glucocorticoid receptor ligand binding domain reveals a novel mode of receptor dimerization and coactivator recognition*. Cell, 2002. **110**(1): p. 93-105.
115. Pike, J.W., H. Yamamoto, and N.K. Shevde, *Vitamin D receptor-mediated gene regulation mechanisms and current concepts of vitamin D analog selectivity*. Adv Ren Replace Ther, 2002. **9**(3): p. 168-74.
116. He, B. and E.M. Wilson, *Electrostatic modulation in steroid receptor recruitment of LXXLL and FXXLF motifs*. Mol Cell Biol, 2003. **23**(6): p. 2135-50.
117. DeLano, W.L., *The PyMOL Molecular Graphics System*. 2002, DeLano Scientific: San Carlos, CA, USA.
118. Matias, P.M., et al., *Structural evidence for ligand specificity in the binding domain of the human androgen receptor. Implications for pathogenic gene mutations*. J Biol Chem, 2000. **275**(34): p. 26164-71.
119. Gustafsson, J.A., *What pharmacologists can learn from recent advances in estrogen signalling*. Trends Pharmacol Sci, 2003. **24**(9): p. 479-85.
120. Hall, J.M., J.F. Couse, and K.S. Korach, *The multifaceted mechanisms of estradiol and estrogen receptor signaling*. J Biol Chem, 2001. **276**(40): p. 36869-72.
121. Vegeto, E., et al., *Estrogen receptor-alpha mediates the brain antiinflammatory activity of estradiol*. Proc Natl Acad Sci U S A. 2003. **100**(16): p. 9614-9.
122. Manolagas, S.C., S. Kousteni, and R.L. Jilka, *Sex steroids and bone*. Recent Prog Horm Res, 2002. **57**: p. 385-409.
123. Losel, R.M., et al., *Nongenomic steroid action: controversies, questions, and answers*. Physiol Rev, 2003. **83**(3): p. 965-1016.
124. Mendelsohn, M.E., *Genomic and nongenomic effects of estrogen in the vasculature*. Am J Cardiol, 2002. **90**(1A): p. 3F-6F.
125. Turgeon, J.L., et al., *Hormone therapy: physiological complexity belies therapeutic simplicity*. Science, 2004. **304**(5675): p. 1269-73.

126. Wong, C.W., et al., *Estrogen receptor-interacting protein that modulates its nongenomic activity-crossstalk with Src/Erk phosphorylation cascade*. Proc Natl Acad Sci U S A, 2002. **99**(23): p. 14783-8.
127. McDonnell, D.P., et al., *Definition of the molecular and cellular mechanisms underlying the tissue-selective agonist/antagonist activities of selective estrogen receptor modulators*. Recent Prog Horm Res, 2002. **57**: p. 295-316.
128. Anzick, S.L., et al., *AIB1, a steroid receptor coactivator amplified in breast and ovarian cancer*. Science, 1997. **277**(5328): p. 965-8.
129. Klinge, C.M., *Estrogen receptor interaction with co-activators and co-repressors*. Steroids, 2000. **65**(5): p. 227-51.
130. Bramlett, K.S. and T.P. Burris, *Effects of selective estrogen receptor modulators (SERMs) on coactivator nuclear receptor (NR) box binding to estrogen receptors*. Mol Genet Metab, 2002. **76**(3): p. 225-33.
131. Shang, Y., et al., *Cofactor dynamics and sufficiency in estrogen receptor-regulated transcription*. Cell, 2000. **103**(6): p. 843-52.
132. Hall, J.M., C.Y. Chang, and D.P. McDonnell, *Development of peptide antagonists that target estrogen receptor beta-coactivator interactions*. Mol Endocrinol, 2000. **14**(12): p. 2010-23.
133. Iannone, M.A., et al., *Correlation between in vitro peptide binding profiles and cellular activities for estrogen receptor-modulating compounds*. Mol Endocrinol, 2004. **18**(5): p. 1064-81.
134. Wu, Z., et al., *Mechanisms controlling mitochondrial biogenesis and respiration through the thermogenic coactivator PGC-1*. Cell, 1999. **98**(1): p. 115-24.
135. Tcherepanova, I., et al., *Modulation of estrogen receptor-alpha transcriptional activity by the coactivator PGC-1*. J Biol Chem, 2000. **275**(21): p. 16302-8.
136. Warnmark, A., et al., *Differential recruitment of the mammalian mediator subunit TRAP220 by estrogen receptors ERalpha and ERbeta*. J Biol Chem, 2001. **276**(26): p. 23397-404.
137. Ko, L., et al., *Ser-884 adjacent to the LXXLL motif of coactivator TRBP defines selectivity for ERs and TRs*. Mol Endocrinol, 2002. **16**(1): p. 128-40.
138. Laudet, V., *Evolution of the nuclear receptor superfamily: early diversification from an ancestral orphan receptor*. J Mol Endocrinol, 1997. **19**(3): p. 207-26.
139. Escriva, H., et al., *Analysis of lamprey and hagfish genes reveals a complex history of gene duplications during early vertebrate evolution*. Mol Biol Evol, 2002. **19**(9): p. 1440-50.
140. Goodwin, B., et al., *A regulatory cascade of the nuclear receptors FXR, SHP-1, and LRH-1 represses bile acid biosynthesis*. Mol Cell, 2000. **6**(3): p. 517-26.
141. Hammer, G.D. and H.A. Ingraham, *Steroidogenic factor-1: its role in endocrine organ development and differentiation*. Front Neuroendocrinol, 1999. **20**(3): p. 199-223.
142. Lu, T.T., et al., *Molecular basis for feedback regulation of bile acid synthesis by nuclear receptors*. Mol Cell, 2000. **6**(3): p. 507-15.
143. del Castillo-Olivares, A. and G. Gil, *Alpha 1-fetoprotein transcription factor is required for the expression of sterol 12alpha -hydroxylase, the specific enzyme for cholic acid synthesis. Potential role in the bile acid-mediated regulation of gene transcription*. J Biol Chem, 2000. **275**(23): p. 17793-9.

144. Nitta, M., et al., *CPF: an orphan nuclear receptor that regulates liver-specific expression of the human cholesterol 7alpha-hydroxylase gene*. Proc Natl Acad Sci U S A, 1999. **96**(12): p. 6660-5.
145. Luo, Y., C.P. Liang, and A.R. Tall, *The orphan nuclear receptor LRH-1 potentiates the sterol-mediated induction of the human CETP gene by liver X receptor*. J Biol Chem, 2001. **276**(27): p. 24767-73.
146. Schoonjans, K., et al., *Liver receptor homolog 1 controls the expression of the scavenger receptor class B type I*. EMBO Rep, 2002. **3**(12): p. 1181-7.
147. Roberts, L.M., J. Shen, and H.A. Ingraham, *New solutions to an ancient riddle: defining the differences between Adam and Eve*. Am J Hum Genet, 1999. **65**(4): p. 933-42.
148. Ingraham, H.A., et al., *The nuclear receptor steroidogenic factor 1 acts at multiple levels of the reproductive axis*. Genes Dev, 1994. **8**(19): p. 2302-12.
149. Luo, X., Y. Ikeda, and K.L. Parker, *A cell-specific nuclear receptor is essential for adrenal and gonadal development and sexual differentiation*. Cell, 1994. **77**(4): p. 481-90.
150. Parker, K.L. and B.P. Schimmer, *Steroidogenic factor 1: a key determinant of endocrine development and function*. Endocr Rev, 1997. **18**(3): p. 361-77.
151. Steinmetz, A.C., J.P. Renaud, and D. Moras, *Binding of ligands and activation of transcription by nuclear receptors*. Annu Rev Biophys Biomol Struct, 2001. **30**: p. 329-59.
152. Xu, P.L., et al., *Molecular mechanism for the potentiation of the transcriptional activity of human liver receptor homolog 1 by steroid receptor coactivator-1*. Mol Endocrinol, 2004. **18**(8): p. 1887-905.
153. Seol, W., H.S. Choi, and D.D. Moore, *An orphan nuclear hormone receptor that lacks a DNA binding domain and heterodimerizes with other receptors*. Science, 1996. **272**(5266): p. 1336-9.
154. Seol, W., M. Chung, and D.D. Moore, *Novel receptor interaction and repression domains in the orphan receptor SHP*. Mol Cell Biol, 1997. **17**(12): p. 7126-31.
155. Lee, Y.K. and D.D. Moore, *Dual mechanisms for repression of the monomeric orphan receptor liver receptor homologous protein-1 by the orphan small heterodimer partner*. J Biol Chem, 2002. **277**(4): p. 2463-7.
156. Lee, Y.K., et al., *Activation of the promoter of the orphan receptor SHP by orphan receptors that bind DNA as monomers*. J Biol Chem, 1999. **274**(30): p. 20869-73.
157. Achermann, J.C., J.J. Meeks, and J.L. Jameson, *Phenotypic spectrum of mutations in DAX-1 and SF-1*. Mol Cell Endocrinol, 2001. **185**(1-2): p. 17-25.

U
San Francisco
LIBRARY

M
San Francisco
LIBRARY

U
San Francisco
LIBRARY

U
San Francisco
LIBRARY

M
San Francisco
LIBRARY

U
San Francisco
LIBRARY

U
San Francisco
LIBRARY

M
San Francisco
LIBRARY

U
San Francisco
LIBRARY

U
San Francisco
LIBRARY

M
San Francisco
LIBRARY

U
San Francisco
LIBRARY

U
San Francisco
LIBRARY

M
San Francisco
LIBRARY

U
San Francisco
LIBRARY

U
San Francisco
LIBRARY

M
San Francisco
LIBRARY

U
San Francisco
LIBRARY

U
San Francisco
LIBRARY

M
San Francisco
LIBRARY

U
San Francisco
LIBRARY

U
San Francisco
LIBRARY

M
San Francisco
LIBRARY

U
San Francisco
LIBRARY

U
San Francisco
LIBRARY

M
San Francisco
LIBRARY

U
San Francisco
LIBRARY

U
San Francisco
LIBRARY

M
San Francisco
LIBRARY

U
San Francisco
LIBRARY

U
San Francisco
LIBRARY

M
San Francisco
LIBRARY

U
San Francisco
LIBRARY

U
San Francisco
LIBRARY

M
San Francisco
LIBRARY

U
San Francisco
LIBRARY

U
San Francisco
LIBRARY

M
San Francisco
LIBRARY

U
San Francisco
LIBRARY

For Not to be taken
from the room.
reference

7433314



3 1378 00743 3314

